Institute for Physical Science and Technology

University of Maryland
College Park

FINAL REPORT

to the

OFFICE OF NAVAL RESEARCH

on

Grant N00014-82-K-0208

Acceleration of Ions and Electrons by Wave-Particle Interactions

C. S. Wu
Principal Investigator

John D. Goffey, Jr.
Co-Principal Investigator

Funding Period:

March 1, 1982 - March 31, 1984

CONTENTS

III. REPRINTS AND PREPRINTS

1. Calculation of the spontaneous cyclotron emissivity using the complete relativistic resonance condition, H. P. Freund, C. S. Wu, and J. D. Gaffey, Jr., Phys. Fluids, in press (1984).

2. Electron-cyclotron maser instability in hot electron mirror machines, H. K. Wong, C. S. Wu, and J. D. Gaffey, Jr., Phys. Rev. Lett., submitted (1984).

3. Instabilities excited by an energetic ion beam and electron temperature anisotropy in tandem mirrors, E. H. da Jornada, J. D. Gaffey, Jr., and D. Winske, Phys. Fluids, submitted (1984).

4. Effect of electron thermal anisotropy on the kinetic cross-field streaming instability, S. T. Tsai, M. Tanaka, J. D. Gaffey, Jr., E. H. da Jornada, C. S. Wu, and L. F. Ziebell, J. Plasma Phys., in press (1984).

5. Acceleration of auroral electrons by lower-hybrid turbulence and a quasistatic parallel electric field, J. D. Gaffey, Jr., Z. X. Liu, and S. C. Guo, J. Plasma Phys., submitted (1984).

6. Comments on "Energization of ionospheric ions by electrostatic hydrogen cyclotron waves," by N. Singh, R. W. Schunk, and J. J. Sojka, in Geophys. Res. Lett. 8, 1249 (1981), J. D. Gaffey, Jr., Geophys. Res. Lett., submitted (1983).

IV. ABSTRACTS

1. Statistical acceleration of electrons by lower-hybrid turbulence in the presence of a parallel electric field, J. D. Gaffey, Jr., Z. X. Liu, and C. S. Wu, EOS Trans. Am. Geophys. Union 63, 409 (1982).

2. Acceleration of auroral electrons by lower-hybrid turbulence and a quasistatic parallel electric field, J. D. Gaffey, Jr., Z. X. Liu, and S. C. Guo, Bull. Am. Phys. Soc. 27, 1024 (1982).

3. Instabilities at the bow shock. I. Kinetic cross-field streaming instability, M. Tanaka, J. D. Gaffey, Jr., D. Winske, C. S. Wu, Y. M. Zhou, S. T. Tsai, and K. Papadopoulos, EOS, Trans. Am. Geophys. Union 63, 1070 (1982).

4. Instabilities at the bow shock. III. Cross-field streaming instability with temperature anisotropy, S. T. Tsai, M. Tanaka, C. S. Wu, and J. D. Gaffey, Jr., EOS, Trans. Am. Geophys. Union 63, 1070 (1982).

5. A cross-field streaming instability with electron temperature anisotropy in tandem mirrors, J. D. Gaffey, Jr., M. Tanaka, and S. T. Tsai, Proc. 1983 Sherwood Theory Meeting, Annual Controlled Fusion Theory Conf., Arlington, VA, USA (Mar., 1983).

6. Effect of electron thermal anisotropy on the kinetic cross-field streaming instability in the bow shock, J. D. Gaffey, Jr., Motohiko Tanaka, C. S. Wu, and E. H. da Jornada, EOS, Trans. Am. Geophys. Union 64, 228 (1983).

7. Spontaneous emission of radiation at cyclotron harmonics by electrons with a loss-cone or hollow-beam distribution function, C. S. Wu, H. P. Freund, and J. D. Gaffey, Jr., Bull. Am. Phys. Soc. 28, 1068 (1983).

8. Effect of electron temperature anisotropy on the kinetic cross-field streaming instability, J. D. Gaffey, Jr., E. H. da Jornada, M. Tanaka, D. Winske, and C. S. Wu, Bull. Am. Phys. Soc. 28, 1195 (1983).

9. Electron-cyclotron maser instability in magnetic mirror machines, H. K. Wong, J. D. Gaffey, Jr., and C. S. Wu, Proc. 1984 Sherwood Theory Meeting, Annual Controlled Fusion Theory Conf., Incline Village, NV, USA (Apr., 1984).

10. Instabilities excited by an energetic ion beam and electron temperature anisotropy in tandem mirrors, J. D. Gaffey, Jr., E. H. da Jornada, and D. Winske, Proc. 1984 Sherwood Theory Meeting, Annual Controlled Fusion Theory Conf., Incline Village, NV, USA (Apr., 1984).

11. Instabilities due to transmitted and reflected ions in the quasiperpendicular bow shock, J. D. Gaffey, Jr., E. H. da Jornada, D. Winske, EOS Trans. Am. Geophys. Union 65, 270 (1984).

I. SUMMARY OF RESEARCH ACCOMPLISHMENTS

I. SUMMARY OF RESEARCH ACCOMPLISHMENTS

This report summarizes the research activites carried out at the Institute for Physical Science and Technology, University of Maryland, under the auspices of the Office of Naval Research Grant N00014-82-K-0208 from March 1, 1982 to March 31, 1984. We are pleased to report that significant progress has continued in the study of the acceleration of electrons and ions by wave-particle interactions. Several theoretical and numerical investigations of these acceleration processes with applications to space physics and laboratory plasmas have been conducted. Copies of the six completed papers are attached. The ONR grant was acknowledged appropriately. Several other manuscripts are presently in preparation. Also included for your information are eleven abstracts of talks presented at scientific meetings. Dr. Gaffey chaired two sessions at the Spring 1984 Meeting of the American Geophysical Union.

1. Overview

The research program is devoted to analyzing the processes responsible for the acceleration of ions and electrons in plasmas, to studying instabilities resulting from energetic ion beams streaming across a magnetic field, or other non-equilibrium features, such as temperature anisotropy or a loss-cone distribution function, and to calculating the spontaneous emission of radiation at the fundamental and harmonics of the cyclotron frequency.

The program is divided into six closely related projects. The first and second parts deal with electromagnetic and electrostatic instabilities resulting from an energetic ion beam streaming across the magnetic field and electron temperature anisotropy in the earth's bow shock and in magnetic mirrors. The third part treats the acceleration of electrons by plasma turbulence and an electric field parallel to the magnetic field. The fourth part considers the electron-cyclotron maser instability in a high temperature

plasma with a loss-cone distribution function. In the fifth part, the spectral emissivity of spontaneous synchrotron radiation at the fundamental and harmonics of the cyclotron frequency is calculated using the complete relativistic resonance condition. In the sixth part, the stochastic acceleration of ions by a large amplitude ion cyclotron wave is discussed.

The problems discussed above are all interrelated. For example, the kinetic cross-field streaming instability considered in sections 2 and 3 can generate the plasma turbulence which results in the electron acceleration considered in section 4. Moreover, the acceleration of the electrons along the magnetic field can result in a loss-cone distribution function, which can be unstable to the electron cyclotron maser instability discussed in section 5. The expression for the spontaneous cyclotron emissivity obtained in section 6 has been used to calculate the radiation spectrum from energetic trapped electrons with a loss-cone distribution function. Finally, the electron current along the magnetic field discussed in section 4 can excite the ion cyclotron waves which produce the stochastic ion acceleration considered in section 7.

We now briefly describe the key results and major accomplishments achieved thus far in our research program. A detailed report on each problem is given in Chapter III.

2. Effect of Electron Thermal Anisotropy on the Kinetic Cross-Field Streaming Instability

We have investigated both numerically and analytically the kinetic cross-field streaming instability, which is excited by a relative electron-ion cross-field drift and enhanced by an electron temperature anisotropy $T_{e\perp} > T_{e\parallel}$. This investigation is motivated by the research on collisionless shock waves and applied to the earth's bow shock.[1,2] The unstable waves have been

shown to be obliquely propagating whistlers, and the instability is not suppressed by electromagnetic effects when the drift velocity V_0 exceeds the Alfven velocity v_A and the plasma parameter β is of order unity. The effect of increasing V_0/v_A is to shift the direction of propagation more nearly parallel to the magnetic field. The effect of increasing the electron temperature ratio $T_{e\perp}/T_{e\parallel}$ is to increase the growth rate and to shift the direction of propagation more nearly perpendicular to the magnetic field. The mode has mixed electrostatic and electromagnetic polarization. However, for $\beta \sim 1$ and for nearly perpendicular propagation, the mode is predominantly electrostatic; whereas, for more oblique propagation, the electromagnetic and electrostatic components are nearly equal. Finally, for small β, the mode becomes the well-known modified two-stream instability.[3]

In summary, we have studied the plasma instability resulting from a cross-field drift and an electron temperature anisotropy, $T_{e\perp}/T_{e\parallel} > 1$. We find that both effects significantly affect the instability. In particular, the present study has led to the following major conclusions:

(1) A relative electron-ion cross-field drift can cause instability, even if $V_0/v_A > 1$.

(2) An electron temperature anisotropy $T_{e\perp}/T_{e\parallel} > 1$ significantly enhances the peak growth rate.

(3) The unstable waves have both electrostatic and electromagnetic components in general. For $\beta \sim 1$ and nearly parallel propagation, the electrostatic and electromagnetic components are comparable and the polarization is mixed.

(4) The instability is highly kinetic for high $\beta \sim 1$. From numerical solutions of the dispersion equation, we find that

$$\frac{\omega_r}{k_\parallel v_{e\parallel}} \lesssim 1 \quad \text{and} \quad \frac{|\omega_r - k_\perp v_0|}{k v_i} \gtrsim 1$$

over the entire range of angles of propagation. Moreover, electromagnetic effects, high-order electron cyclotron harmonics, and ion terms all affect the dispersion equation significantly and, therefore, it is difficult to treat the dispersion equation accurately by analytic techniques.

3. Instabilities Excited by an Energetic Ion Beam and Electron Temperature Anisotropy in Tandem Mirrors

Tandem Mirrors are magnetic confinement devices in which the ions in the central (solenoidal) cell are prevented from leaking out the end by means of an electrostatic potential maintained by a denser plasma in mirror-end cells. The basic concept has been successfully verified in the Tandem Mirror Experment (TMX).[4] In order to generate the barrier, the density in this region is reduced by pumping out some of the ions. This is achieved by injecting neutral beams at oblique angles to create "sloshing ion distributions," which have a density minimum at the center of the barrier. Furthermore, a hot electron population is also created in the barrier by means of ECRH to reduce the power transfer between the plug and central-cell electrons. The thermal barrier concept is presently being tested in the upgraded TMX-U experiment.[5]

While the inclusion of such complexity into the end cell of the Tandem Mirror may improve the overall confinement significantly, it is implicitly assumed that such configurations can be stably maintained. However, the introduction of (neutral) ion beams and hot anisotropic electrons in the barrier region suggests a variety of possible microinstabilities. Injection of neutral beams to form the sloshing ion distribution allows the possibility of various streaming instabilities.[6,7] The formation of hot anisotropic electrons may also give rise to unstable modes, such as the whistler[8-11] and the electron cyclotron maser instabilities.[12-21]

In a recent paper, we have investigated such a combination of ions drifting across a magnetic field in which the background electron temperature was anisotropic in the environment of the earth's bow shock.[22] In that situation, the ion streaming results from ion reflection at supercritical shocks and the electron anisotropy arises from adiabatic compression at the shock surface.[2] We have found that the well-known (low-beta) modified two-stream instability[23] is modified by finite-beta effects[1] and further enhanced by the temperature anisotropy.[22]

Using the same basic model (local linear theory, homogeneous plasma, unmagnetized ions, etc.), we extend the theory of cross-field ion streaming instabilities to the parameter regime of the end cells of the upgraded Tandem Mirror Experiment with neutral beam injection. The cross-field ion drift as well as the electron thermal anisotropy $T_{e\perp} > T_{e\parallel}$ provides the free-energy which drives various instabilities. Three instabilities, a nearly perpendicular propagating modified two-stream instability, an obliquely propagating ion-ion streaming instability, and an obliquely propagating electromagnetic lower-hybrid instability, have been identified. The first two waves are electrostatic and have the largest growth rate. For the actual operation conditions of the Tandem Mirror Experiment, it is found that the ion-ion streaming instability has the largest growth rate. When more energetic neutral beams become available, the modified two-stream instability may play the dominant role in the stability of these devices.

4. Acceleration of Electrons by Plasma Turbulence and a Quasistatic Parallel Electric Field

Recently, some laboratory experiments have demonstrated that the combined effect of a parallel electric field and plasma turbulence is effective in producing energetic electrons.[24] This phenomenon has been observed in

a tokamak, and we expect that the physical mechanism should be operative in the auroral region also. It is based on this notion that we were motivated to proceed with the present study.

The acceleration of electrons along the magnetic field by large amplitude plasma turbulence and a quasistatic parallel electric field has been investigated. The plasma amplifies perturbations excited by a cross-field current due to a relative electron-ion drift. The fluctuating electric field is primarily electrostatic and propagates nearly perpendicularly to the magnetic field. The instability is assumed to saturate rapidly. The time evolution of the velocity and energy of an individual test electron is calculated from the moment equations. A Green's function is constructed for the quasi-linear diffusion equation, with a power law spectral energy density.[25] The time evolution of an initial Maxwellian distribution is given; and the average electron velocity, energy, and velocity spread are obtained for various cases by taking moments of the distribution function. We have found that the combined effect of a parallel electric field and electrostatic plasma turbulence is especially effective in producing energetic electrons. In particular, the present study has led to the following major conclusions:

(1) A larger electric field produces greater acceleration; however, acceleration by an electric field alone does not increase the velocity spread of the electron distribution function.

(2) A larger spectral index, i.e., a narrower spectrum of waves, produces greater turbulent acceleration. Turbulent acceleration increases both the velocity spread and the average energy of the electron distribution function.

(3) The turbulent acceleration mechanism is more effective at higher altitudes, whereas the electric field acceleration is independent of altitude.

(4) For some values of the parameters which are typical of the auroral zones the turbulent acceleration and the electric field acceleration are comparable.

(5) When both acceleration mechanisms are operable the acceleration is greater than when only one acceleration mechanism is operable.

Although the results have been applied to the auroral regions, they also have important implications for laboratory experiments as well, for example, radio frequency current drive in tokamaks.[24]

5. Electron-Cyclotron Maser Instability in Hot Electron Mirror Machines

It has now been firmly established that energetic electrons with a loss-cone distribution function are unstable to the electron-cyclotron maser instability. The basic physical mechanism of the instability is a resonant wave-particle interaction via a Doppler-shifted cyclotron resonance process.[12-18] The relativistic resonance condition has been shown to represent an ellipse in velocity-space, which is qualitatively different from the usual nonrelativistic resonance condition, which represents a line in velocity-space. If the portion of the distribution function covered by the resonant ellipse has a positive derivative, then the electron-cyclotron maser instability will develop. This is a sufficient condition for instability. The free-energy which drives the instability is the velocity-space anisotropy of the distribution function. The result of the instability is the transfer of energy from the energetic electrons to the electromagnetic waves via a relativistic Doppler-shifted cyclotron resonance process.

This instability has received considerable attention in the past few years by the space physics community as a possible source mechanism of the auroral kilometric radiation.[12-18] More recently, it has been suggested that

this instability may also occur in some laboratory experiments, such as the Tandem Mirror Machine and the EBT device. In a recent paper by Lau and Chu,[19] a special case of the cyclotron maser instability associated with a loss-cone distribution function is discussed for hot electron mirror experiments. Their analysis is restricted to the case that the radiation propagates parallel to the applied magnetic field $\underset{\sim}{B}_0$ ($k_\perp = 0$) and, moreover, emphasis is placed on the limit $k_\parallel \to 0$. Actually, before Ref. 19 was published, the theory of such an instability had been extensively developed by numerous authors[12-18,20,26] (mostly in the space physics community), although the research has been motivated by the investigation of the auroral kilometric radiation.

In view of the fact that strong bursts of cyclotron radiation have been observed in hot electron mirror machines,[5,27] it is important and interesting to study the cyclotron maser instability for such experiments more fully.

We have generalized the work of Lau and Chu to treat the case of a plasma consisting of a background of low-energy electrons as well as a population of suprathermal electrons, and our analysis is carried out for arbitrary direction of propagation. The major conclusions of our preliminary study are:

(1) The cyclotron maser instability can occur at all angles of propagation over a wide range of parameters.

(2) In general, the instability at large θ (i.e., $\theta \sim 90^\circ$) is more serious than that at $\theta = 0^\circ$.

(3) The peak of the growth rate maximized over k increases with the temperature T and, for large T, occurs at a finite k rather than $k = 0$.

(4) The range of unstable values of ω_e/Ω_e broadens as T increases.

(5) The instability can be supressed by the presence of a sufficiently large population of cold electrons if T is not too high.

In passing, we remark that, besides the maser instability, a whistler instability may also occur in the mirror experiments as pointed out by Gladd.[11] Experimentally, it should not be difficult to distinguish the maser instability from the whistler instability, even if both should be operative, because the extraordinary mode can be unstable at all angles of propagation, whereas the whistler mode is most unstable for parallel or nearly parallel propagation.

Finally, we hope that more observations will be carried out in the near future so that a comparison between experimental results and theoretical predictions may become possible.

6. Calculation of Spontaneous Cyclotron Emissivity Using the Complete Relativistic Resonance Condition

General expression for the emissivity of cyclotron radiation from high-temperature plasmas including collective effects have been derived and discussed in two recent articles by Freund and Wu[28] and by Audenaerde[29] (relevant bibliographies concerning earlier publications are cited in these articles). Although sufficient generality has been retained in these results, practical evaluations of these expresions are, however, difficult. As a result, emissivity has been discussed in two distinct regimes: (1) $N \cos\theta \gg \bar{v}/c$ and (2) $N \cos\theta \ll \bar{v}/c$, where N is the index refraction of the radiation, θ is the angle between the wavevector and the ambient magnetic field, $\bar{v}$ denotes a characteristic velocity of the electrons, and c is the speed of light. In the first regime, the Doppler effect prevails over the relativistic effect in the wave-particle resonance condition and vice versa for the second regime. It is evident that when the refractive index is close to unity the

later regime only occurs in the very small range of θ (i.e., $\theta \simeq 90^{o}$) for weakly relativistic electron energies ($\lesssim$ 10 keV). Obviously the aforementioned approximations become invalid in the intermediate regime where $N \cos\theta \simeq \bar{v}/c$. The range of θ which defines the intermediate regime increases with electron energy, and results in a serious limitation of the previous calculations.[28,29]

Spurred by efforts to explain the auroral kilometric radiation,[30] considerable progress has been made in treating the general resonance condition, and in obtaining general expressions for the growth rates of the escape modes (ordinary and extraordinary) in the presence of a population of suprathermal electrons with a loss-cone distribution function.[12-18,31,32] The success of these efforts provides the motivation for the present work in which we extend the previous[28,29] work on the emissivity to treat arbitrary angles of propagation with no approximation imposed on the resonance condition. In this work we specifically consider the emissions of the escape modes due to energetic electrons with a loss-cone distribution. The applications of the results of our calculation to the study of both the auroral kilometric radiation and to magnetic mirror machine experiments, however, will be presented in separate articles.

In summary, the spontaneous cyclotron emissivity has been calculated using the complete relativistic resonance condition. Unlike prior calculations of synchrotron radiation,[28,29] the result is valid over the entire angular range of propagation without regard to the bulk energy of the electron population. We are specifically interested in the evaluation of the radiation spectrum from an energetic population of trapped electrons having a loss-cone distribution in a low-density plasma. The particular feature of such a plasma (i.e., $\omega_e < \Omega_e$) is that a relatively high radiation intensity is found in the

X-mode at frequencies just above cutoff due to the fundamental gyroresonance which, since this is an escape mode, can readily propagate out of the plasma. While cyclotron damping due to the backgroun plasma can be expected to be negligible for sufficiently low-bulk temperatures of background plasma, amplification of the radiation can occur due to the anisotropic nature of the suprathermal electron distribution. The detailed nature of this instability has been amply discussed in the literature dealing with auroral kilometric ration.[12-18]

Finally, it should be observed that, while the overall level of spontaneous synchrotron radiation is greatest for the X-mode above cutoff, the detailed angular spectrum is more complex. In particular, the X-mode radiation intensity at the higher gyroharmonics actually exceeds that near the fundamental ($\omega \gtrsim \Omega_e$, $\omega \gtrsim \omega_{x0}$) for angles of propagation nearly perpendicular to the ambient magnetic field.

7. Preferential Stochastic Acceleration of Heavy Ions by a Coherent Electrostatic Hydrogen Cyclotron Wave

In a hydrogen dominated multi-ion plasma, the minority ion species with large mass to charge ratios are preferentially accelerated by a coherent electrostatic hydrogen cyclotron wave propagating nearly perpendicularly to the magnetic field. The equations of motion have been studied analytically and numerically using an appropriate Hamiltonian formalism. Surfaces of sections have been plotted numerically to visualize the solutions and to make comparisons between the numerical results and the analytical predictions. Stochasticity has been found to onset rather abruptly when the wave amplitude exceeded a critical threshold. The stochastic region has an upper bound as well as a lower bound on the ion kinetic energy. The maximum ion kinetic energy is proportional to the ion mass to the 5/3 power. The agreement

between the theoretically predicted values and the numerically calculated values is quite good in most cases. In general, the numerical v_{min} is slightly less than the theoretical value, and the numerical v_{max} is slightly larger than the theoretical value. The effect of increasing the wave amplitude is to decrease v_{min} and to increase v_{max}, thus broadening the stochastic region. A diffusion equation which describes the stochastic acceleration of the ions has been derived and the resulting ion distribution function has been determined. The importance of this process to the acceleration of O^+ ions in magnetosphere, as observed by satellites, has been discussed. We expect similar behavior during stochastic acceleration by other types of waves. Hence, these results may have important implications for radio frequency heating experiments in tokamaks and other devices.

In a recent paper, Singh et al.[33] make a comparison between the stochastic acceleration of ionospheric ions by electrostatic hydrogen cyclotron waves observed in their numerical simulations and the predicted acceleration of these ions based on the theory of stochastic acceleration by Papadopoulos et al.[34] The assertion made by Singh et al.[33], that the heating of the helium ions observed in their simulations is appreciably larger than the heating predicted by the theory of stochastic acceleration by Papadopoulos et al.[34], is the result of an algebraic error. In fact, upon correcting the error, we find agreement beween the values of the minimum and maximum velocities of the stochastic region calculated from the theory of Karney[35] and Papadopoulos et al.[34] agree quite well with the numerical simulations of Singh et al.[33] and Gaffey[36] in most cases.

REFERENCES

1. C. S. Wu, Y. M. Zhou, S. T. Tsai, S. C. Guo, D. Winske, and K. Papadopoulos, Phys. Fluids 26, 1259 (1983).

2. C. S. Wu, D. Winske, Y. M. Zhou, S. T. Tsai, P. Rodriguez, M. Tanaka, K. Papadopoulos, K. Akimoto, C. S. Lin, M. M. Leroy, and C. C. Goodrich, Space Sci. Rev. 37, 63 (1984).

3. J. B. McBride and E. Ott, Phys. Lett. A39, 363 (1972).

4. D. L. Correll et al., Nucl. Fusion 22, 223 (1982).

5. T. A. Casper, Y.-J. Chen, R. Ellis, R. James, and C. Lasnier, Lawrence Livermore Lab., Report No. UCID-19783, Apr., unpublished (1983).

6. P. L. Auer, R. W. Kilb, and W. F. Crevier, J. Geophys. Res. 76, 2927 (1971).

7. K. Papadopoulos, R. C. Davidson, J. M. Dawson, I. Haber, D. A. Hammer, N. A. Krall, and R. Shanny, Phys. Fluids 14, 849 (1971).

8. C. F. Kennel and H. E. Petschek, J. Geophys. Res. 71, 1 (1966).

9. J. E. Scherer and A. W. Trivelpiece, Phys. Fluids 10, 591 (1967)

10. A. B. Mihkailovskii, Theory of Plasma Instabilities, Vol. 1 (Consultants Bureau, New York, NY, USA, 1974), p. 235.

11. N. T. Gladd, Phys. Fluids 26, 974 (1983).

12. C. S. Wu and L. C. Lee, Astrophys. J. 230, 621 (1979).

13. L. C. Lee and C. S. Wu, Phys. Fluids 23, 1348 (1980).

14. C. S. Wu, H. K. Wong, D. J. Gorney, and L. C. Lee, J. Geophys. Res. 87, 4476 (1982).

15. N. Omidi and D. Gurnett, J. Geophys. Res. 87, 2377 (1982).

16. P. B. Dusenberry and L. R. Lyons, J. Geophys. Res. 87, 7467 (1982).

17. D. B. Melrose, R. G. Hewitt, and K. G. Rönnmark, J. Geophys. Res. 87, 5140 (1982).

18. R. G. Hewitt, D. B. Melrose, and K. G. Rönnmark, Aust. J. Phys 35, 447 (1982).

19. Y. Y. Lau and K. R. Chu, Phys. Rev. Lett. 50, 243 (1983).

20. H. K. Wong, C. S. Wu, F. J. Ke, R. S. Schneider, and L. F. Ziebell, J. Plasma Phys. 28, 503 (1982).

21. H. K. Wong, C. S. Wu, and J. D. Gaffey, Jr., Phys. Rev. Lett. 52, submitted (1984).

22. S. T. Tsai, M. Tanaka, J. D. Gaffey, Jr., E. H. da Jornada, C. S. Wu, and L. F. Ziebell, J. Plasma Phys. 31, in press (1984).

23. J. B. McBride, E. Ott, J. P. Boris, and J. H. Orens, Phys. Fluids 15, 2367 (1972).

24. Y. Yamamoto, T. Imai, M. Shinada, N. Suzuki, M. Maeno, S. Konoshima, T. Fujii, K. Uehara, T. Nakashima, A. Funahashi, and N. Fujisawa, Phys. Rev. Lett. 45, 716 (1980).

25. C. S. Wu, J. D. Gaffey, Jr., and B. Liberman, J. Plasma Phys. 25, 391 (1981).

26. C. S. Wu, C. S. Lin, H. K. Wong, S. T. Tsai, and R. L. Zhou, Phys. Fluids 24, 2191 (1981).

27. N. T. Gladd, in Proc. Workshop on Hot Electron Ring Physics, N. A. Uckan (ed.), San Diego, CA, USA (Oak Ridge National Lab., Oak Ridge, NT, 1982), CONF-811203, Vol. 1, p. 247.

28. H. P. Freund and C. S. Wu, Phys. Fluids 20, 963 (1977); Phys. Fluids 20, 2157 (1977).

29. K. Audenaerde, Plasma Phys. 19, 299 (1977).

30. D. A. Gurnett, J. Geophys. Res. 79, 4227 (1974).

31. H. P. Freund, H. K. Wong, C. S. Wu, and M. J. Xu, Phys. Fluids 26, 2263 (1983).

32. C. S. Wu and H. P. Freund, Radio Sci., 19, 519 (1984).

33. N. Singh, R. W. Schunk, and J. J. Sojka, Geophys. Res. Lett. 8, 1249 (1981).

34. K. Papadopoulos, J. D. Gaffey, Jr., and P. J. Palmadesso, Geophys. Res. Lett. 7, 1014 (1980).

35. C. F. F. Karney, Phys. Fluids 21, 1584 (1978).

36. J. D. Gaffey, Jr., EOS 62, 1005 (1981).

II. LIST OF PUBLICATIONS

II. LIST OF PUBLICATIONS

A. Papers

1. Comments on "Energization of ionospheric ions by electrostatic hydrogen cyclotron waves," by N. Singh, R. W. Schunk, and J. J. Sojka, Geophys. Res. Lett. 8, 1249 (1981); J. D. Gaffey, Jr., Geophys. Res. Lett., submitted (1983).

2. Acceleration of auroral electrons by lower-hybrid turbulence and a quasistatic parallel electric field, J. D. Gaffey, Jr., Z. X. Liu, and S. C. Guo, J. Plasma Phys., submitted (1983).

3. Effect of electron thermal anisotropy on the kinetic cross-field streaming instability S. T. Tsai, M. Tanaka, J. D. Gaffey, Jr., E. H. da Jornada, C. S. Wu, and L. F. Ziebell, J. Plasma Phys., in press (1984).

4. Calculation of the spontaneous cyclotron emissivity using the complete relativistic resonance condition, H. P. Freund, C. S. Wu, and J. D. Gaffey, Jr., Phys. Fluids, in press (1984).

5. Electron-cyclotron maser instability in hot electron mirror machines, H. K. Wong, C. S. Wu, and J. D. Gaffey, Jr., Phys. Rev. Lett., submitted (1984).

6. Instabilities excited by an energetic ion beam and electron temperature anisotropy in Tandem mirrors, E. H. da Jornada, J. D. Gaffey, Jr., and D. Winske, Phys.Fluids, submitted (1984).

7. Weak magnetic field limit of electromagnetic and electrostatic waves, J. D. Gaffey, Jr. and B. Liberman, J. Plasma Phys., to be submitted (1984).

8. The velocity distribution of alpha particles and collisional transport in a thermonuclear plasma, J. D. Gaffey, Jr. and R. S. Schneider, J. Plasma Phys., to be submitted (1984).

9. Green's functions for a general class of diffusion equations, J. D. Gaffey, Jr., J. Plasma Phys., to be submitted (1984).

10. The influence of quasilinear diffusion of resonant particles on high energy tail formation, J. D. Gaffey, Jr. and M. Zales Caponi, in preparation (1984).

11. An ion cyclotron instability excited by energetic ion beams, J. D. Gaffey, Jr., A. T. Bernardes, and E. H. da Jornada, in preparation (1984).

12. Preferential acceleration of heavy ions by a coherent electrostatic wave, J. D. Gaffey, Jr., in preparation (1984).

13. Instabilities due to transmitted and reflected ions in the quasiperpendicular bow shock, J. D. Gaffey, Jr., E. H. da Jornada, and D. Winske, J. Geophys. Res., in preparation (1984).

B. Talks at Scientific Meetings

1. Statistical acceleration of electrons by lower-hybrid turbulence in the presence of a parallel electric field, EOS Trans. Am. Geophys. Union 63, J. D. Gaffey, Jr., Z. X. Liu, and C. S. Wu, 409 (1982).

2. Acceleration of auroral electrons by lower-hybrid turbulence and a quasistatic parallel electric field, J. D. Gaffey, Jr., Z. X. Liu, and S. C. Guo, Bull. Am. Phys. Soc. 27, 1024 (1982).

3. Instabilities at the bow shock. I. Kinetic cross-field streaming instability, M. Tanaka, J. D. Gaffey, Jr., D. Winske, C. S. Wu, Y. M. Zhou, S. T. Tsai, and K. Papadopoulos, EOS, Trans. Am. Geophys. Union 63, 1070 (1982).

4. Instabilities at the bow shock. III. Cross-field streaming instability with temperature anisotropy, S. T. Tsai, M. Tanaka, C. S. Wu, and J. D. Gaffey, Jr., EOS, Trans. Am. Geophys. Union 63, 1070 (1982).

5. A cross-field streaming instability with electron temperature anisotropy in tandem mirrors, J. D. Gaffey, Jr., M. Tanaka, and S. T. Tsai, Proc. 1983 Sherwood Theory Meeting, Annual Controlled Fusion Theory Conf., Arlington, VA, USA (Mar., 1983).

6. Effect of electron thermal anisotropy on the kinetic cross-field streaming instability in the bow shock, J. D. Gaffey, Jr., Motohika Tanaka, C. S. Wu, and E. H. da Jornada, EOS, Trans. Am. Geophys. Union 64, 228 (1983).

7. Spontaneous emission of radiation at cyclotron harmonics by electrons with a loss-cone or hollow-beam distribution function, C. S. Wu, H. P. Freund, and J. D. Gaffey, Jr., Bull. Am. Phys. Soc. 28, 1068 (1983).

8. Effect of electron temperature anisotropy on the kinetic cross-field streaming instability, J. D. Gaffey, Jr., E. H. da Jornada, M. Tanaka, D. Winske, and C. S. Wu, Bull. Am. Phys. Soc. 28, 1195 (1983).

9. Electron-cyclotron maser instability in magnetic mirror machines, H. K. Wong, J. D. Gaffey, Jr., and C. S. Wu, Proc. 1984 Sherwood Theory Meeting, Annual Controlled Fusion Theory Conf., Incline Village, NV, USA (Apr., 1984).

10. Instabilities excited by an energetic ion beam and electron temperature anisotropy in tandem mirrors, J. D. Gaffey, Jr., E. H. da Jornada, and D. Winske, Proc. 1984 Sherwood Theory Meeting, Annual Controlled Fusion Theory Conf., Incline Village, NV, USA (Apr., 1984).

11. Instabilities due to transmitted and reflected ions in the quasiperpendicular bow shock, J. D. Gaffey, Jr., E. H. da Jornada, D. Winske, EOS Trans. Am. Geophys. Union 65, 270 (1984).

III. REPRINTS AND PREPRINTS

Phyfld840600
005406PHf

Calculation of the spontaneous cyclotron emissivity using the complete relativistic resonance condition

H. P. Freund[a], C. S. Wu, and J. D. Gaffey, Jr.
Institute for Physical Science and Technology, University of Maryland, College Park, Maryland 20742

(Received 5 October 1983; accepted 13 February 1984)

An expression for the spectral emissivity of spontaneous synchrotron radiation for a plasma which consists of both thermal and suprathermal electron components is derived using the complete relativistic cyclotron resonance condition. The expression is valid over all angles of propagation. The result is applied to the study of the emission of radiation from an energetic population of electrons with a loss-cone distribution in a relatively low-density plasma (i.e., the electron plasma frequency is less than the cyclotron frequency).

PACS numbers: 52.25.Ps, 52.60. + h

I. INTRODUCTION

General expressions for the emissivity of cyclotron radiation from high-temperature plasmas including collective effects are derived and discussed in two recent articles by Freund and Wu[1] and Audenaerde[2] (relevant bibliographies concerning earlier publications are cited in these articles). Although sufficient generality has been retained in these results, practical evaluations of these expressions are difficult. As a result, the emissivity has been discussed in two distinct regimes: (1) $N\cos\theta \gg \bar{v}/c$ and (2) $N\cos\theta \ll \bar{v}/c$, where N is the index refraction of the radiation, θ is the angle between the wave vector and the ambient magnetic field, $\bar{v}$ denotes a characteristic velocity of the electrons, and c is the speed of light. In the first regime, the Doppler effect prevails over the relativistic effect in the wave-particle resonance condition and vice versa for the second regime. It is evident that when the refractive index is close to unity the latter regime only occurs in a very small range of θ (i.e., $\theta \simeq 90°$) for weakly relativistic electron energies (< 10 keV). Obviously the aforementioned approximations become invalid in the intermediate region where $N\cos\theta \simeq \bar{v}/c$. The range of θ which defines the intermediate regime increases with electron energy and results in serious drawback of the calculations presented in Refs. 1 and 2.

Spurred by efforts to explain the auroral kilometric radiation,[3] considerable progress has been made in treating the general resonance condition and in obtaining general expressions for the growth rates of the escape modes (ordinary and extraordinary) in the presence of a population of suprathermal electrons with a loss-cone type of distribution function.[4–12] The success of these efforts provides the motivation for the present work in which we extend the previous[1,2] work on the emissivity to treat arbitrary angles of propagation with no approximation imposed on the resonance condition. In this paper we specifically consider the emissions of the escape modes due to energetic electrons with a loss-cone distribution. The applications of the results of our calculation are to the study of both the auroral kilometric radiation and to magnetic mirror machine experiments. In the case of the auroral kilometric radiation (AKR), the most commonly accepted theory involves the induced emission of extraordinary mode radiation due to the presence of a suprathermal electron component with a loss-cone distribution function. Indeed, observations of energetic electron distributions in the auroral regions confirm the existence of such energetic populations.[13] However, while growth rates for such an instability have been calculated, the basic level of spontaneous radiation which determines the initial condition has not been discussed. The present work addresses the issue of the spontaneous emissivity at both the fundamental and higher harmonics. The topic is highly relevant to the question of why the observed second harmonic AKR is often more effective than the theory predicts, since the growth rate is one order of magnitude smaller than that for the fundamental AKR. We will show later that for nearly perpendicular propagation the spontaneous emissions of the X mode at the second harmonic is much stronger than that at the fundamental. This finding may explain the question mentioned earlier.

In addition to the theory of AKR, the discussion of the spontaneous emission presented in this paper is also relevant to the magnetic mirror machine experiments for controlled fusion research. In particular, in the planned MFTF-B experiment at the Lawrence Livermore National Laboratory it is anticipated that the suprathermal electron energies will be of the order of 100 keV. In each of these cases, the relativistic effects on the electron cyclotron resonance condition is important and will be included in the present analysis in a self-consistent manner. Finally, we note that the relativistic effects on the resonance condition have recently been shown to be important to the application of electron cyclotron current drive in tokamaks even for weakly relativistic electron energies.[14]

The organization of the paper is as follows. The general formulation of the emissivity is given in Sec. II, along with a discussion of the complete resonance condition. The emissivity is evaluated numerically in Sec. III for the specific case of a loss-cone distribution using the fully general resonance condition. A summary and discussion are given in Sec. IV.

II. GENERAL CONSIDERATIONS

The physical configuration under consideration is that of a uniformly magnetized plasma ($\mathbf{B}_0 = B_0\hat{\mathbf{e}}_z$) which consists of a thermal background as well as a population of suprathermal electrons. Since the suprathermal electrons are assumed to have a much lower density than the thermal species, the dielectric properties of the plasma are deter-

[a] Permanent address: Science Applications, Inc., McLean, Virginia 22102.

mined primarily by the thermal background, and the suprathermal electrons may be considered to act solely as a source of emission for the normal modes of the plasma. Within the context of this model, the emissivity η (defined as the power radiated per unit volume per unit frequency and per unit solid angle subtended by the wave vector $\mathbf{k}$) can be expressed in the form

$$\eta_{\pm}(\omega,\theta) = \frac{e^2 n_s}{2\pi}\frac{\omega^2}{c} N_{\pm} \frac{\rho \mp \sin^2\theta}{2\rho} \int d^3u F_s(\mathbf{u}) \times \sum_{m=-\infty}^{\infty} [V_{\pm} J_m(b_{\pm}) + \beta_{\perp} J'_m(b_{\pm})]^2 \times \delta(\omega - m\Omega_e/\gamma - k_{\parallel} v_{\parallel}), \quad (1)$$

where $(\omega,\mathbf{k})$ are the frequency and wave vector of the radiation, $k_{\parallel} \equiv \mathbf{k}\cdot\hat{\mathbf{e}}_z$, $\theta \equiv \cos^{-1}(k_{\parallel}/k)$, $\mathbf{k}_{\perp} = \mathbf{k}_{\parallel}$, n_s denotes the suprathermal electron density, $\mathbf{u} \equiv \mathbf{p}/m = \gamma\mathbf{v}$ is the momentum per unit mass, $\gamma \equiv (1 + u^2/c^2)^{1/2} = (1 - v^2/c^2)^{-1/2}$ is the relativistic factor, F_s is the suprathermal electron distribution, $\Omega_e \equiv |eB_0/m_e c|$ is the electron cyclotron frequency, $v_{\perp}$ and $v_{\parallel}$ are the components of the velocity in directions perpendicular and parallel to $\mathbf{B}_0$, $\beta_{\perp,\parallel} \equiv v_{\perp,\parallel}/c$, and J_m and J'_m are the regular Bessel function of the first kind of order m and its derivative, respectively. In addition,

$$V_{\pm} \equiv 2\frac{\omega}{\Omega_e}\frac{[(1-\alpha^2)(1 - N_{\pm}\beta_{\parallel}\cos\theta) - N_{\pm}^2 \sin^2\theta]}{N_{\pm}\sin\theta(\sin^2\theta \mp \rho)}, \quad (2)$$

$$b_{\pm} \equiv \frac{mN_{\pm}\beta_{\perp}\sin\theta}{(1 - N_{\pm}\beta_{\parallel}\cos\theta)}, \quad (3)$$

$$\rho^2 \equiv \sin^4\theta + 4(\omega^2/\Omega_e^2)(1-\alpha^2)^2\cos^2\theta, \quad (4)$$

where $\alpha^2 \equiv \omega_e^2/\omega^2$, ω_e is the background electron plasma frequency, $N = ck/\omega$ is the refractive index, and the subscript $\pm$ refers to the ordinary and extraordinary modes, respectively. The indices of refraction for these wave modes are given by the Appleton–Hartree dispersion relation[15]

$$N_{\pm}^2 = 1 - 2\alpha^2(1-\alpha^2)/[2(1-\alpha^2) - \beta^2(\sin^2\theta \mp \rho)], \quad (5)$$

where $\beta^2 \equiv \Omega_e^2/\omega^2$.

The resonance condition described by the delta function in Eq. (1) may be expressed in the form

$$u_{\perp}^2/a_m^2 + (u_{\parallel} - \bar{u}_m)^2/b_m^2 = 1, \quad (6)$$

where

$$\frac{\bar{u}_m}{c} \equiv \frac{m\Omega_e}{\omega}\frac{N\cos\theta}{1 - N^2\cos^2\theta}, \quad (7)$$

$$\frac{a_m^2}{c^2} \equiv \frac{1}{1 - N^2\cos^2\theta}\left(\frac{m^2\Omega_e^2}{\omega^2} + N^2\cos^2\theta - 1\right), \quad (8)$$

and

$$b_m^2 \equiv a_m^2/(1 - N^2\cos^2\theta). \quad (9)$$

In the regime applicable to the escape modes ($N^2\cos^2\theta < 1$) the reality of the solutions requires that

$$m^2\Omega_e^2/\omega^2 > 1 - N^2\cos^2\theta, \quad (10)$$

and the resonance condition describes an ellipse in $(u_{\perp},u_{\parallel})$ space, centered at $(0,\bar{u}_m)$, with extrema at $(a_m,\bar{u}_m)$ and $(0,\bar{u}_m \mp b_m)$. This is illustrated schematically in Fig. 1(a). Observe that in this case a_m^2 and b_m^2 are both positive. We restrict our consideration to that section of the ellipse for which $u_{\perp} > 0$. From the resonance condition we find that resonance occurs for $u_{\perp} = u_m$, where

$$\frac{u_m^2}{c^2} = (N^2\cos^2\theta - 1)\frac{u_{\parallel}^2}{c^2} + 2\frac{m\Omega_e}{\omega}N\cos\theta\frac{u_{\parallel}}{c} + \frac{m^2\Omega_e^2}{\omega^2} - 1. \quad (11)$$

However, the range of $u_{\parallel}$ over which this is valid is not infinite and must be restricted to within the $u_{\parallel}$ extrema of the ellipse. The resulting integral over $u_{\parallel}$, therefore, is defined by the range $u_m^{(-)} \leqslant u_{\parallel} \leqslant u_m^{(+)}$, where

$$u_m^{(\pm)} \equiv \bar{u}_m \pm b_m. \quad (12)$$

In the opposite regime, in which $N^2\cos^2\theta > 1$, Eq. (6) may be rewritten in the form

$$(u_{\parallel} - \bar{u}_m)^2/b_m^2 - u_{\perp}^2/|a_m^2| = 1, \quad (13)$$

where we observe that $a_m^2 < 0$ and $b_m^2 > 0$. This case is schematically illustrated in Fig. 1(b) in which it is evident that the resonance curve is a hyperbola with $u_{\parallel}$ intercepts at $\bar{u}_m \pm b_m$. Hence, resonance is possible only for $u_{\parallel} \leqslant \bar{u}_m - b_m$ and $u_{\parallel} \geqslant \bar{u}_m + b_m$.

The normal modes described by the Appleton–Hartree dispersion equation are shown schematically in Fig. 2 for $0 < \theta \leqslant \pi/2$. The ordinary mode (i.e., $N^2 = N_+^2$) exhibits a cutoff at $\omega = \omega_e$ and a resonance at $\omega = \omega_{\text{lh}}(\theta)$, where

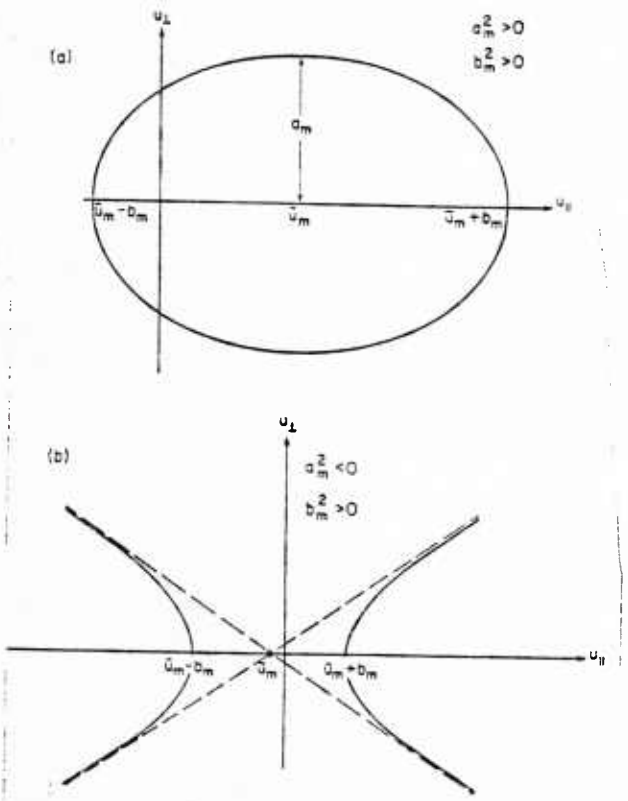

FIG. 1. Schematic representations of (a) elliptical and (b) hyperbolic resonance curves.

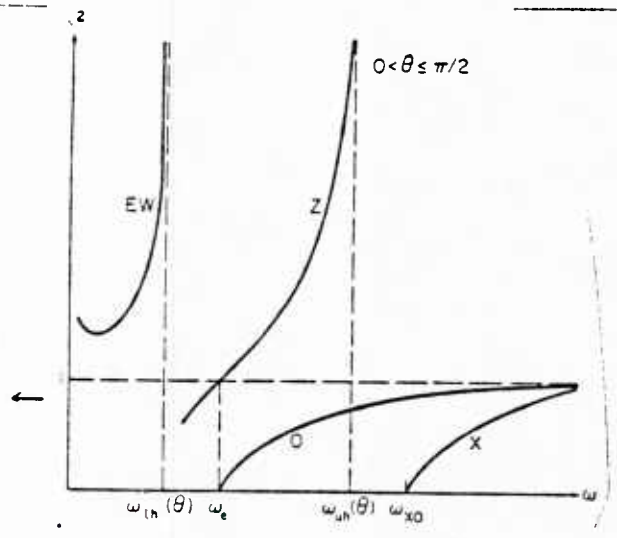

FIG. 2. Schematic illustration of the magneto-ionic wave modes.

$$\omega_{lh}^2(\theta)\equiv\tfrac{1}{2}(\omega_e^2+\Omega_e^2)\times\left[1-\left(1-4\frac{\omega_e^2\Omega_e^2}{(\omega_e^2+\Omega_e^2)^2}\cos^2\theta\right)^{1/2}\right] \quad (14)$$

is a resonance frequency for which $\omega_{lh}(\theta)\simeq\omega_e\cos\theta$ when $\omega_e\ll\Omega_e$, and $\omega_{lh}(\theta)\simeq\Omega_e\cos\theta$ when $\omega_e\gg\Omega_e$. It should be remarked that this expression becomes invalid in the limit as $\theta\to\pi/2$ since $\omega_{lh}(\theta)\to 0$ and ion contributions become important. The branch above the cutoff frequency is the escape mode ($N^2<1$) and is usually referred to as the O mode, which below the resonance the mode is called the electron whistler (EW) branch. Similar results apply to the extraordinary mode (i.e., $N^2=N_-^2$) which displays a resonance at

$$\omega_{uh}^2(\theta)\equiv\tfrac{1}{2}(\omega_e^2+\Omega_e^2)\times\left[1+\left(1-4\frac{\omega_e^2\Omega_e^2}{(\omega_e^2+\Omega_e^2)^2}\cos^2\theta\right)^{1/2}\right], \quad (15)$$

and a cutoff at

$$\omega_{xo}=\tfrac{1}{2}\Omega_e\{1+[1+4(\omega_e^2/\Omega_e^2)]^{1/2}\}. \quad (16)$$

The branch below the resonance is called either the Z mode or the slow extraordinary mode. The escape mode is above the cutoff and is termed either the fast extraordinary mode or simply the X mode. We shall confine our attention in this work to the escape modes for which $N^2\cos^2\theta<1$ and the resonance curve is an ellipse. However, it should be noted that while $N^2>1$ over much of the Z and EW modes, it is still possible to describe the resonance curve as an ellipse at sufficiently large angles of propagation.

The conditions under which the complete relativistic form of the resonance condition must be employed involve a complex relationship between the wave frequency and angle of propagation and the bulk energy of the electrons. In general, the relativistic corrections become important whenever either

$$N\cos\theta\lesssim\langle v\rangle/2c, \quad (17)$$

or

$$\langle v^2\rangle/2c^2\gtrsim|1-m\Omega_e/\omega|. \quad (18)$$

From these inequalities [(17) and (18)] it is evident that relativistic corrections to the resonance condition become important whenever (1) the wave propagation direction is nearly normal to the ambient magnetic field, (2) the index of refraction of the wave is much less than unity (i.e., near cutoff), or (3) the wave frequency is near the cyclotron harmonic.

Finally, it should be remarked that, while we are primarily concerned with the spontaneous radiation in this paper, the relativistic effects on the resonance condition also apply to the study of the growth or damping of the coherent emissions.

Utilizing the resonance condition (11), we obtain the following expression for the emissivity of a gyrotropic distribution $F_s(u_\parallel,u_\perp)$,

$$\eta_\pm(\omega,\theta)=e^2n_s\omega cN_\pm\frac{\rho\mp\sin^2\theta}{2\rho}\sum_{m=-\infty}^{\infty}\int_{u_m^{(-)}}^{u_m^{(+)}}du_\parallel F_s\times(u_\parallel,u_m)\left[\gamma_mV_\pm J_m(b_\pm)+(u_m/c)J_m'(b_\pm)\right]^2\times H(m^2\Omega_e^2/\omega^2+N_\pm^2\cos^2\theta-1), \quad (19)$$

where the relativistic factor $\gamma_m=(m\Omega_e/\omega)+(u_\parallel/c)N_\pm\cos\theta$, H is the Heaviside function, and $b_\pm=mN_\pm\sin\theta(u_m/\gamma_mc)(1-N_\pm\beta\cos\theta)^{-1}$.

III. NUMERICAL ANALYSIS

Because of the complexity of this expression for the emissivity, there is no recourse at this stage but to turn to numerical integration for specific choices of the suprathermal electron distribution function. We choose a loss-cone type of distribution,

$$F_s(u_\parallel,u_\perp)=(\pi\alpha_\perp^2)^{-1}(\pi\alpha_\parallel^2)^{-1/2}(u_\perp/\alpha_\perp)^2\times\exp(-u_\parallel^2/\alpha_\parallel^2)\exp(-u_\perp^2/\alpha_\perp^2), \quad (20)$$

where $\alpha_{\parallel,\perp}$ describes the parallel and perpendicular momentum spreads, respectively. Such a distribution function might be used to model the hot electrons in the end cells of a tandem mirror machine or a population of energetic electrons trapped in a dipole-like magnetic field, such as might be found at relatively low amplitudes in planetary magnetic fields or the solar corona.

Equations (19) and (20) have been evaluated numerically for the escape modes in a low-density plasma ($\omega_e<\Omega_e$), and the results are shown in Figs. 3–5 for the choice of parameters such that $\omega_e=0.1\,\Omega_e$, and $\alpha_\perp/c=\alpha_\parallel/c=0.14$ (corresponding to thermal energies of 5 keV). Note that for this choice of parameters the X-mode cutoff frequency occurs at $\omega_{xo}\simeq 1.01\,\Omega_e$, and the stop band between $\omega_{uh}(\theta)$ and the cutoff frequency is narrow. Significant levels of spontaneous emission are possible, therefore, because of the fundamental X-mode gyroresonance (i.e., $m=1$) at frequencies $\omega>\omega_{xo}$. Such an interaction (at frequencies $\omega>\Omega_e$), however, occurs by means of the contribution of Doppler shift to the gyroresonance and consequently vanishes when $\mathbf{k}\cdot\mathbf{B}_0=0$ (i.e., $\theta=90°$). A spectrum is shown in Fig. 3 in which we plot $\eta/(n_s\Omega_e)$ vs ω/Ω_e at $\theta=60°$ (where η is in units of erg-sr^{-1}-cm^{-3}), and the solid (dashed) line represents the X(O) mode. Evidently the X-mode emission near

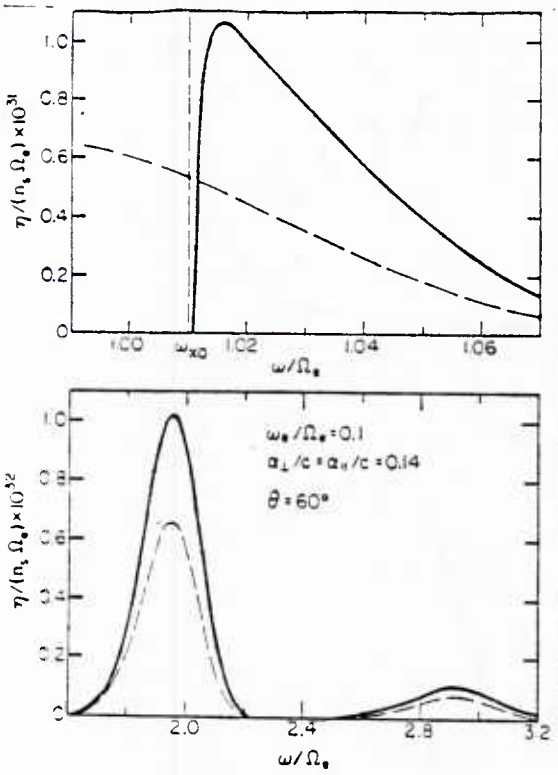

FIG. 3. Spontaneous synchrotron spectra for the O and X modes at $\theta = 60°$, $\omega_e/\Omega_e = 0.1$, and $\alpha_\perp/c = \alpha_\parallel/c = 0.14$. The solid (dashed) line represents the X(O) mode.

the fundamental gyroharmonic is peaked at $\omega \sim 1.016\,\Omega_e$. In addition, the peak decreases in intensity by about an order of magnitude and broadens in width (as measured by the full-width-half-maximum) at successively higher harmonics.

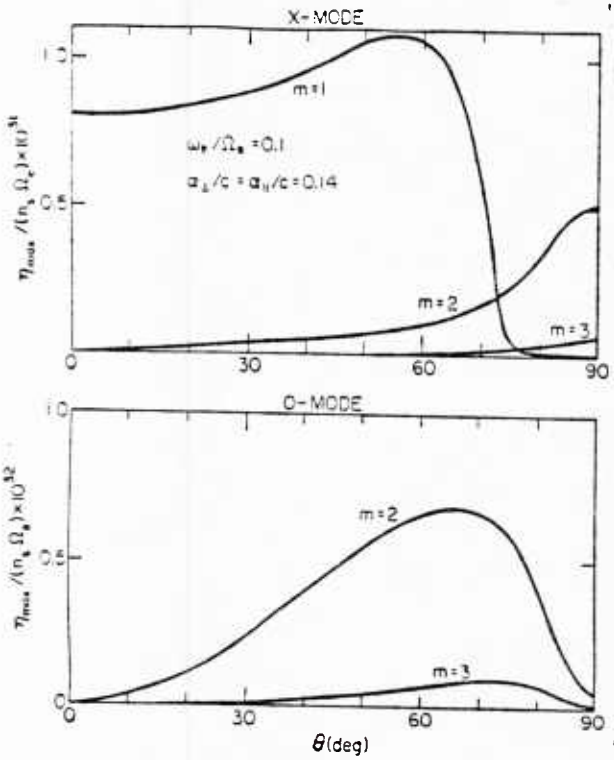

FIG. 4. Angular variations in peak radiation intensity of the O and X modes for $\omega_e/\Omega_e = 0.1$, and $\alpha_\perp/c = \alpha_\parallel/c = 0.14$.

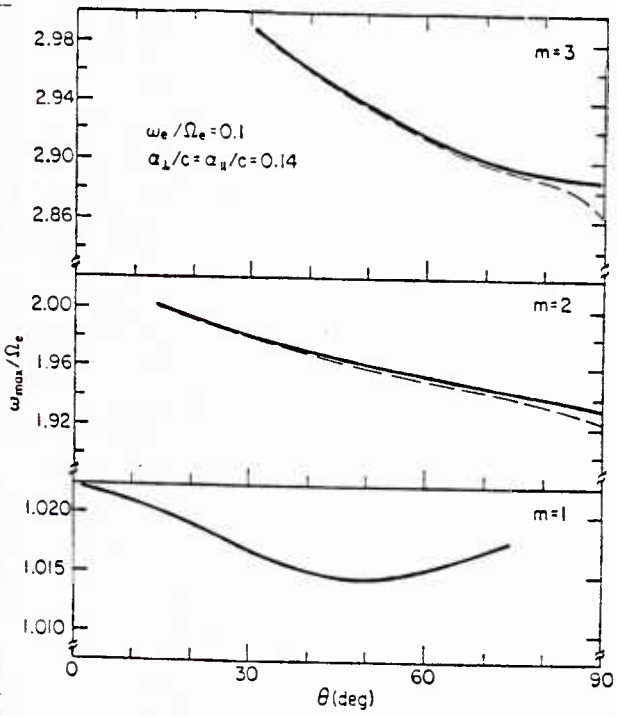

FIG. 5. Angular variations in the frequency corresponding to the peak emissivity of the O and X modes. The solid (dashed) line corresponds to the X(O) mode.

Similar results are found for the O mode which, at each harmonic, is found to peak at approximately 65% of the X-mode maximum at this angle. It should also be observed that we have not shown the entire O-mode peak near the fundamental gyroresonance. The reason for this is that as waves with frequencies below the local cyclotron frequency propagate out of the plasma (i.e., through regions of decreasing magnetic field), they will encounter a layer in which the wave frequency is sufficiently close to the local gyrofrequency that strong cyclotron damping due to the thermal electrons will occur. As a consequence, the observed radiation spectrum at these frequencies will bear little resemblance to the spontaneous emissivity. The X-mode radiation near the fundamental ($\omega \gtrsim \omega_{xo}$), as well as both X-mode and O-mode radiation, will in the course of propagation out of the plasma encounter only higher harmonic cyclotron resonance layers for which the cyclotron resonant damping is relatively weak. Finally, it is implicitly assumed that the temperature of the background electrons is sufficiently low that they do not participate in the X-mode resonance above the cutoff, and cylotron damping of these waves is negligible. This is true, for example, for thermal energies less than about 100 eV.

The variation in the peak of the emissivity versus angle of propagation is shown in Fig. 4 for the X mode at the first three harmonics and for the O mode at the second and third harmonics. The frequency at which the peak occurs is shown in Fig. 5 where the solid (dashed) line refers to the X(O) mode. It is evident from the figures that the fundamental X mode emission occurs over an extremely broad angular range ($\theta \lesssim 70°$) with a small peak at $\theta \simeq 57°$, and that the emission frequency varies little with angle. In contrast, there is a very strong angular dependence in the emission of both the X and O modes at the higher harmonics. In particular, the

X-mode emissivity is maximum for perpendicular propagation while the O mode peaks for propagation at oblique angles ($\theta \simeq 68°$ for the parameters considered).

IV. CONCLUSIONS

In this work the spontaneous cyclotron emissivity has been calculated using the complete relativistic resonance condition. Unlike prior calculations of synchrotron radiation,[1,2] the result is valid over the entire angular range of propagation without regard to the bulk energy of the electron population. We are specifically interested in the evaluation of the radiation spectrum from an energetic population of trapped electrons (i.e., having a loss-cone distribution) in a low-density plasma, because the study is motivated by the research of the auroral kilometric radiation and possible applications to the mirror machine experiments. The particular feature of such a plasma (i.e., $\omega_e < \Omega_e$) is that a relatively high radiation intensity is found in the X mode at frequencies just above cutoff due to the fundamental gyroresonance which, since this is an escape mode, can readily propagate out of the plasma. While cyclotron damping due to the background plasma can be expected to be negligible for sufficiently low bulk temperatures of the background plasma, amplification of the radiation can occur due to the anisotropic nature of the suprathermal electron distribution. The detailed nature of this instability has been amply discussed in the literature dealing with the auroral kilometric radiation.[4–10] Detailed discussion of the present results and their application to AKR will be elaborated in a forthcoming article.

Finally, it should be observed that while the overall level of spontaneous synchrotron radiation is greatest for the X mode above cutoff the detailed angular spectrum is more complex. In particular, the X-mode radiation intensity at the higher gyroharmonics actually exceeds that near the fundamental ($\omega \gtrsim \Omega_e$, $\omega \lesssim \omega_{xo}$) for angles of propagation near the perpendicular to the ambient magnetic field.

ACKNOWLEDGMENTS

The present research was supported in part by the National Aeronautics of Spain Administration Grant No. NGL 21-002-005 and in part by the Office of Naval Research No. N00014-82-K-0208.

MARGIN

[1] H. P. Freund and C. S. Wu, Phys. Fluids **20**, 963 (1977); Phys. Fluids **20**, 2157 (1977).
[2] K. Audenaerde, Plasma Phys. **19**, 299 (1977).
[3] D. A. Gurnett, J. Geophys. Res. **79**, 4227 (1979).
[4] C. S. Wu and L. C. Lee, Astrophys. J. **230**, 621 (1979).
[5] L. C. Lee and C. S. Wu, Phys. Fluids **23**, 1348 (1980).
[6] C. S. Wu, H. K. Wong, D. J. Gorney, and L. C. Lee, J. Geophys. Res. **87**, 4476 (1982).
[7] M. Omidi and D. A. Gurnett, J. Geophys. Res. **87**, 2377 (1982).
[8] D. B. Melrose, R. G. Hewitt, and K. G. Rönmark, J. Geophys. Res. **87**, 5140 (1982).
[9] P. B. Dusenberry and J. R. Lyons, J. Geophys. Res. **87**, 7467 (1982).
[10] R. G. Hewitt, D. B. Melrose, and K. G. Rönmark, Aust. J. Phys. **35**, 447 (1982).
[11] H. P. Freund, H. K. Wong, C. S. Wu, and M. J. Xu, Phys. Fluids **26**, 2263 (1983).
[12] C. S. Wu and H. P. Freund, Radio Sci. (in press).
[13] J. F. Fennell, D. J. Gorney, and P. F. Mizera, in *Physics of Auroral Arc Formation*, edited by S.-I. Akasofu and J. R. Kan (American Geophysical Union, Washington, D. C., 1981), p. 91.
[14] R. A. Cairns, J. Owen, and C. N. Lashmore-Davies, Phys. Fluids **26**, 3475 (1983).
[15] T. Stix, *The Theory of Plasma Waves* (McGraw-Hill, New York, 1962), Chap. 2.

FOOTNOTE LINE LIMIT

LIMIT OF TEXT

ELECTRON-CYCLOTRON MASER INSTABILITY IN HOT ELECTRON MIRROR MACHINES

H. K. Wong

Laboratory for Extraterrestrial Physics
NASA-Goddard Space Flight Center
Greenbelt, Maryland 20771

C. S. Wu and J. D. Gaffey, Jr.

Institute for Physical Science and Technology
University of Maryland
College Park, Maryland 20742

ABSTRACT

The electron-cyclotron maser instability for energetic electrons with a loss-cone distribution function is studied for hot electron mirror experiments. The instability can occur at all angles of propagation for a wide range of parameters. The growth rate is significantly reduced by the presence of a population of cold electrons, and the instability can be suppressed if the density of the cold electrons is sufficiently large and the temperature of the energetic electrons is not too high.

In a recent paper by Lau and Chu,[1] a special case of the cyclotron maser instability associated with a loss-cone distribution function is discussed for hot electron mirror experiments. Their analysis is restricted to the case that the radiation propagates parallel to the applied magnetic field $\underset{\sim}{B}_0$ ($k_\perp = 0$) and moreover emphasis is placed on the limit $k_\parallel \to 0$. Actually, before Ref. 1 was published, the theory of such an instability had been extensively developed by numerous authors[2-9] (mostly in the space physics community), although the research has been motivated by the investigation of the auroral kilometric radiation. (Early publications which discussed the physics of the maser instability have been cited in Ref. 1 and are not repeated here.)

In view of the fact that strong bursts of cyclotron radiation have been observed in hot electron mirror machines,[10,11] it is pertinent and interesting to study the cyclotron maser instability for such experiments more fully than was done in Ref. 1.

In the following, we report the results of our investigation. We have carried out a fairly general analysis in which not only radiation with $k_\perp \neq 0$ and $k_\parallel \neq 0$ is considered, but also a population of cold electrons is included. The purpose of including the latter effect is to examine the possibility of whether the instability can be stabilized by these electrons.

To proceed with the discussion, we consider an unperturbed distribution of the form[12]

$$F_e\,(u_\perp, u_\parallel) = \frac{n_e}{\pi^{3/2}\alpha^3(\ell!)}\left(\frac{u_\perp^2}{\alpha^2}\right)^\ell \exp\left(-\frac{u^2}{\alpha^2}\right), \qquad (1)$$

where $\underset{\sim}{u}$ is the electron momentum per unit mass; α denotes the thermal spread;

$u_\perp$ is the component of $\underset{\sim}{u}$ perpendicular to the applied magnetic field $\underset{\sim}{B}_0$; ℓ is an index which measures the steepness of the loss-cone feature; and n_e is the density of the energetic electrons. The dispersion equation may be written as

$$\det \mid D_{ij} (\underset{\sim}{k},\omega) \mid = 0, \tag{2}$$

where

$$D_{ij} (\underset{\sim}{k},\omega) = \left(1 - \frac{c^2 k^2}{\omega^2} \right) \delta_{ij} + \frac{c^2 k_i k_j}{\omega^2} + \sum_s Q^s_{ij} (\underset{\sim}{k},\omega)$$

and the superscript s on Q_{ij} denotes the particle species. In the present discussion, ions are ignored. We shall consider that, in general, there exists a population of cold electrons in addition to the main component which has a thermal energy of several tens of keV. Since we are interested in waves with refractive indices $N \lesssim 1$ and frequency ω close to the electron cyclotron frequency Ω_e, in calculating Q^e_{ij} (for the energetic electrons) we may ignore terms associated with high harmonic numbers (i.e., $|n| > 1$),[5] and thus obtain

$$Q^e_{ij} = Q^e_{ij} (n = 1) + \eta^e_{ij}$$

where

$$Q^e_{ij} (n=1) = - i \frac{n_e}{n_t} \frac{\omega_e^2}{\omega^2} \frac{c^2}{\alpha^2} \exp (- h^2) \int_0^\infty d\tau \frac{M_{ij}}{(1-i\tau)^{\ell+3/2}} \exp \left[iz\tau + \frac{h^2}{1-i\tau} \right] \tag{3}$$

with

$$M_{xx} = \ell \left(1 - \frac{h^2\alpha^2}{c^2} \right) + \frac{1}{1-i\tau} \left[\ell \frac{h^2\alpha^2}{c^2} - (\ell + 1) \right] = M_{yy} ,$$

$$M_{xy} = - iM_{xx} = - M_{yx} ,$$

$$M_{xz} = \frac{k_\perp \alpha}{\Omega_e} h \left\{ \ell \left(1 - \frac{h^2\alpha^2}{c^2} \right) - \frac{1}{1-i\tau} \left[2\ell + 1 + \frac{\ell}{2} \frac{\alpha^2}{c^2} (1 - 4h^2) \right] \right.$$

$$\left. + \frac{1}{(1-i\tau)^2} \left[\ell + 1 - \ell \frac{h^2\alpha^2}{c^2} \right] \right\}$$

$$= M_{zx} = iM_{zy} = - iM_{yz} ,$$

(4)

$$M_{zz} = \frac{k_\perp^2\alpha^2}{\Omega_e^2} \left\{ \ell h^2 \left(1 - \frac{h^2\alpha^2}{c^2} \right) \right.$$

$$+ \frac{1}{(1-i\tau)} \left[\frac{\ell}{2} (1 - 4h^2) - (\ell + 1) h^2 - \frac{3\ell}{2} \frac{h^2\alpha^2}{c^2} + 3\ell \frac{h^4\alpha^2}{c^2} \right]$$

$$+ \frac{1}{(1-i\tau)^2} \left[\ell h^2 - \frac{\ell+1}{2} (1 - 4h^2) + \frac{3\ell}{2} \frac{h^2\alpha^2}{c^2} - 3\ell \frac{h^4\alpha^2}{c^2} \right]$$

$$\left. + \frac{1}{(1-i\tau)^3} \left[- (\ell + 1) h^2 + \ell \frac{h^4\alpha^2}{c^2} \right] \right\} ,$$

$$h \equiv \frac{k_\parallel c^2}{\omega\alpha} \quad \text{and} \quad z \equiv \frac{2c^2}{\alpha^2} \left(1 - \frac{\Omega_e}{\omega} \right) - h^2 ;$$

and

$$\eta^e_{xx} = \eta^e_{yy} = -\frac{n_e}{2n_t}\frac{\omega_e^2}{\omega(\omega+\Omega_e)}$$

$$\eta^e_{xy} = -\eta^e_{yx} = \frac{in_e}{2n_t}\frac{\omega_e^2}{\omega(\omega+\Omega_e)} \qquad (5)$$

$$\eta^e_{zz} = -\frac{n_e}{n_t}\frac{\omega_e^2}{\omega^2}$$

$$\eta^e_{xz} = \eta^e_{zx} = \eta^e_{yz} = \eta^e_{zy} = 0 \ .$$

For the cold electrons, Q^c_{ij} may simply be written as

$$Q^c_{xx} = Q^c_{yy} = -\frac{n_c}{n_t}\frac{\omega_e^2}{(\omega^2-\Omega_e^2)} \ ,$$

$$Q^c_{xy} = -Q^c_{yx} = i\frac{n_c}{n_t}\frac{\omega_e^2\Omega_e}{\omega(\omega^2-\Omega_e^2)} \ , \qquad (6)$$

$$Q^c_{zz} = -\frac{n_c}{n_t}\frac{\omega_e^2}{\omega^2} \ ,$$

$$Q^c_{xz} = Q^c_{zx} = Q^c_{yz} = Q^c_{zy} = 0 \ .$$

In Eqs. (3), (5), and (6), $\omega_e^2 = 4\pi n_t e^2/m$; n_t is the total electron density; and n_c is the density of the cold electrons. Eq. (2) has been solved numerically and the results are presented in Figs. 1-5. The real part of the frequency is close to the electron cyclotron frequency in most cases and the graphs of the real frequency are very similar to those in Ref. 1. Henceforth, we discuss only the imaginary part of the frequency. The growth rate

normalized by the cyclotron frequency is plotted in Fig. 1 as a function of the normalized wavenumber kc/Ω_e for T ($\equiv m\alpha^2/2$) = 50 keV, $\omega_e/\Omega_e = 0.5$, $n_c = 0$, and $\ell = 1$. Four values of θ, 0°, 30°, 60°, and 90°, have been considered. We note that, although the maximum growth rate occurs at the cutoff, k = 0, in this case, the range of wavenumbers over which the growth rate is large increases as the angle of propagation θ increases and for perpendicular propagation the growth rate is nearly constant for $0 < k \lesssim 0.6\ \Omega_e/c$.

In Fig. 2, the normalized growth rate is again plotted as a function of the wavenumber for $\omega_e/\Omega_e = 0.5$; $n_c = 0$; $\ell = 1$; T = 30, 50, 100 keV; and, for perpendicular propagation, $\theta = 90°$. It is seen that the growth rate and the range of unstable wavenumbers increase as the temperature increases. Moreover, for T = 100 keV, the growth rate peaks at $k = 0.63\ \Omega_e/c$, which is a significant fraction of the free-space wavenumber.

In Fig. 3, the growth rate $\omega_{i,max}$ maximized over the wavenumber is plotted versus θ for four values of ω_e/Ω_e, 0.1, 0.3, 0.5, and 0.7. It is seen that as ω_e/Ω_e increases, $\omega_{i,max}$ becomes progressively more independent of θ. The maximized growth rate $\omega_{i,max}$ is also plotted versus ω_e/Ω_e in Fig. 4 for three different energies, T = 30 keV, 50 keV, and 100 keV. For each energy, two indices, $\ell = 1$ and $\ell = 2$, are studied for the case $\theta = 90°$. We see that the peak of $\omega_{i,max}$ increases with increasing energy and with increasing loss-cone index and, furthermore, it shifts to a higher value of ω_e/Ω_e.

In Fig. 5 we plot the growth rate ω_i as a function of k for three values of n_c/n_t, 0, 0.1, and 0.3. In this case we take T = 50 keV, $\omega_e/\Omega_e = 0.5$, $\ell = 1$, and $\theta = 0°$. The case $n_c = 0$ was studied by Lau and Chu.[1] We notice that as n_c/n_t increases the instability diminishes gradually. For $n_c/n_t > 0.3$ the unstable waves are practically suppressed. However, this conclusion is

only valid for the case $\theta = 0^{o}$. Unstable waves can still occur at other angles as shown in Fig. 6, in which the case $\theta = 90^{o}$ is investigated.

In Fig. 6(a) we consider T = 50 keV, $\omega_e/\Omega_e = 0.5$, and $\ell = 1$. It is seen that the maximum growth rate occurs at a certain finite wavenumber k rather than at k = 0. Even when $n_c/n_t = 0.5$, the instability is not completely suppressed. The importance of finite wavenumber k is enhanced when the electron energy T is increased. This fact can be seen in Fig. 6(b) in which T = 100 keV is considered. In this case, even for $n_c = 0$, the maximum growth rate $\omega_{i,max}$ does not occur at k = 0. Moreover, for each value of n_c/n_t, the maximum growth rate is higher than that for the case T = 50 keV.

In summary, the major conclusions of our preliminary study are: (1) the cyclotron maser instability can occur at all angles of propagation over a wide range of parameters; (2) in general, the instability at large θ (i.e., $\theta \sim 90^{o}$) is more serious than that at $\theta = 0^{o}$; (3) the peak of the growth rate maximized over k increases with the temperature T and, for large T, occurs at a finite k rather than k = 0; (4) the range of unstable values of ω_e/Ω_e broadens as T increases; and (5) the instability can be suppressed by the presence of a sufficiently large population of cold electrons if T is not too high.

Readers should be cautioned that the above conclusions are for the extraordinary mode only. Generally, the growth rate for the ordinary mode radiation is much smaller. Nevertheless, the ordinary mode cannot be stabilized easily by the presence of a small population of cold electrons. This and some other relevant results will be discussed more fully in a subsequent article.

In passing, we remark that, besides the maser instability, a whistler instability may also occur in the mirror experiments as pointed out by

Gladd.[13] Experimentally, it should not be difficult to distinguish the maser instability from the whistler instability, even if both should be operative, because the extraordinary mode can be unstable at all angles of propagation, whereas the whistler mode is most unstable for parallel or nearly parallel propagation.

Finally, we hope that more observations will be carried out in the near future so that comparison between experimental results and theoretical predictions may become possible.

ACKNOWLEDGMENTS

The authors thank R. Ellis for informative discussions. The present research was supported in part by the Office of Naval Research under grants N00014-82-K-0208 and N00014-84-C-0255 and in part by the National Aeronautics and Space Administration under grant NGL21-002-005. One of the authors (H.K.W.) is a NAS/NRC Research Associate.

REFERENCES

1. Y. Y. Lau and K. R. Chu, Phys. Rev. Lett. 50, 243 (1983).
2. C. S. Wu and L. C. Lee, Astrophys. J. 230, 621 (1979).
3. L. C. Lee and C. S. Wu, Phys. Fluids 23, 1348 (1980).
4. C. S. Wu, C. S. Lin, H. K. Wong, S. T. Tsai, and R. L. Zhou, Phys. Fluids 24, 2191 (1981).
5. H. K. Wong, C. S. Wu, F. J. Ke, R. S. Schneider, and L. F. Ziebell, J. Plasma Phys. 28, 503 (1982).
6. D. B. Melrose, R. G. Hewitt, and K. G. Rönnmark, J. Geophys. Res. 87, 5140 (1982).
7. R. G. Hewitt, D. B. Melrose, and K. G. Rönnmark, Aust. J. Phys. 35, 447 (1982).
8. C. S. Wu, H. K. Wong, D. J. Gorney, and L. C. Lee, J. Geophys. Res. 87, 4476 (1982).
9. P. B. Dusenberry and L. R. Lyons, J. Geophys. Res. 87, 7467 (1982).
10. T. A. Casper, Y. J. Chen, R. Ellis, R. James, and C. Lasnier, LLNL Report UCID 19783 (unpublished, April 1983).
11. N. T. Glass, in Proc. Workshop on Hot Electron Ring Physics, San Diego, CA, 1981, edited by N. A. Uckan (Oak Ridge National Laboratory, Oak Ridge, TN, 1982), CONF-811203, Vol. 1, p. 247.
12. R. A. Dory, G. E. Guest, and E. G. Harris, Phys. Rev. Lett. 14, 131 (1965).
13. N. T. Gladd, Phys. Fluids 26, 974 (1983).

FIGURE CAPTIONS

Figure 1. Normalized growth rate ω_i/Ω_e as a function of the normalized wavenumber kc/Ω_e for T = 50 keV, $\omega_e/\Omega_e = 0.5$, $\ell = 1$, $n_c = 0$, and $\theta = 0^o, 30^o, 60^o, 90^o$.

Figure 2. Normalized growth rate ω_i/Ω_e as a function of the normalized wavenumber kc/Ω_e for $\omega_e/\Omega_e = 0.5$, $\ell = 1$, $\theta = 90^o$, $n_c = 0$, and T = 30, 50, 100 keV.

Figure 3. Normalized growth rate $\omega_{i,max}/\Omega_e$ maximized over wavenumber as a function of the propagation angle θ for T = 50 keV, $\ell = 2$, $n_c = 0$, and $\omega_e/\Omega_e = 0.1, 0.3, 0.5, 0.7$.

Figure 4. Maximum growth rate $\omega_{i,max}/\Omega_e$ as a function of the plasma density parameter ω_e/Ω_e for $\theta = 90^o$; $\ell = 1, 2$; and three values of the energetic electron temperature: (a) T = 30 keV, (b) T = 50 keV, and (c) T = 100 keV.

Figure 5. Growth rate ω_i/Ω_e as a function of the wavenumber kc/Ω_e for T = 50 keV, $\omega_e/\Omega_e = 0.5$, $\ell = 1$, $\theta = 0^o$, and three values of the cold to total electron density ratio $n_c/n_t = 0, 0.1, 0.3$.

Figure 6. Growth rate ω_i/Ω_e as a function of the wavenumber kc/Ω_e for $\omega_e/\Omega_e = 0.5$; $\ell = 1$; $\theta = 90^o$; $n_c/n_t = 0, 0.1, 0.3, 0.5$; and two values of the termperature: (a) T = 50 keV and (b) T = 100 keV.

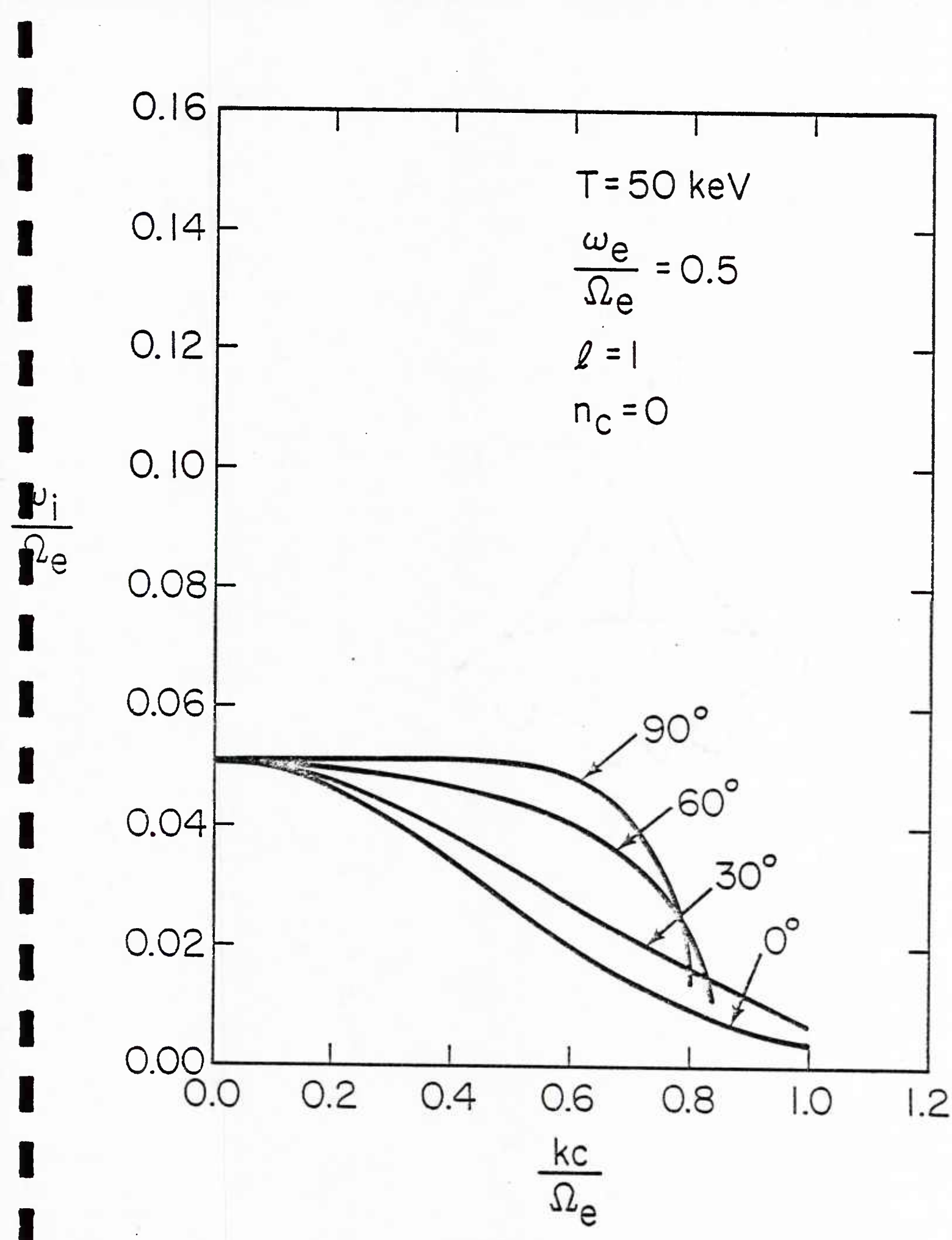
0.16
0.14
0.12
0.10
0.08
0.06
0.04
0.02
0.00
$\frac{\nu_i}{\Omega_e}$
T = 50 keV
$\frac{\omega_e}{\Omega_e}$ = 0.5
ℓ = 1
n_c = 0
90°
60°
30°
0°
0.0
0.2
0.4
0.6
0.8
1.0
1.2
$\frac{kc}{\Omega_e}$

Figure 1.

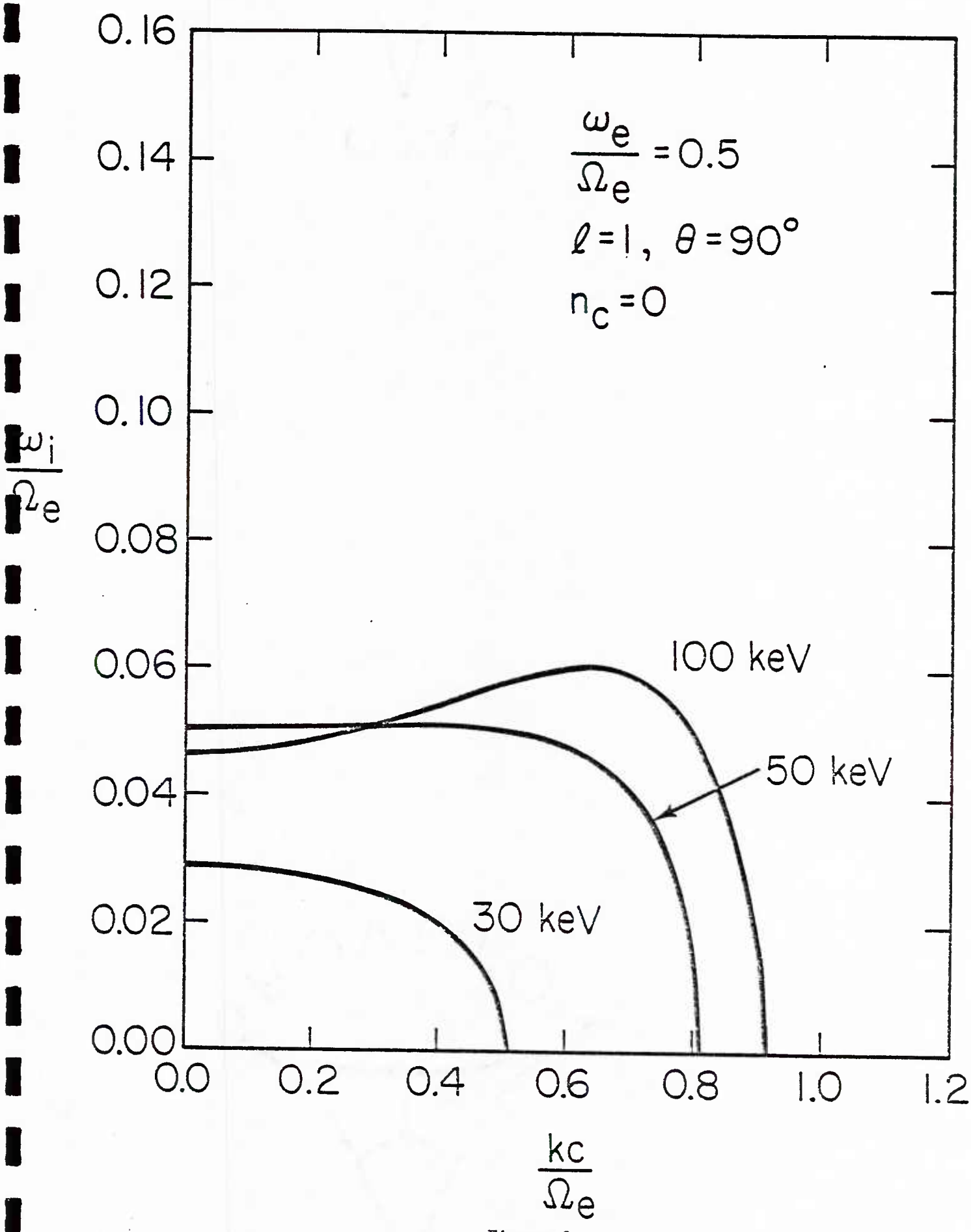
0.16
0.14
0.12
0.10
0.08
0.06
0.04
0.02
0.00
$\frac{\omega_i}{\Omega_e}$
$\frac{\omega_e}{\Omega_e} = 0.5$
$\ell = 1,\ \theta = 90°$
$n_c = 0$
100 keV
50 keV
30 keV
0.0
0.2
0.4
0.6
0.8
1.0
1.2
$\frac{kc}{\Omega_e}$

Figure 2.

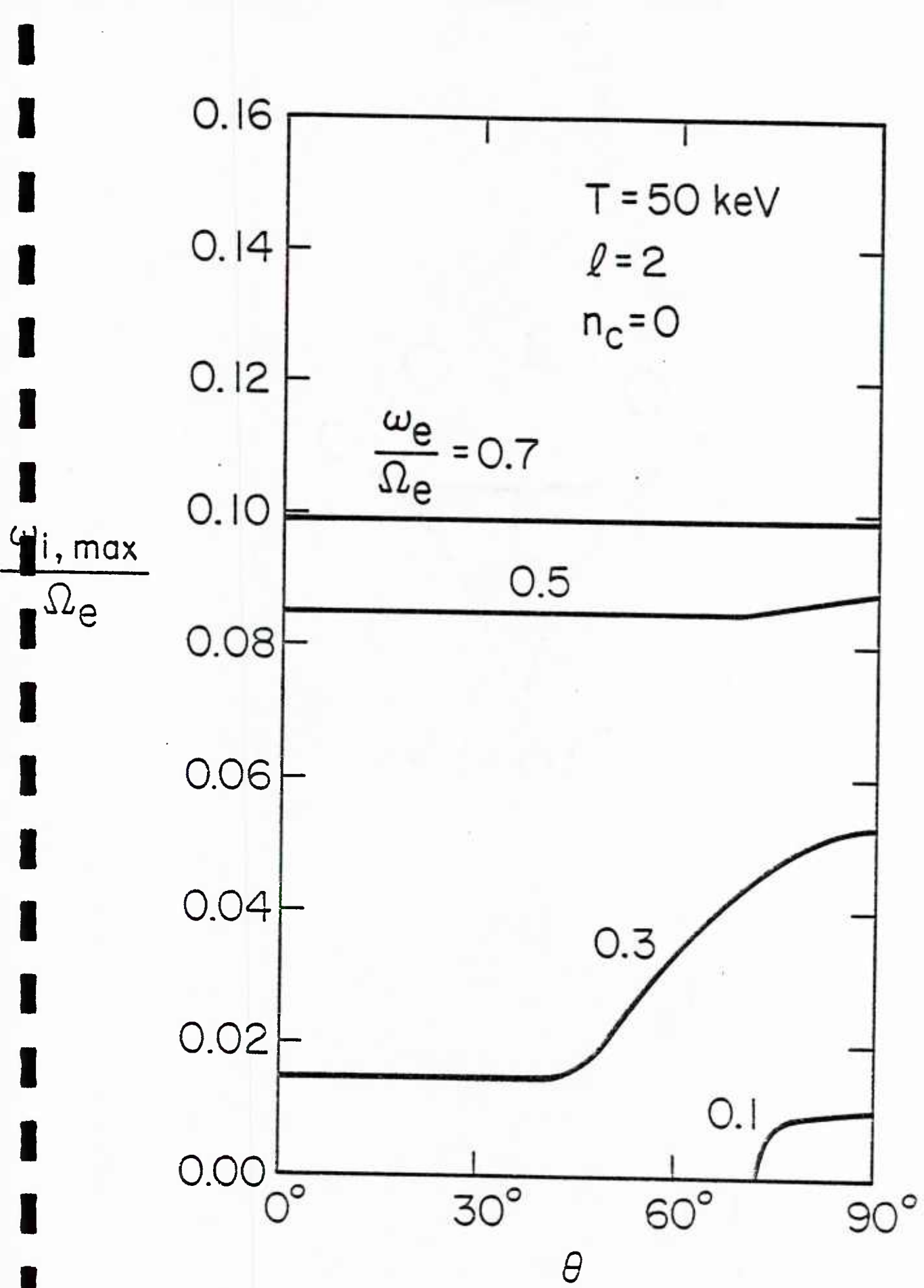
0.16
0.14
0.12
0.10
0.08
0.06
0.04
0.02
0.00
T = 50 keV
ℓ = 2
$n_c = 0$
$\frac{\omega_e}{\Omega_e} = 0.7$
0.5
0.3
0.1
0°
30°
60°
90°
θ
$\frac{\omega_{i,max}}{\Omega_e}$

Figure 3.

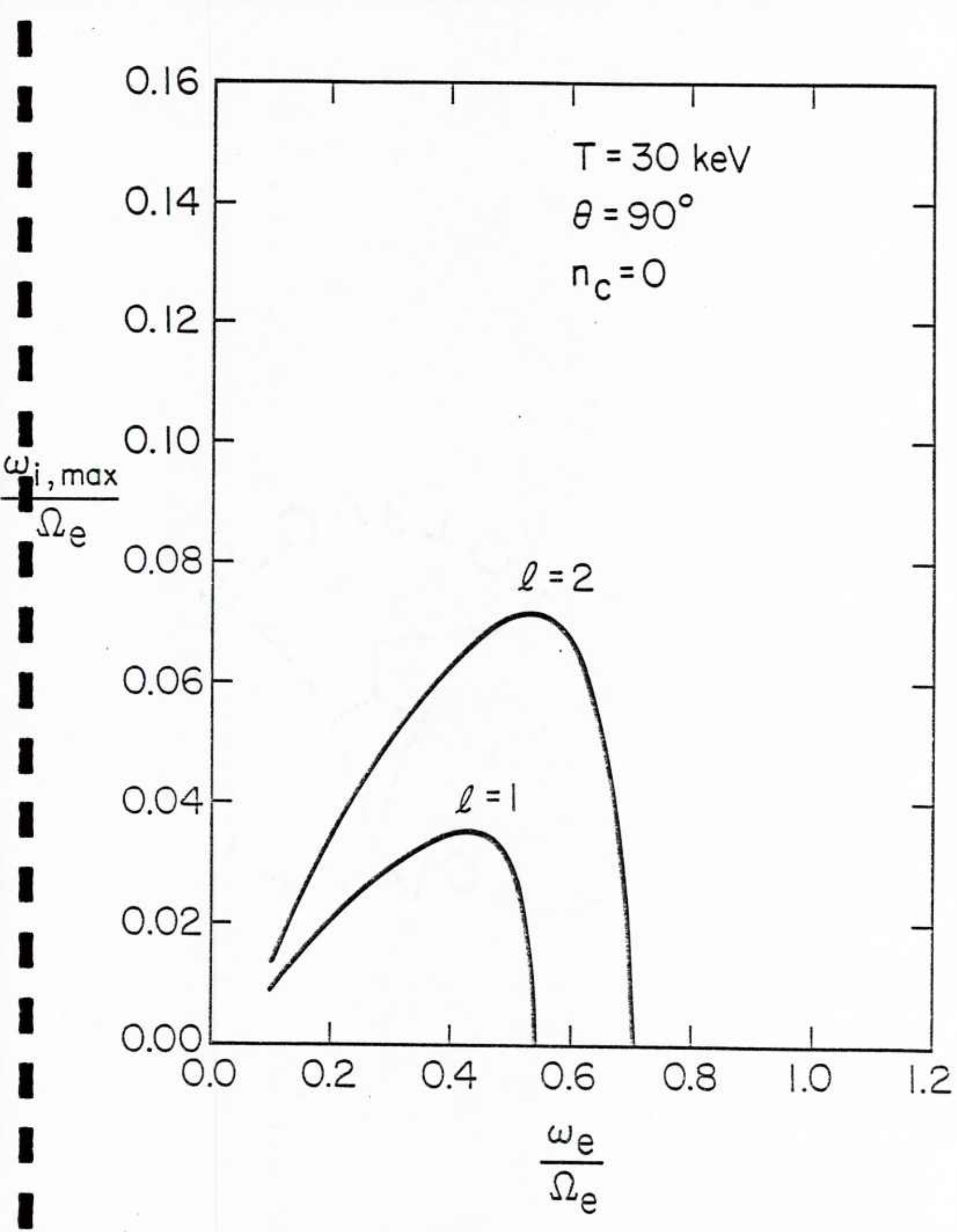
T = 30 keV
θ = 90°
n_c = 0
ℓ = 2
ℓ = 1
ω_i, max / Ω_e
ω_e / Ω_e
0.16
0.14
0.12
0.10
0.08
0.06
0.04
0.02
0.00
0.0
0.2
0.4
0.6
0.8
1.0
1.2

Figure 4a.

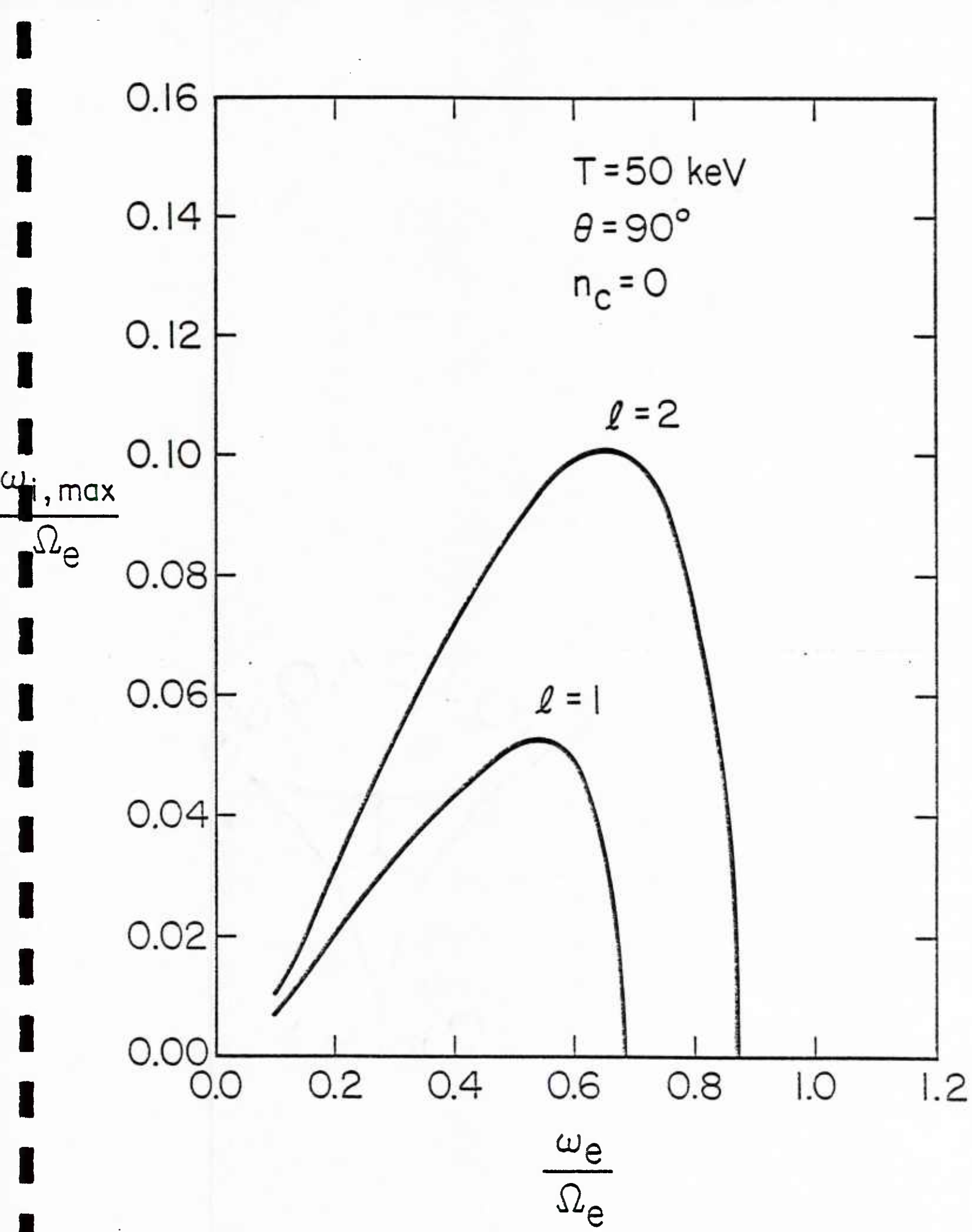
0.16
0.14
0.12
0.10
0.08
0.06
0.04
0.02
0.00
T = 50 keV
θ = 90°
n_c = 0
ℓ = 2
ℓ = 1
ω_i, max / Ω_e
0.0
0.2
0.4
0.6
0.8
1.0
1.2
ω_e / Ω_e

Figure 4b.

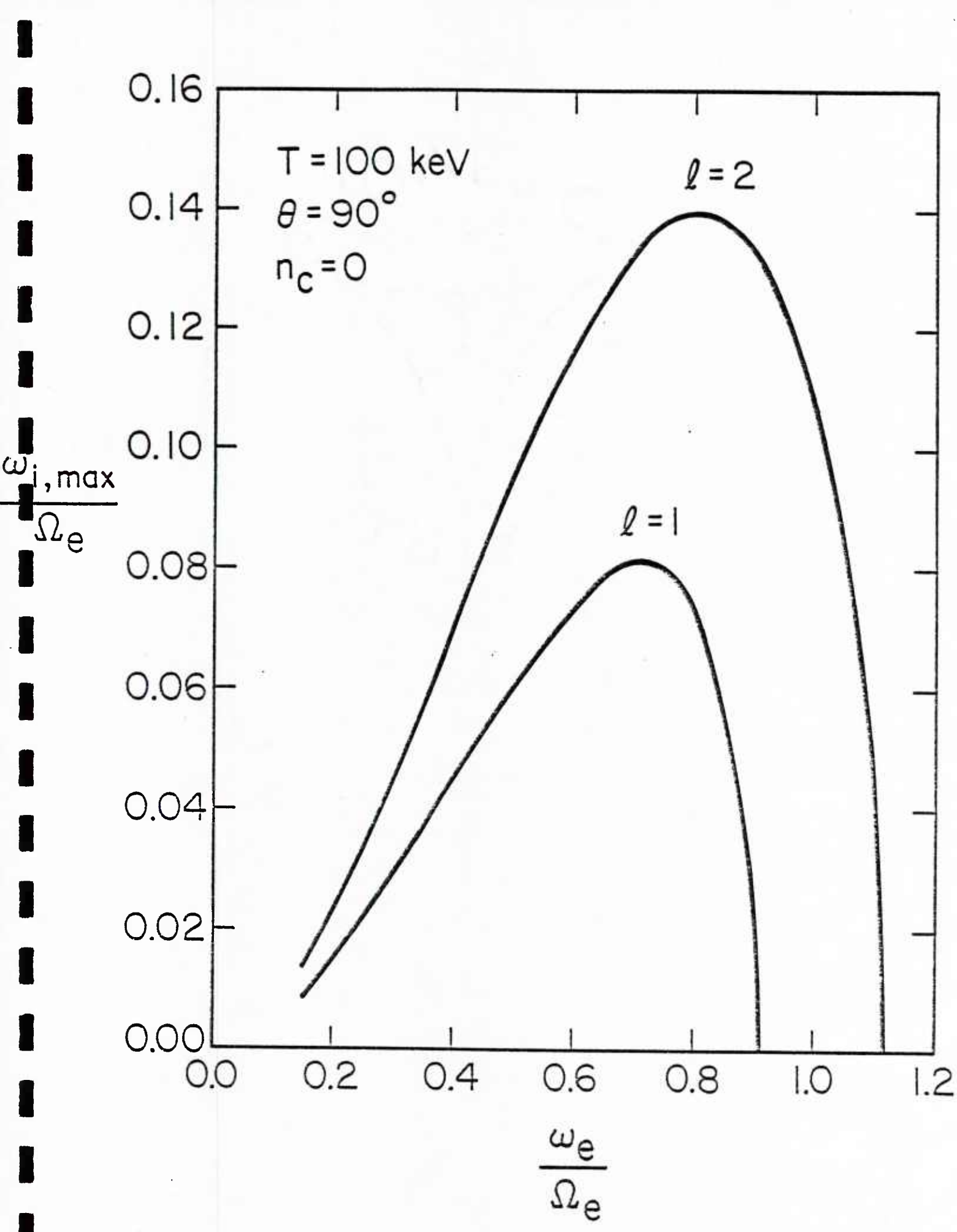
T = 100 keV
θ = 90°
n_c = 0
ℓ = 2
ℓ = 1
0.16
0.14
0.12
0.10
0.08
0.06
0.04
0.02
0.00
0.0
0.2
0.4
0.6
0.8
1.0
1.2
ω_i,max / Ω_e
ω_e / Ω_e

Figure 4c.

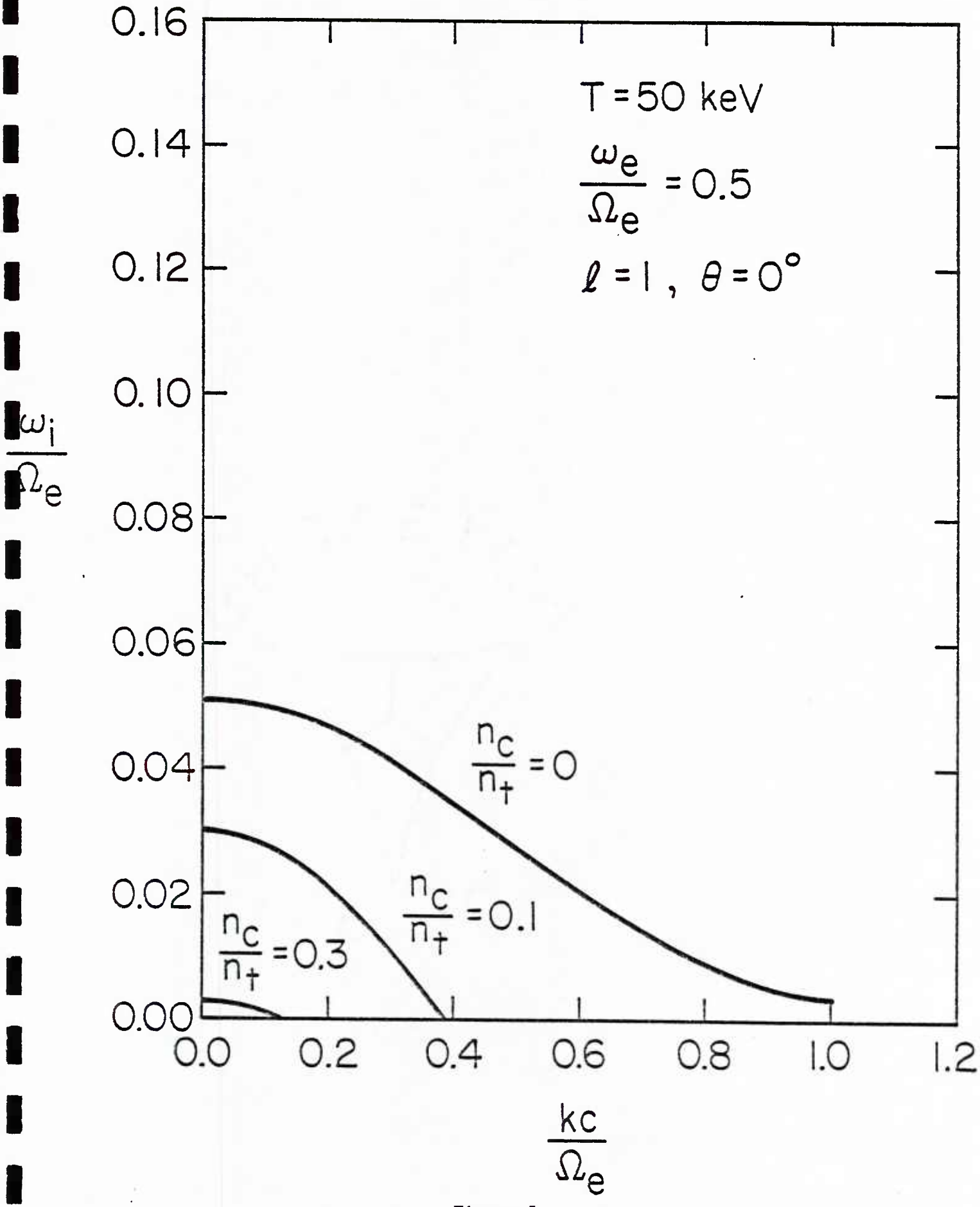
0.16
0.14
0.12
0.10
0.08
0.06
0.04
0.02
0.00
$\frac{\omega_i}{\Omega_e}$
T = 50 keV
$\frac{\omega_e}{\Omega_e} = 0.5$
$\ell = 1$, $\theta = 0°$
$\frac{n_c}{n_t} = 0$
$\frac{n_c}{n_t} = 0.1$
$\frac{n_c}{n_t} = 0.3$
0.0
0.2
0.4
0.6
0.8
1.0
1.2
$\frac{kc}{\Omega_e}$

Figure 5 .

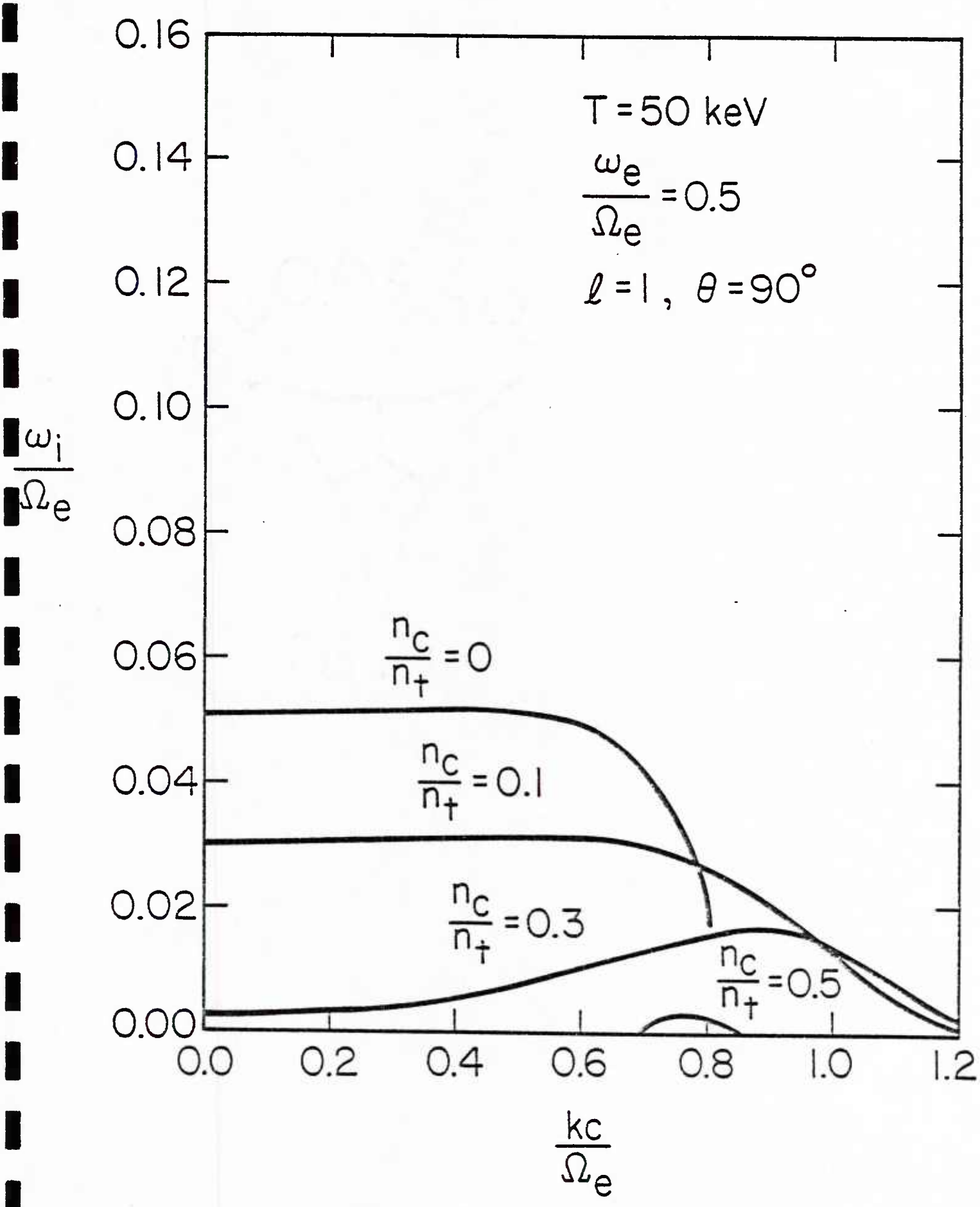
T = 50 keV
$\frac{\omega_e}{\Omega_e} = 0.5$
$\ell = 1, \ \theta = 90°$
$\frac{n_c}{n_t} = 0$
$\frac{n_c}{n_t} = 0.1$
$\frac{n_c}{n_t} = 0.3$
$\frac{n_c}{n_t} = 0.5$
$\frac{\omega_i}{\Omega_e}$
$\frac{kc}{\Omega_e}$
0.16
0.14
0.12
0.10
0.08
0.06
0.04
0.02
0.00
0.0
0.2
0.4
0.6
0.8
1.0
1.2

Figure 6a.

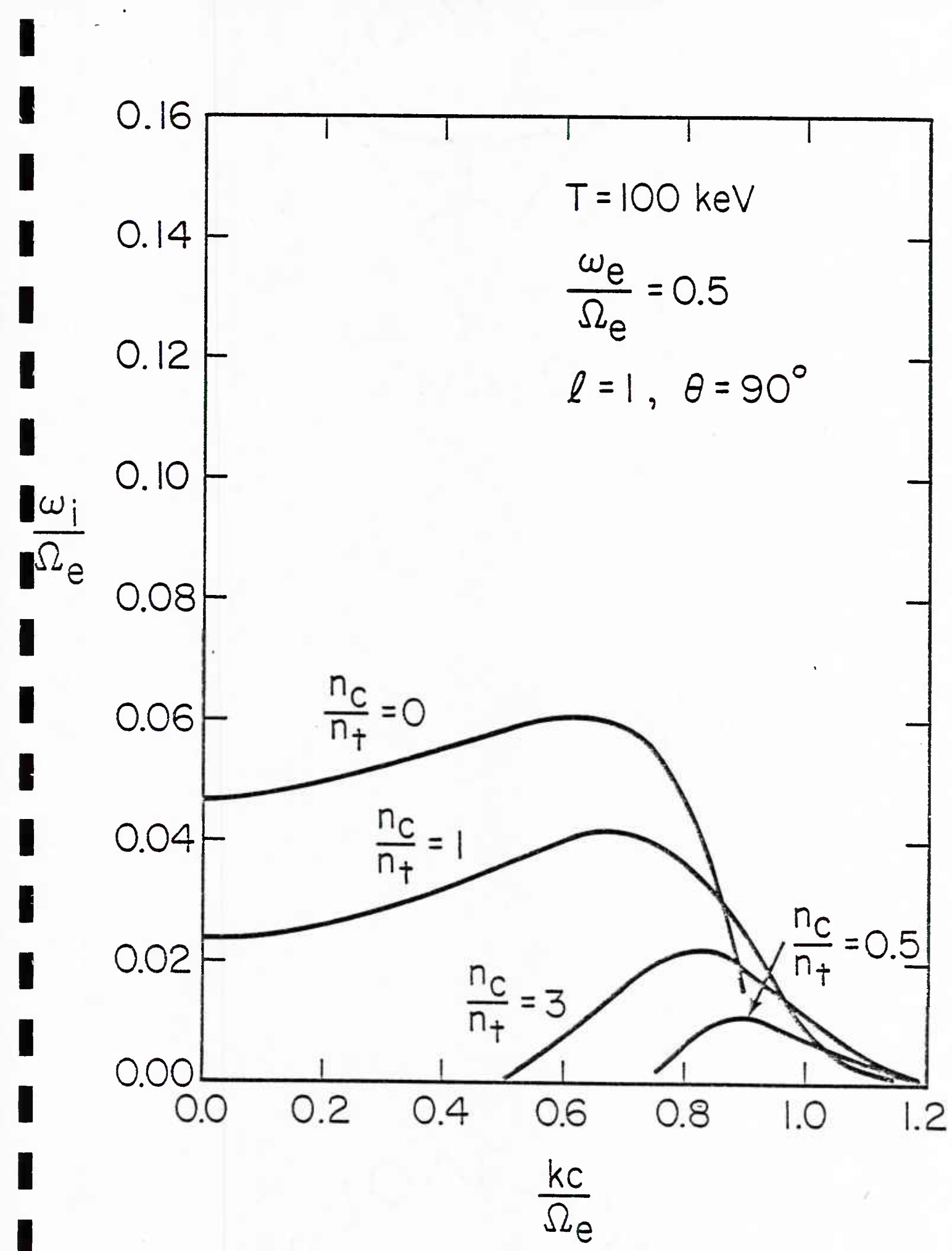
T = 100 keV
$\frac{\omega_e}{\Omega_e} = 0.5$
$\ell = 1, \ \theta = 90°$
$\frac{n_c}{n_t} = 0$
$\frac{n_c}{n_t} = 1$
$\frac{n_c}{n_t} = 0.5$
$\frac{n_c}{n_t} = 3$
$\frac{\omega_i}{\Omega_e}$
$\frac{kc}{\Omega_e}$
0.16
0.14
0.12
0.10
0.08
0.06
0.04
0.02
0.00
0.0
0.2
0.4
0.6
0.8
1.0
1.2

Figure 6b.

INSTABILITIES EXCITED BY AN ENERGETIC ION BEAM AND ELECTRONIC TEMPERATURE ANISOTROPY IN TANDEM MIRRORS

E. H. da Jornada[a], J. D. Gaffey, Jr., and D. Winske[b]

Institute for Physical Science and Technology

University of Maryland

College Park, Maryland 20742

U.S.A.

Permanent Addresses: [a] Instituto de Física
Universidade Federal do Rio Grande do Sul
90.000 Porto Alegre, R. S., Brasil

[b] Los Alamos National Laboratory
X-1, MS E-531
Los Alamos, New Mexico 87545, U.S.A.

ABSTRACT

The theory of cross-field ion streaming instabilities is applied to the parameter regime of the end cells of the upgraded Tandem Mirror Experiment with neutral beam injection. The cross-field ion drift as well as the electron thermal anisotropy $T_{e\perp} > T_{e\parallel}$ provides the free-energy which drives various instabilities. Three instabilities, a nearly perpendicular propagating modified two-stream instability, an obliquely propagating ion-ion streaming instability, and an obliquely propagating electromagnetic lower-hybrid instability, have been identified. The first two waves are electrostatic and have the largest growth rate. For the actual operation conditions of the Tandem Mirror machines, it is found that the ion-ion streaming instability has the largest growth rate. When more energetic neutral beams become available, the two-stream instability may play the dominant role in the stability of these devices.

I. INTRODUCTION

Tandem Mirrors are magnetic confinement devices in which the ions in a central (solenoidal) cell are prevented from leaking out the end by means of an electrostatic potential maintained by a denser plasma in mirror end cells.[1,2] The basic concept has been successfully verified in the Tandem Mirror Experiment (TMX).[3] However, it was also apparent from the initial work that the simple Tandem Mirror could not be easily scaled to a reactor-size device, because of the severe technological demands of producing and maintaining the dense mirror plasma. Alternative solutions were thereby investigated, leading to the development of the concept of a thermal barrier.[4,5,6] The thermal barrier is located between the central cell and the plug and allows the electrons in these two regions to be maintained at different temperatures, thus producing the confining potential with a smaller plug density. In order to generate the barrier, the density in this region is reduced by pumping out some of the ions.[4] This is achieved by injecting neutral beams at oblique angles to create "sloshing ion distributions," which have a density minimum at the center of the barrier. Futhermore, a hot electron population is also created in the barrier by means of ECRH to reduce the power transfer between the plug and central cell electrons; the hot electrons also act as an MHD anchor.[5,6] The thermal barrier concept is presently being tested in the upgraded TMX-U experiment[7] and has been incorporated into various reactor designs.[8,9]

While the inclusion of such complexity into the end cell of the Tandem Mirror may improve the overall confinement significantly, it is implicitly assumed that such configurations can be stably maintained. However, the introduction of (neutral) ion beams and hot anisotropic electrons in the barrier region suggests a variety of possible microinstabilities.[4] Injection of

neutral beams to form the sloshing ion distribution allows the possibility of various streaming instabilities.[10,11] The formation of hot anisotropic electrons will also give rise to unstable modes, such as the whistler[12-15] and the electron cyclotron maser instabilities.[16-20] Instabilities resulting from a combination of these two effects are also possible, but as yet have not been examined. In a recent paper, we have investigated such a combination of ions drifting across a magnetic field in which the background electron temperature was anisotropic in the environment of the earth's bow shock.[21] In that situation the ion streaming results from ion reflection at supercritical shocks and the electron anisotropy arises from adiabatic compression at the shock surface.[22] We have found that the well-known (low-beta) modified two-stream instability[23] is modified by finite beta effects[24] and further enhanced by the temperature anisotropy.[21] In another paper the nonlinear development of the instability in a finite beta plasma with isotropic electrons has been studied.[25]

Using the same basic model (local linear theory, homogeneous plasma, unmagnetized ions, etc.), we extend the calculations in this paper to the parameter regime of the Tandem Mirror. We find that three instabilities can occur: an oblique ion-ion mode which has the largest growth rate whenever the ratio of the drift to the thermal background ion velocities is not too large (typically, when $V_o/v_{io} \lesssim 4$); a modified two-stream mode which has the largest growth rate when $V_o/v_{io} \gtrsim 4$ and is most unstable for wave propagation nearly perpendicular to the magnetic field $\vec{B}$; and an electromagnetic lower-hybrid, instability with a peak growth rate for wave propagation between 60° and 75° relative to $\vec{B}$. The first two modes are electrostatic and their real frequencies are insensitive to the electron thermal anisotropy. The modified two-stream mode and the electromagnetic lower-hybrid mode are the low-beta

limits of the kinetic cross-field streaming modes with electron temperature anisotropy discussed by Tsai et al.[21]

The plan of this paper is as follows. In Section II the basic model and assumptions are reviewed and the dispersion tensor elements are given. Numerical solutions over a range of parameters relevant to Tandem Mirrors are shown in Section III. In Section IV the results are discussed, and the summary and conclusions are given in Section V.

II. BASIC CONSIDERATIONS

A. Physical Model and Assumptions

The main purpose of this work is to apply and to extend the theory of cross-field ion streaming instabilities with electron thermal anisotropy,[21,24] to the Tandem Mirror Machines. In previous studies, the relative electron-ion cross-field drift was the result of ions reflected by a high Mach number quasiperpendicular shock wave.[22] The stability analysis was done in a plane where inhomogeneities could be neglected and only one species of ions was included in the theory. Although the source of the cross-field ion-drift and the plasma parameters in the present work are different from those in previous papers, the same physical model and assumptions are adequate for describing both problems. In the following, we discuss the physical model and assumptions for the problem under consideration.

The drifting current in the mirror devices comes from the injection of a neutral beam into the plasma. Under the present operation conditions, the Mach number is low and an ion-ion instability may play an important role. Thus, we have to include both ion species in our theory. In the background plasma frame we have electrons and ions at rest with respect to drifting ions of the beam. We introduce a coordinate system in such a way that the $\hat{z}$ direction is parallel to the ambient magnetic field $\vec{B}_o$, and the beam injection velocity $\vec{V}_o$ and the wave vector $\vec{k}$ lie in the x-z plane. We use a linear local dispersion relation for a homogeneous plasma. The effect of electron temperature anisotropy is again taken into account, because in magnetic mirrors the electrons are preferentially heated perpendicularly to $\vec{B}_o$.

We assume that the unstable waves have frequencies much higher than the ion gyrofrequency, so that the two ion species may be treated as unmagnetized. We take the electrons to be magnetized and include electron thermal

anisotropy with $T_{e\perp} > T_{e\parallel}$ in the theory, where the perpendicular and parallel directions are relative to the magnetic field. We will return to these assumptions in Section IV.

B. Dispersion Tensor

We consider an infinite, homogeneous, collisionless plasma, immersed in a uniform static magnetic field $\vec{B}_o$, consisting of three components: Maxwellian electrons at rest with temperatures $T_{e\perp}$ and $T_{e\parallel}$ relative to $\vec{B}_o$ and density n_e; Maxwellian ions at rest with temperature T_{io} and density n_{io}; and a Maxwellian ion beam, with a temperature T_{is}, density n_{is}, streaming with velocity $\vec{V}_o$ at an angle α with respect to the magnetic field. Hereafter, we consider waves with the following properties: $\mu_{i(o,s)} = \dfrac{k_\perp^2 v_{i(o,s)}^2}{2\Omega_i^2} \gg 1$, $\Omega_i \ll \omega \ll \Omega_e$; where Ω_i and $v_{i(o,s)}$ are, respectively, the ion cyclotron frequency and ion thermal velocity (background, beam). The component of the wavevector $\vec{k}$ perpendicular to $\vec{B}_o$ is denoted by $k_\perp \equiv k \sin\theta$. In such a plasma, the ions are effectively unmagnetized. Moreover, because the ions are massive, we can neglect their contributions to the electromagnetic perturbations.

In the following, we write the elements of the dispersion tensor[21] as,

$$D_{xx} = 1 - N^2\cos^2\theta + \frac{\omega_e^2}{\omega^2}\left[\left(\frac{T_{e\perp}}{T_{e\parallel}} - 1\right) + \frac{T_{e\perp}}{T_{e\parallel}}\frac{e^{-\mu}}{\mu}\sum_{n=-\infty}^{\infty} n^2 I_n(\mu)\bar{z}_n Z(z_n)\right] + \varepsilon^{(i)}\sin^2\theta$$

$$D_{xy} = -D_{yx} = \frac{i\omega_e^2}{\omega^2}\frac{T_{e\perp}}{T_{e\parallel}} e^{-\mu} \sum_{n=-\infty}^{\infty} n\left[I_n(\mu) - I_n'(\mu)\right] \bar{z}_n Z(z_n)$$

$$D_{yy} = 1 - N^2 + \frac{\omega_e^2}{\omega^2}\left(\left(\frac{T_{e\perp}}{T_{e\parallel}} - 1\right) + \frac{T_{e\perp}}{T_{e\parallel}} e^{-\mu}\mu \sum_{n=-\infty}^{\infty} \left\{ \frac{n^2}{\mu^2} I_n(\mu) + 2\left[I_n(\mu) - I_n'(\mu)\right] \right\} \bar{z}_n Z(z_n)\right)$$

$$D_{xz} = D_{zx} = N^2 \sin\theta\cos\theta + \frac{\omega_e^2}{\omega^2}\left[-\frac{k_\perp}{k_\parallel}\left(\frac{T_{e\perp}}{T_{e\parallel}} - 1\right) + \frac{2\Omega_e}{k_\perp v_{e\parallel}} e^{-\mu} \sum_{n=-\infty}^{\infty} n I_n(\mu) \bar{z}_n z_n Z(z_n) \right] + \varepsilon^{(i)} \sin\theta\cos\theta \qquad (1)$$

$$D_{yz} = -D_{zy} = -\frac{i2\omega_e^2}{\omega^2}\frac{\Omega_e}{k_\perp v_{e\parallel}} e^{-\mu}\mu \sum_{n=-\infty}^{\infty} \left[I_n(\mu) - I_n'(\mu)\right] \bar{z}_n z_n Z(z_n)$$

$$D_{zz} = 1 - N^2\sin^2\theta + \frac{\omega_e^2}{\omega^2}\left[\frac{k_\perp^2}{k_\parallel^2}\left(\frac{T_{e\perp}}{T_{e\parallel}} - 1\right) + 2z_o^2 + 2e^{-\mu} \sum_{n=-\infty}^{\infty} I_n(\mu) \bar{z}_n z_n^2 Z(z_n) \right] + \varepsilon^{(i)} \cos^2\theta;$$

where

$$\varepsilon^{(i)} = \frac{2\omega_{io}^2}{k^2 v_{io}^2}\left[1 + \zeta_{io} Z(\zeta_{io}) \right] + \frac{2\omega_{is}^2}{k^2 v_{is}^2}\left[1 + \zeta_{is} Z(\zeta_{is}) \right], \qquad (2)$$

I_n is a modified Bessel function of order n, Z is the plasma dispersion function, and the following definitions have been introduced: $\omega_j^2 = \frac{4\pi n_j e^2}{m_j}$, $\Omega_j = \left| \frac{e_j B_o}{m_j c} \right|$, $v_j^2 = \frac{2T_j}{m_j}$, $\mu = \frac{k_\perp^2 v_{e\perp}^2}{2\Omega_e^2}$, $z_n = \frac{\omega - n\Omega_e}{k_\parallel v_{e\parallel}}$, $\bar{z}_n = \frac{\omega - n\Omega_e\left(1 - \frac{T_{e\parallel}}{T_{e\perp}}\right)}{k_\parallel v_{e\parallel}}$, $\zeta_{io} = \frac{\omega}{k v_{io}}$, and $\zeta_{is} = \frac{\omega - \vec{k}\cdot\vec{v}_o}{k v_{is}}$.

C. Plasma Parameters

Our study is applied to the end cells of the Tandem Mirror device. The parameters chosen are intended to reproduce the current and future operation conditions in the TMX-U machine and are the following[7]

Magnetic Field: $B_o = 5$ kG

Electrons:

$T_{e\perp} = 50\text{-}85$ keV

$T_{e\parallel} = 17$ keV

$n_e = 5.5 \times 10^{12}$ cm^{-3}

$\Omega_e = 8.8 \times 10^{10}$ rad/sec

$\omega_e = 1.3 \times 10^{11}$ rad/sec

$\beta_{e\perp} = 0.45\text{-}0.75$

$\beta_{e\parallel} = 0.15$

Background Ions:

$T_{io} = 1.1$ keV

$n_{io} = 2.7 \times 10^{12}$ cm^{-3}

$\Omega_i = 4.8 \times 10^{7}$ rad/sec

$\omega_{io} = 2.2 \times 10^{9}$ rad/sec

$\beta_{io} = 0.005$

Sloshing Ions: $T_{is\parallel,\perp} = 0.7$ keV

$E_s = \frac{1}{2} m_{is} V_o^2 = 10\text{-}30$ keV

$n_{is} = 2.7 \times 10^{12}$ cm^{-3}

$\Omega_i = 4.8 \times 10^7$ rad/sec

$\omega_{is} = 2.2 \times 10^9$ rad/sec

$\beta_{is} = 0.003$

III. NUMERICAL RESULTS

The numerical analysis of the unstable waves propagating in the plasma described in the previous section are shown in Figs. 1 through 14. In these curves, the growth rate is maximized over wavenumber and the real (ω_r) and imaginary (γ) parts of the frequency are normalized to the frequency $\omega_{LH} = (\Omega_e \Omega_i)^{1/2}$. The numerical solutions were obtained from the complete dispersion equation (1), including harmonics up to $n = \pm 20$. To facilitate our discussion, we classify the waves in two modes, called mode I and mode II. In the following we describe the main characteristics of each mode separately.

For mode I, the assumption of magnetized electrons and unmagnetized ions is satisfied. For this mode, the values of ck/ω_e are of order unity. We find that in the region of maximum growth rate, $1 \lesssim ck/\omega_e \lesssim 2$ for the whole set of solutions. The maximum of the peak growth rate is situated between 58^o and 72^o relative to the magnetic field direction. In Fig. 1 we have plotted ω_r/ω_{LH} and γ/ω_{LH} as a function of the angle of propagation θ, for $T_{e\perp}/T_{e\parallel} = 5$ and 4, $T_{is}/T_{io} = 0.6$, $T_{e\parallel}/T_{io} = 15$, $V_o/v_{io} = 3$, $\alpha = 45^o$, and $n_{io}/n_e = n_{is}/n_e = 0.5$. The curves show that the growth rate and the real part of the frequency decrease very rapidly with decreasing anisotropy and that the angle at which the peak of the maximum growth occurs increases as $T_{e\perp}/T_{e\parallel}$ decreases. The dependence of the real and imaginary parts of the frequency on the drift velocity is shown in Figs. 2 and 3. In these curves $T_{e\perp}/T_{e\parallel} = 5$, $n_{io}/n_e = n_{is}/n_e = 0.5$, $\alpha = 45^o$, and $T_{e\parallel}/T_{io} = 15$. Figure 2 shows ω_r/ω_{LH} and γ/ω_{LH} versus θ for $V_o/v_{io} = 3$, 4, and 5. Increasing the drift velocity, increases γ and ω_r and also the angle at which the peak of the growth rate occurs. In Fig. 3 the variation with drift velocity of the normalized growth rate, maximized over wavenumber and wave propagation direction and the corresponding real part of the frequency are shown. The maximum value of γ/ω_{LH}

occurs for $V_o/v_{io} = 7$ and $\theta = 64^o$. For $V_o/v_{io} = 10$, we find $\theta = 62^o$ for the angle of propagation of the most unstable wave. In Fig. 4 we analyze the instability as a function of the beam injection direction. For these curves, $T_{e\perp}/T_{e\parallel} = 5$, $V_o/v_{io} = 4$, and we vary the angle α from 45^o to 90^o. The remaining parameters are the same as in Fig. 2. The growth rate peaks at $\alpha \simeq 62^o$ and it does not change significantly when α increases up to 75^o. However, when $\alpha > 75^o$ the growth rate decreases more noticeably. At $\alpha = 90^o$, γ/ω_{LH} is nearly 95% of the value at $\alpha = 75^o$. The way the instability is affected by the variation of the densities of the background and beam ions is shown in Fig. 5, where the real and imaginary parts of the wave frequency are plotted as a function of n_{is}/n_e for the values of wavenumber and propagation angle which maximize γ. The paramenters are the same as in Fig. 2, except for $V_o/v_{io} = 4$ and for the values of ion densities, which now vary from $n_{is}/n_e = 0.25$ up to 0.60. The background ion density can be calculated for each curve from the condition of the quasineutrality $n_{io}/n_e = 1 - n_{is}/n_e$. As the ion beam density increases, the growth rate increases and the real frequency decreases. We also find that the angle at which the growth rate peaks decreases with increasing n_{is}/n_e. In Fig. 6 the real frequency $\omega_r(k)$ corresponding to the maximum growth rate is plotted as a function of the wavenumber k. Electromagnetic effects are important because $ck/\omega_e \lesssim 2$. In Fig. 7 we show the real part of the arguments of the plasma dispersion functions for the electrons ($z_o = \omega_r/k_\parallel v_{e\parallel}$), background ions ($\zeta_{io} = \omega_r/kv_{io}$), and ion beam ($|\zeta_{is}| = |\omega_r - \vec{k}_i \cdot \vec{V}_o|/kv_{is}$). For smaller values of the drift velocity and large angles of propagation the instability is highly kinetic, since ζ_{io} and $|\zeta_{is}|$ are approximately unity.

For mode II, the assumption of unmagnetized ions is again valid. However, the numerical results show that $\mu_{io}, \mu_{is} \gg \mu_e > 1$. So the electrons are

now only weakly magnetized compared with the ions species. This mode exhibits two peaks for the growth rate maximized over wavenumber. One is located nearly perpendicular to the magnetic field ($\theta \simeq 89.5^{o}$) and nearly disappears for $V_o/v_{io} < 4$. The second peak is situated at an angle between 52^{o} and 70^{o}, approximately, and has a larger peak growth rate than the nearly perpendicular peak when $V_o/v_{io} \lesssim 4$. In Fig. 8 the normalized imaginary and real parts of the frequency are given as a function of the wave propagation direction for $T_{e\perp}/T_{e\parallel} = 5$, 4, and 3. The other parameters are the same as in Fig. 1. The growth rate peaks at $\theta \simeq 52^{o}$ and increases as the anisotropy increases. The real part of the frequency is very insensitive to the ratio $T_{e\perp}/T_{e\parallel}$. In Figs. 9 and 10 we repeat for mode II the study done in Figs. 2 and 3 for mode I, taking $T_{e\perp}/T_{e\parallel} = 4$. The peak at $\theta \simeq 89.5^{o}$ decreases very rapidly with decreasing V_o/v_{io}. The second peak moves toward the perpendicular direction to the magnetic field as the drift velocity increases. In Fig. 10 both peaks are analyzed as a function of V_o/v_{io}. The peak at $\theta \simeq 89.5^{o}$ (curve A) is maximized at $V_o/v_{io} \simeq 6.8$ and the less oblique peak (curve B) at $V_o/v_{io} \simeq 4.5$. When $V_o/v_{io} \simeq 4.85$, both peaks have the same amplitude. Above this value of drift velocity, the nearly perpendicular wave has the larger growth rate and below , the less oblique peak has the larger one. In Fig. 11 the dependence of the unstable waves on the beam direction is studied, taking $V_o/v_{io} = 3$ with the reamining parameters the same as in Fig. 4. The less oblique peak (curve B) is maximized when $70^{o} < \alpha < 75^{o}$. The growth rate of the perpendicular peak (curve A) increases with increasing beam injection angle. We also find the the angle θ of the maximum growth rate moves toward the direction of the injected beam. The suggestion of an ion-ion interaction as the instability mechanism for the unstable wave with a maximum growth peak less perpendicular to $\vec{B}_o$ is shown in Fig. 12, where the real frequency and

growth rate maximized over wavenumber and propagation angle θ are given as a function of n_{is}/n_e, for $T_{e\perp}/T_{e\parallel} = 4$, $V_o/v_{io} = 3$, and $\alpha = 45^o$. The maximum growth rate occurs for equal background and ion beam densities. We also find that the angle at which the growth rate peaks is insensitive to the variation of n_{is}/n_e. In Fig. 13 the same analysis done in Fig. 6 for mode I has been made for mode II. We can see that the electromagnetic corrections can be neglected in mode II since $ck/\omega_e \gg 1$. Finally, in Fig. 14 we plot the real part of the arguments of the plasma dispersion function for the three plasma components. The perpendicular mode is kinetic in nature, since $\omega_r/k_\parallel v_{e\parallel} \sim 1$ when $\theta \simeq 89.5^o$.

Summarizing, we have observed three kinds of instabilities. The first, described as mode I, is an oblique wave which has a relatively small growth rate compared to the other two. It is an electromagnetic wave with frequency $\omega_r < \omega_{LH}$ and is the low β limit of the smaller growth rate peaks in Figs. 2 and 3 of Tsai et al.[21] for $\beta \simeq 1$. It is instructive to emphasize that this mode is distinct from the kinetic cross-field streaming instability (KCFSI), becoming stable when $T_{e\perp} \simeq T_{e\parallel}$ and remaining electromagnetic even when β is small. The basic sources of free energy arise from the electron temperature anisotropy and ion beam streaming energy. In mode II, there is a nearly perpendicular wave which, as will be shown in the next section, is a modified two-stream instability. As discussed by Wu et al.[24], this mode is the low β limit of the KCFSI and corresponds to the nearly perpendicular growth rate peaks in Figs. 2 and 3 of Tsai et al.[21] The third wave, described in mode II, is also an oblique wave and has the largest growth rate for the actual operating conditions of the Tandem Mirror Machines. It is an ion-ion streaming wave. Both waves in Mode II are electrostatic. In Section IV, we present a discussion of these waves.

IV. DISCUSSION

Numerical solution of the complete dispersion equation (1) for the parameters of the end cells of the upgraded Tandem Mirror Experiment with neutral beam injection have been presented in the previous section. Three kinds of unstable waves have been identified. One is electromagnetic and two are electrostatic. In order to give a better interpretation of these waves we will next present an analytical analysis of each mode, using appropriate approximations to the dispersion equation, based on the results of the previous section.

We start with mode I. For convenience we normalize the frequency to the usual whistler frequency $\omega_o = c^2k^2\Omega_e\cos\theta/\omega_e^2$. Because the electrons are strongly magnetized, we retain only the terms associated with harmonics $n = 0, \pm 1$ in (1). Introducing the index of refraction $N = ck/\omega$, using the small argument expansion of the Bessel functions and the large argument expansion of the electron plasma dispersion function for $n = \pm 1$, the elements of the dispersion matrix D_{ij} can be written approximately as

$$D_{xx} = N^2\{-\cos^2\theta + \frac{\omega^2}{\omega_o^2}\frac{c^2k^2}{\omega_e^2}\cos^2\theta - \frac{1}{2}(\beta_{e\perp}-\beta_{e\parallel})\cos^2\theta + ig + \frac{\omega^2}{\omega_o^2}\cdot\frac{\omega_o^2}{c^2k^2}\varepsilon^{(i)}\sin^2\theta\}$$

$$D_{yy}=N^2\{-1+\frac{\omega^2}{\omega_o^2}\frac{c^2k^2}{\omega_e^2}\cos^2\theta+\beta_{e\perp}[(\frac{T_{e\perp}}{T_{e\parallel}}-1)+\frac{T_{e\perp}}{T_{e\parallel}}z_oZ(z_o)]\sin^2\theta-\frac{1}{2}(\beta_{e\perp}-\beta_{e\parallel})\cos^2\theta+ig\}$$

$$D_{zz}=N^2\{-\sin^2\theta+\frac{2}{\beta_{e\parallel}}\frac{\omega^2}{\omega_o^2}[1+z_oZ(z_o)]-\frac{1}{2}(\beta_{e\perp}-\beta_{e\parallel})\sin^2\theta+ig\tan^2\theta+\frac{\omega^2}{\omega_o^2}\frac{\omega_0^2}{c^2k^2}\varepsilon^{(i)}\cos^2\theta\} \tag{3}$$

$$D_{xy} = -D_{yx} = -iN^2\left(\frac{\omega}{\omega_o}\cos\theta + if\right)$$

$$D_{xz} = D_{zx} = N^2\{ \sin\theta\cos\theta + \tfrac{1}{2}(\beta_{e\perp} - \beta_{e\parallel})\sin\theta\cos\theta - ig\tan\theta + \frac{\omega^2}{\omega_o^2}\frac{\omega_o^2}{c^2k^2}\varepsilon^{(i)}\sin\theta\cos\theta \}$$

$$D_{yz} = -D_{zy} = -iN^2\{ \frac{\omega}{\omega_o}\frac{T_{e\perp}}{T_{e\parallel}}[1 + z_o Z(z_o)]\sin\theta + if\tan\theta \} ;$$

where $\varepsilon^{(i)}$ is given in Eq. (2),

$$f = \frac{\pi^{1/2}\omega\omega_e}{2\beta_{e\parallel}^{1/2}\omega_o ck}\{ \frac{T_{e\perp}}{T_{e\parallel}}\Phi_- - \frac{\Omega_e}{\omega}\left(\frac{T_{e\perp}}{T_{e\parallel}} - 1\right)\Phi_+ \}$$

$$g = \frac{\pi^{1/2}\omega\omega_e}{2\beta_{e\parallel}^{1/2}\omega_o ck}\{ \frac{T_{e\perp}}{T_{e\parallel}}\Phi_+ - \frac{\Omega_e}{\omega}\left(\frac{T_{e\perp}}{T_{e\parallel}} - 1\right)\Phi_- \} \qquad (4)$$

$$\Phi_\pm = \exp\left[-\frac{(\omega - \Omega_e)^2}{k_\parallel^2 v_{e\parallel}^2}\right] \pm \exp\left[-\frac{(\omega + \Omega_e)^2}{k_\parallel^2 v_{e\parallel}^2}\right] .$$

For $\omega_r \gg |\gamma|$, the real and imaginary parts of the frequency can be calculated by the standard approach,

$$\text{Re } D(\vec{k},\omega_r) = 0$$

$$\gamma = -\frac{\text{Im } D(\vec{k},\omega_r)}{\frac{\partial}{\partial\omega_r}\text{Re } D(\vec{k},\omega_r)} , \qquad (5)$$

where D denotes the determinant of D_{ij}.

For the real part of the frequency, we can neglect the term $(\omega^2/\omega_o^2)_x (c^2k^2/\omega_e^2)\cos^2\theta$ in D_{xx} and D_{yy}, because $\omega_r^2 \ll \omega_o^2$ and $ck/\omega_e \lesssim 2$. Using this, we obtain an equation similar to Tsai et al.[21], equation (B6),

$$\frac{\omega_r^2}{\omega_o^2} = \frac{B}{A}\,, \tag{6}$$

where

$$A = 1+\left[1+\frac{2}{\beta_{e\parallel}}\sin^2\theta-\sin^4\theta\left(\frac{T_{e\perp}}{T_{e\parallel}}-1\right)^2+3\sin^2\theta\cos^2\theta\left(\frac{T_{e\perp}}{T_{e\parallel}}-1\right)\right]\frac{k^2 v_{e\parallel}^2}{2\omega_e^2}\,\mathrm{Re}\,\varepsilon^{(i)}$$

$$B=\left(1+\frac{\beta_{e\perp}}{2}-\frac{\beta_{e\parallel}}{2}\right)\left\{\frac{\beta_{e\parallel}}{2}\left(\frac{T_{e\perp}}{T_{e\parallel}}-1\right)^2\sin^2\theta+\left[1-\beta_{e\perp}\left(\frac{T_{e\perp}}{T_{e\parallel}}-1\right)\sin^2\theta+\left(\frac{\beta_{e\perp}}{2}-\frac{\beta_{e\parallel}}{2}\right)\cos^2\theta\right]\right. \tag{7}$$

$$\left.x\left(1+\frac{k^2 v_{e\parallel}^2}{2\omega_e^2}\,\mathrm{Re}\,\varepsilon^{(i)}\right)\right\}.$$

Equation (6) reduces to the usual whistler dispersion equation when $T_{e\perp} = T_{e\parallel}$ and $\theta = 0^o$. The waves we are discussing satisfy neither of these conditions and the numerical solution gives $\omega_r/\omega_o \lesssim 10^{-3}$ at the peak growth rate. The expressions for the growth rate are very similar to those given in Ref. (21). The significant differences are that in the present case, $\beta \ll 1$, two ion species have been considered and $\vec{V}_o$ typically makes an angle $\alpha = 45^o$ relative to $\vec{B}$, whereas in the case treated in Ref. (21), $\beta \sim 1$, only one species of ions is considered, and $\alpha = 90^o$.

Next, we analyze Mode II. Since these are low frequency waves and the normalized wavenumber ck/ω_e is large compared to unity, we treat them in the electrostatic approximation. Neglecting electromagnetic corrections, the dispersion relation becomes

$$D\,(\vec{k},\omega) = \frac{k_\perp^2}{k^2}\,D_{xx} + \frac{2\,k_\perp k_\parallel}{k^2}\,D_{xz} + \frac{k_\parallel^2}{k^2}\,D_{zz} = 0. \tag{8}$$

Substituting (1) into (8), we obtain

$$D(\vec{k},\omega) = 1 + \varepsilon^{(i)} + \frac{2\omega_e^2}{k^2 v_{e\parallel}^2}\left\{1 + e^{-\mu_e}\sum_{n=-\infty}^{+\infty} I_n(\mu_e)\,\bar{z}_n\,Z(z_n)\right\}. \qquad (9)$$

This expression can be simplified by using the large argument expansion of the plasma dispersion function for the electron cyclotron harmonics with $n \neq 0$ and the large argument expansion of the Bessel function I_o. The use of these expansions is justified by the numerical solutions. For instance, from the previous section it is possible to show that typically $\mu_e \simeq 10$, while $\mu_{i(s,o)} > 10^2$. Hence,

$$D(\vec{k},\omega) = 1 + \frac{2\omega_e^2}{k^2 v_{e\perp}^2} - \frac{\cos^2\theta}{(2\pi\,\mu_e)^{1/2}}\,\frac{\omega_e^2}{\omega^2}\,z_o^2\,Z'(z_o) - \frac{\omega_{io}^2}{\omega^2} - \frac{\omega_{is}^2}{(\omega - \vec{k}\cdot\vec{V}_o)^2}, \qquad (10)$$

where the prime denotes the derivative of Z with respect to the argument.

For the obliquely propagating waves, z_o is small, as shown in Fig. 14 and the dispersion relation (10) can be approximated by

$$D(\vec{k},\omega) \simeq 1 + \frac{2\omega_e^2}{k^2 v_{e\perp}^2} - \frac{\omega_{io}^2}{\omega^2} - \frac{\omega_{is}^2}{(\omega - \vec{k}\cdot\vec{V}_o)^2}. \qquad (11)$$

This is essentially the dispersion equation for the ion-ion streaming instability.[12-14,22] The solution of Eq. (11) is independent of the electron mass and the parallel electron temperature. The dependence on the perpendicular electron temperature is weak because the second term in (11) is small. Furthermore, the only angular dependence is on the absolute value of the difference between θ and α, rather than on θ and α separately.

It can be shown that the largest value of the growth rate occurs for $\omega_{io} = \omega_{is} \equiv \omega_i$, i.e., for $n_{io} = n_{is} = n_e/2$ in agreement with Fig. 12. For

this case, eq. (11) is easily solved and gives unstable waves if $|\vec{k}\cdot\vec{V}_o| < 2^{3/2}\omega_i$. The maximum growth rate occurs for $|\vec{k}\cdot\vec{V}_o| = 3^{1/2}\,\omega_i$, in which case $\omega = \omega_i\,(3^{1/2} + i)/2$.

For the nearly perpendicular propagating mode, $\theta \lesssim 90^o$ and z_o becomes nearly unity, as can be seen in Fig. 14. In this case the dispersion equation (10) becomes similar to the dispersion equation for the modified two-stream mode[22,24] in the electrostatic limit. It is again independent of the parallel electron temperature and depends only weakly on the perpendicular electron temperature. However, a significant difference is that there is a dependence on the electron mass in this case.

We emphasize that this modified two-stream mode can occur only in a very limited range of angles $\theta \lesssim 90^o$. As θ decreases, the parallel component of the wavevector increases and z_o becomes smaller than unity, as shown in Fig. 14. The applicable dispersion equation then becomes (11), which gives the ion-ion streaming mode. On the other hand, if $\theta \simeq \theta_c$, where

$$\theta_c = \cos^{-1}\left\{ \frac{n_{io}}{n_e}\,\frac{m_e}{m_i}\,\frac{(2\pi\,\mu_e)^{1/2}}{z_o^2\,Z'(z_o)} \right\}^{1/2}, \qquad (12)$$

the electron-ion beam interaction is comparable to the ion-ion interaction and the mode becomes a modified two-stream mode.

Figure 10 can now be easily interpreted. The nearly perpendicular mode (which has $z_o \simeq 1$) is more strongly electron Landau damped than the oblique mode (which has $z_o \ll 1$), while the difference in the background ion Landau damping on either of the modes is not so pronunciated for a given value of V_o/v_{io}. On the other hand, the electron Landau damping is rather insensitive to V_o/v_{io}, in contrast to what occurs for the background ion damping and ion

beam growth rate, as can be inferred from Fig. 14. Therefore, for plasma parameters such that at smaller values of V_o/v_{io} the electron Landau damping (γ_e) is larger than the background ion damping (γ_{io}), we expect that at a sufficient large value of the drift velocity, $\gamma_{io} > \gamma_e$. In this way, the nearly perpendicular mode, which is governed by an electron-ion beam interaction and has the damping mechanism provided essentially by the electrons, will have the greater growth rate when V_o/v_{io} is sufficiently large.

V. SUMMARY AND CONCLUSIONS

In this paper, we have studied analytically and numerically three instabilities associated with the injection of a neutral beam into the end cells of the Tandem Mirror Machine. These unstable waves, which are excited by the relative electron-ion cross-field drift and by the electron temperature anisotropy, may also occur in the perpendicular bow shock. However, since the two problems deal with different situations, a particular unstable wave may have distinct relative importance and the growth rate may be maximized for different values of the parameters appropriate to the space and laboratory plasmas, even though they result from the same source of free energy. Also, in the present work, more parameters are free to vary, for example, the beam injection angle α, which provide more ways to optimize a particular instability.

For propagation oblique to the magnetic field $\vec{B}$, we find two unstable waves. One has been identified as an electromagnetic lower-hybrid instability (EMLHI) and the second, as an electrostatic ion-ion streaming instability (IISI).

It is found that the EMLHI has the following properties:

(1) The growth rate γ is maximized for $60^{o} \leq \theta \leq 75^{o}$.

(2) γ and ω_r increase with increasing $T_{e\perp}/T_{e\parallel}$. The mode becomes stable when the electron temperature anisotropy is reduced, i.e., $T_{e\perp} \simeq T_{e\parallel}$.

(3) γ is nearly constant with respect to the angle of beam injection for $45^{o} \leq \alpha \leq 75^{o}$ and decreases more rapidly for larger values of α.

(4) γ increases and ω_r decreases with increasing n_{is} (density of beam ions).

(5) The instability is highly kinetic for smaller drift velocities and large angles of propagation.

The IISI has the characteristics that:

(1) The growth rate γ is maximized for $50^{o} < \theta < 70^{o}$.

(2) The growth rate is the largest compared to the other two modes, when $V_o/v_{io} < 4$.

(3) γ exhibits a peak for $70^{o} < \alpha < 75^{o}$.

(4) γ is maximized for $n_{is} = n_{io}$.

For propagation nearly perpendicular to $\vec{B}$, we find an electrostatic modified two-stream mode (MTSI) with the properties that:

(1) The growth rate γ is maximized for $\theta = 89.5^{o}$.

(2) γ increases, but ω_r remains nearly constant, as $T_{e\perp}/T_{e\parallel}$ increases.

(3) The growth rate is the largest compared to the other to modes when $V_o/v_{io} > 4$.

(4) γ increases with increasing V_o/v_{io}.

(5) The mode is kinetic in nature because $\omega_r/k_{\parallel} v_{e\parallel} \sim 1$ when $\theta = 89.5^{o}$.

The parameters have been chosen to describe typical operation conditions of the TMX-U device. Since presently $V_o/v_{io} < 4$, we expect the ion-ion streaming mode to play the dominant role in the stability of the Tandem Mirror Machines. However, new experiments are likely to have larger values of the ratio V_o/v_{io}, and we expect that the nearly perpendicular two-stream mode may have the largest growth rate in the future experiments.

ACKNOWLEDGEMENTS

The authors thank Dr. M. Tanaka for helpful discussions about the computer codes used in the numerical computation. The present research was supported in part by the U. S. Office of Naval Research under grants N00014-82-K-0208 and N00014-84-C-0255, in part by the National Aeronautics and Space Administration under grant NGL21-002-005, and in part by the Conselho Nacional de Desenvolvimento Científico e Tecnológico of Brazil, CNPq.

REFERENCES

1. G. I. Dimov, V. V. Zakaidakov, and M. E. Kishinevsky, Fiz. Plasmy 2, 597 (1976) [Sov. J. Plasma Phys. 2, 326 (1976)], in Proceedings of the Sixth International Conference on Plasma Physics and Controlled Nuclear Fusion Research, Berchtesgaden, West Germany, 1976 (International Atomic Energy Agency, Vienna, 1977). Paper No. C4.
2. T. K. Fowler and B. G. Logan, Comments Plasma Phys. Controlled Fusion 2, 167 (1977).
3. D. L. Correll et al., Nucl. Fusion 22, 223 (1982).
4. D. E. Baldwin and B. G. Logan, Phys. Rev. Lett. 43, 1318 (1979).
5. J. Kesner, R. S. Post, D. K. Smith, D. E. Baldwin and Y. C. Lee, Nucl. Fusion 22, 577 (1982).
6. J. Kesner, R. S. Post, B. D. McVey and D. K. Smith, Nucl. Fusion 22, 549 (1982).
7. T. A. Casper, Y.-J. Chen, R. Ellis, R. James and C. Lasnier, Lawrence Livermore National Laboratory, Report No. UCID-19783, April, 1983 (unpublished).
8. R. W. Conn, V. K. Dhir, N. M. Ghoniem, D. M. Goebel, S. P. Grotz, F. Kantrowitz, N. S. Kim, T. K. Mau, G. W. Shuy and M. Z. Youssef, Nucl. Tech./Fusion 2, 563 (1982).
9. MARS Study Group, Lawrence Livermore National Laboratory, Report No. TB-047 [GPO No. 689-504], March, 1983 (unpublished)
10. P. L. Auer, R. W. Kilb and W. F. Crevier, J. Geophys. Res. 76, 2927 (1971).
11. K. Papadopoulos, R. C. Davidson, J. M. Dawson, I. Haber, D. A. Hammer, N. A. Krall and R. Shanny, Phys. Fluids 14, 849 (1971).
12. C. F. Kennel and H. E. Petschek, J. Geophys. Res. 71, 1 (1966).

13. J. E. Scherer and A. W. Trivelpiece, Phys. Fluids 10, 591 (1967).

14. A. B. Mihkailovskii, Theory of Plasma Instabilities, Vol. 1 (Consultants Bureau, New York, NY, 1974), p. 235.

15. N. T. Gladd, Phys. Fluids 26, 974 (1983).

16. L. C. Lee and C. S. Wu, Phys. Fluids 23, 1348 (1980).

17. R. G. Hewitt, D. B. Melrose and K. G. Rönnmark, Aust. J. Phys. 35, 447 (1982).

18. Y. Y. Lau and K. R. Chu, Phys. Rev. Lett. 50, 243 (1983).

19. H. K. Wong, C. S. Wu, F. J. Ke, R. S. Schneider and L. F. Ziebell, J. Plasma Phys. 28, 503 (1982).

20. H. K. Wong, C. S. Wu and J. D. Gaffey, Jr., Phys. Rev. Lett. 52 (1984), submitted.

21. S. T. Tsai, M. Tanaka, J. D. Gaffey, Jr., E. H. da Jornada, C. S. Wu and L. F. Ziebell, J. Plasma Phys. 31 (1984), in press.

22. C. S. Wu, D. Winske, Y. M. Zhou, S. T. Tsai, P. Rodriguez, M. Tanaka, K. Papadopoulos, K. Akimoto, C. S. Liu, M. M. Leroy and C. C. Goodrich, Space Sci. Rev. 37, 63 (1984).

23. J. B. McBride, E. Ott, J. P. Boris and J. H. Orens, Phys. Fluids 15, 2367 (1972).

24. C. S. Wu, Y. M. Zhou, S. T. Tsai, S. C. Guo, D. Winske and K. Papadopoulos, Phys. Fluids 26, 1259 (1983).

25. D. Winske, M. Tanaka and C. S. Wu, Phys. Fluids 27 (1984), to be submitted.

FIGURE CAPTIONS

Figure 1. Mode I growth rate (dashed curve) maximized over wavenumber and real part of the frequency (solid curve) as a function of propagation angle θ for two values of electron temperature anisotropy $T_{e\perp}/T_{e\parallel} = 4,5$; $V_o/v_{io} = 3$; $T_{e\parallel}/T_{io} = 15$; $\alpha = 45^o$, $T_{is}/T_{io} = 0.6$, and $n_{io} = n_{is} = 0.5\ n_e$.

Figure 2. Mode I growth rate (dashed curve) maximized over wavenumber and real part of the frequency (solid curve) as a function of propagation angle θ for several values of the relative electron-ion beam drift velocity normalized to the background ion thermal velocity $V_o/v_{io} = 3,4,5$; $T_{e\perp}/T_{e\parallel} = 5$; $n_{io} = n_{is} = 0.5\ n_e$; $\alpha = 45^o$; $T_{is}/T_{io} = 0.6$, and $T_{e\parallel}/T_{io} = 15$.

Figure 3. Mode I growth rate (dashed curve) maximized over wavenumber and propagation angle θ and the corresponding real frequency (solid curve) versus relative electron-ion beam drift velocity V_o/v_{io}. The remaining parameters are the same as in Fig. 2.

Figure 4. Mode I growth rate (dashed curve) maximized over wavenumber and propagation angle θ and the corresponding real frequency (solid curve) versus beam injection angle α for $V_o/v_{io} = 4$, $T_{e\perp}/T_{e\parallel} = 5$, $n_{io} = n_{is} = 0.5\ n_e$, and $T_{e\parallel}/T_{io} = 15$.

Figure 5. Mode I growth rate (dashed curve) maximized over wavenumber and propagation angle θ and the corresponding real frequency (solid curve) as a function of the ion beam density n_{is}/n_e for $V_o/v_{io} = 4$, $T_{e\perp}/T_{e\parallel} = 5$, $T_{e\parallel}/T_{io} = 15$, and $\alpha = 45^o$.

Figure 6. Mode I real part of the frequency versus wavenumber ck/ω_e corresponding to maximum growth rate for $V_o/v_{io} = 3,5$; $T_{e\perp}/T_{e\parallel} = 5$ (dashed curve), 4 (solid curve); $n_{io} = n_{is} = 0.5\ n_e$; and $T_{e\parallel}/T_{io} = 15$.

Figure 7. Mode I values of $|\ \omega_r - \vec{k}\cdot\vec{V}_o\ |/kv_{is}$, ω_r/kv_{io}, and $\omega_r/k_\parallel v_{e\parallel}$ corresponding to maximum growth versus angle of propagation θ for $V_o/v_{io} = 3,5$; $T_{e\perp}/T_{e\parallel} = 5$; $n_{io} = n_{is} = 0.5\ n_e$; $\alpha = 45^o$; and $T_{e\parallel}/T_{io} = 15$.

Figure 8. Mode II growth rate (dashed curve) maximized over wavenumber and the real frequency (solid curve) as a function of propagation angle θ for $T_{e\perp}/T_{e\parallel} = 3,4,5$; $V_o/v_{io} = 3$, $T_{e\parallel}/T_{io} = 15$; $n_{io} = n_{is} = 0.5\ n_e$; and $\alpha = 45^o$.

Figure 9. Mode II growth rate (dashed curve) maximized over wavenumber and the real frequency (solid curve) as a function of propagation angle θ for $V_o/v_{io} = 3,4,5$; $T_{e\perp}/T_{e\parallel} = 4$; $T_{e\parallel}/T_{io} = 15$; $n_{io} = n_{is} = 0.5\ n_e$; and $\alpha = 45^o$.

Figure 10. Mode II nearly perpendicular (A) and oblique (3) growth rates (dashed curves) maximized over propagation angle θ and wavenumber and the real part of the frequency (solid curves) versus drift velocity V_o/v_{io} for $T_{e\perp}/T_{e\parallel} = 4$, $T_{e\parallel}/T_{io} = 15$, $n_{io} = n_{is} = 0.5\ n_e$, and $\alpha = 45^o$.

Figure 11. Mode II nearly perpendicular (A) and oblique (B) growth rates (dashed curves) maximized over wavenumber and propagation angle θ and the corresponding real frequency (solid curves) versus beam injection angle α for $V_o/v_{io} = 3$, $T_{e\perp}/T_{e\parallel} = 5$, $T_{e\parallel}/T_{io} = 15$, and $n_{io} = n_{is} = 0.5\ n_e$.

Figure 12. Mode II maximum oblique growth rate (dashed curve) and real frequency (solid curve) as a function of ion beam density n_{is}/n_e for $V_o/v_{io} = 3$, $T_{e\perp}/T_{e\parallel} = 4$, $T_{e\parallel}/T_{io} = 15$, and $\alpha = 45^o$.

Figure 13. Mode II real part of the frequency versus wavenumber ck/ω_e for several values of the drift velocity $V_o/v_{io} = 3,4,5$; $T_{e\perp}/T_{e\parallel} = 4$ (dashed curve), 5 (solid curve); $T_{e\parallel}/T_{io} = 15$; $n_{io} = n_{is} = 0.5\ n_e$; and $\alpha = 45^o$.

Figure 14. Mode II values of $|\ \omega_r - \vec{k}\cdot\vec{V}_o\ |/kv_{is}$, ω_r/kv_{io}, and $\omega_r/k_\parallel v_{e\parallel}$ corresponding to maximum growth rate versus angle of propagation θ for $V_o/v_{io} = 4,5$; $T_{e\perp}/T_{e\parallel} = 4$; $T_{e\parallel}/T_{io} = 15$; and $\alpha = 45^o$.

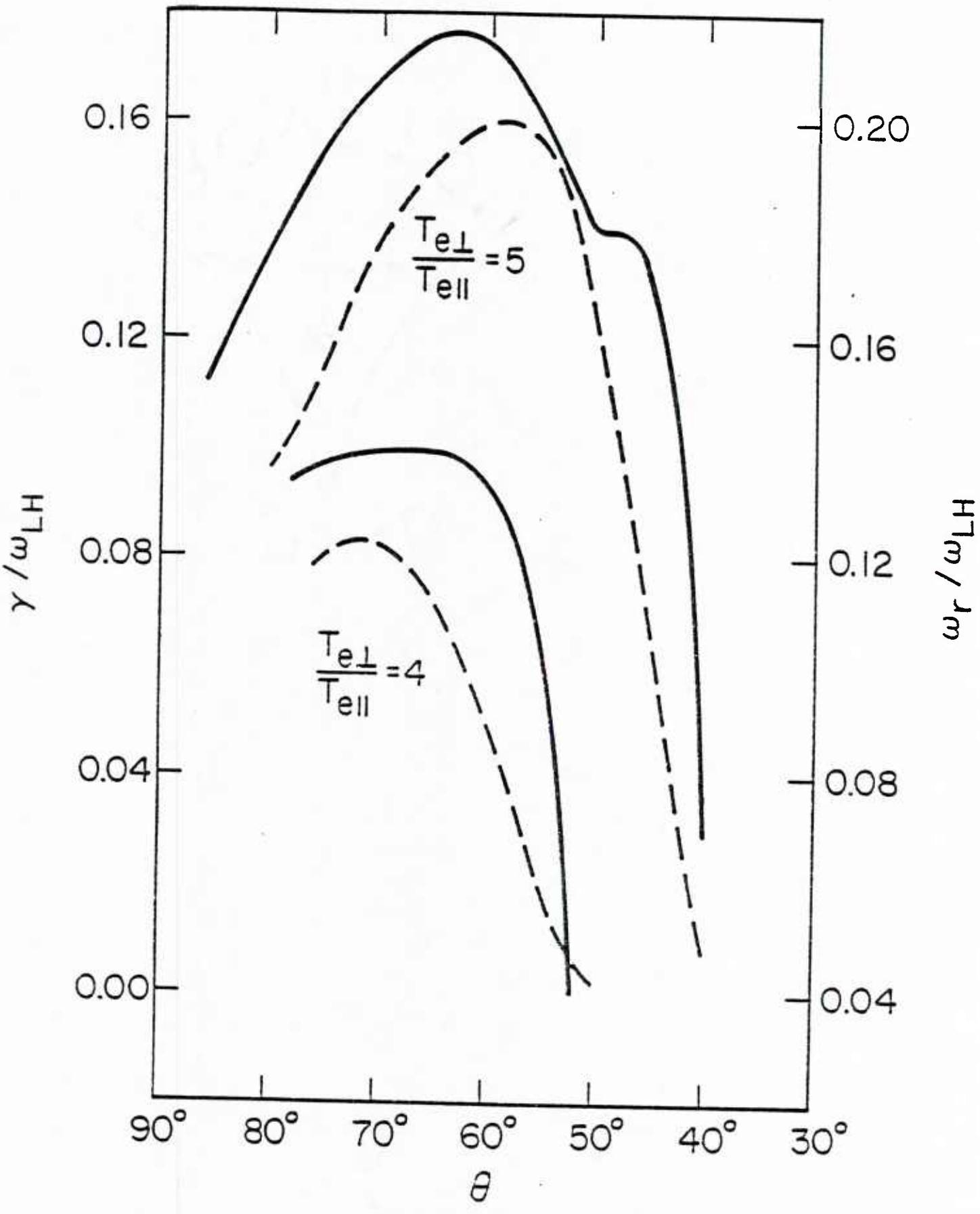
0.16
0.12
0.08
0.04
0.00
0.20
0.16
0.12
0.08
0.04
γ/ω_{LH}
ω_r/ω_{LH}
$\frac{T_{e\perp}}{T_{e\parallel}}=5$
$\frac{T_{e\perp}}{T_{e\parallel}}=4$
90°
80°
70°
60°
50°
40°
30°
θ

Figure 1.

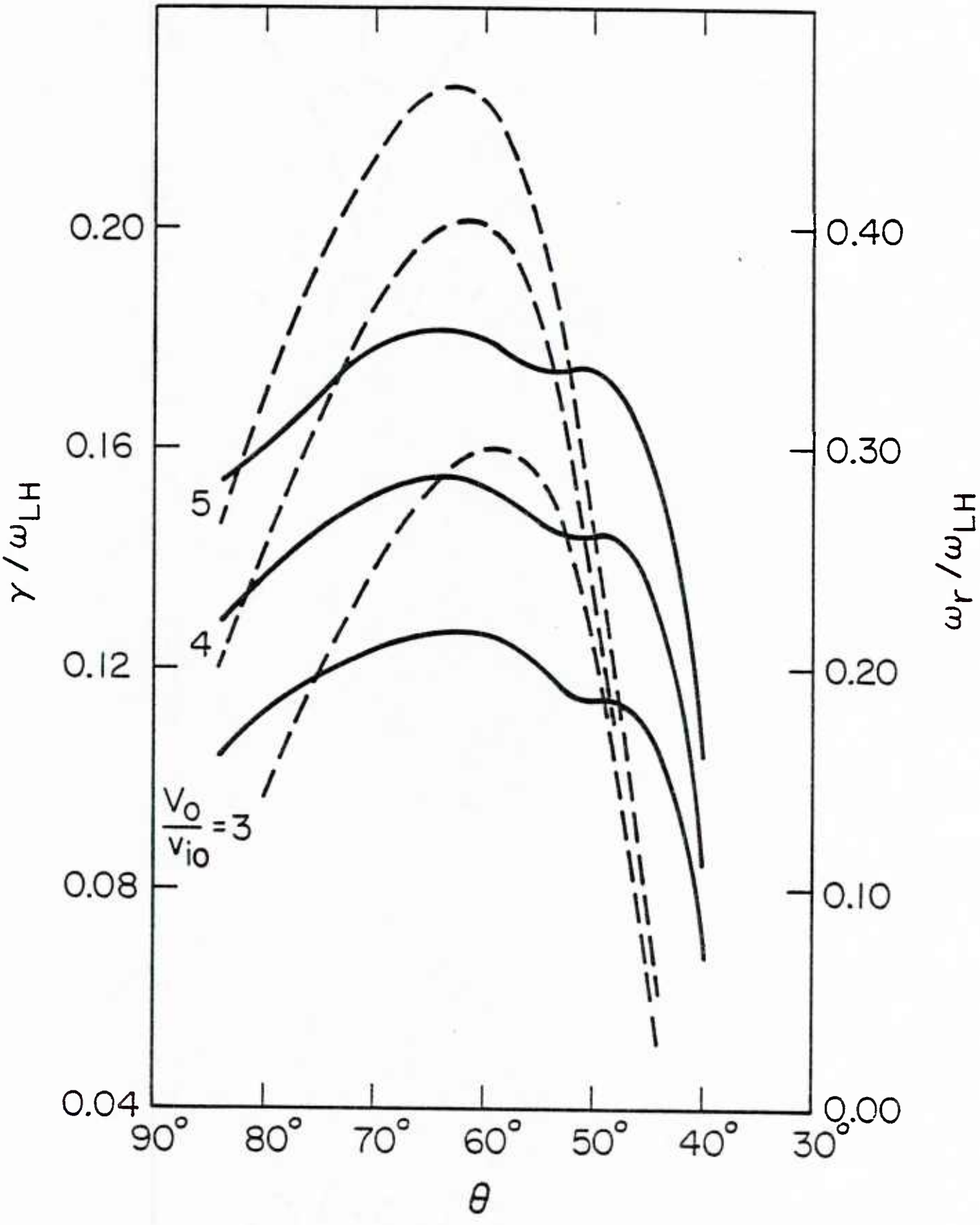
0.20
0.16
0.12
0.08
0.04
γ / ω_{LH}
0.40
0.30
0.20
0.10
0.00
ω_r / ω_{LH}
5
4
$\frac{V_o}{v_{io}} = 3$
90°
80°
70°
60°
50°
40°
30°
θ

Figure 2.

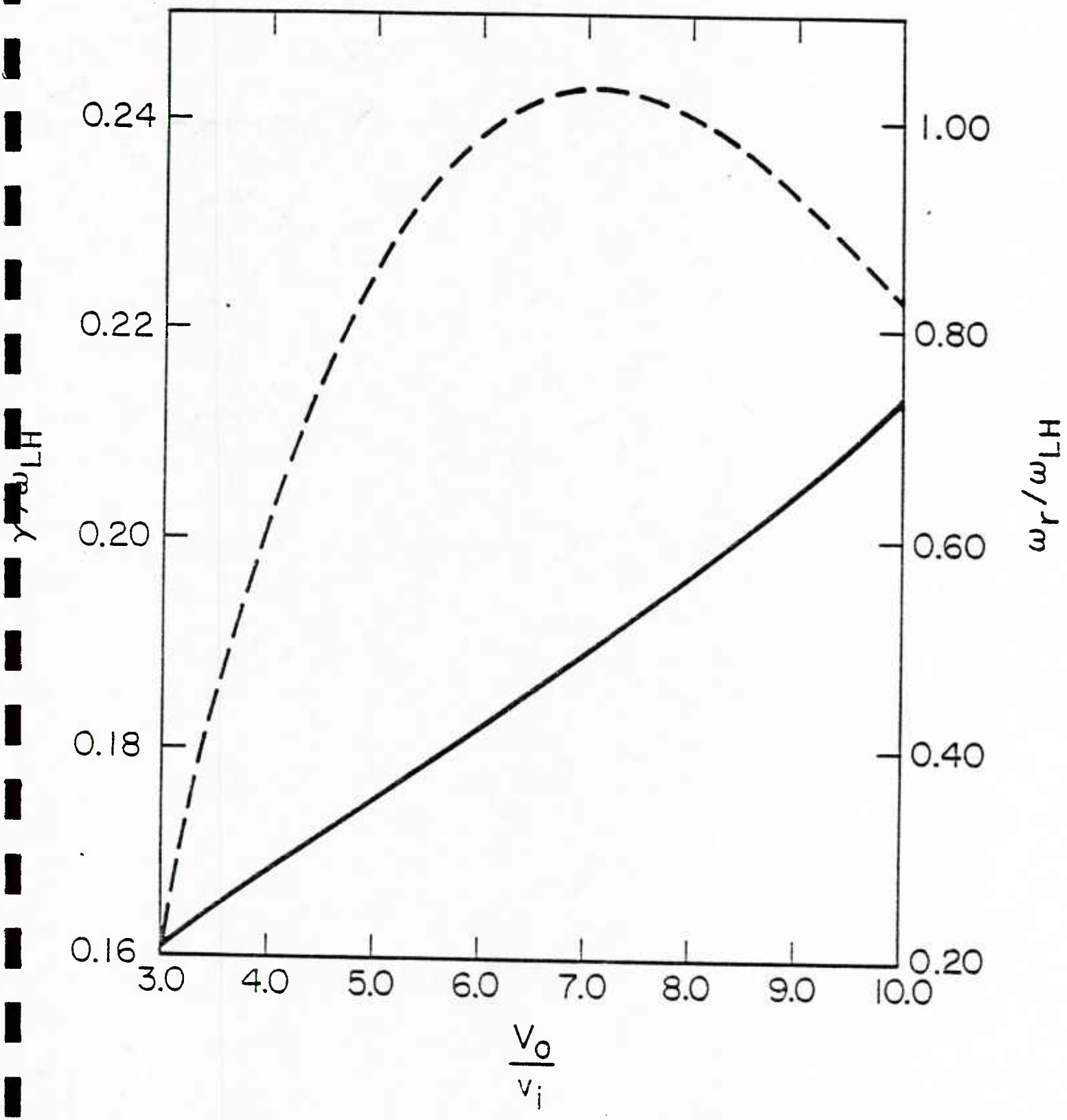
0.24
0.22
0.20
0.18
0.16
γ/ω_{LH}
1.00
0.80
0.60
0.40
0.20
ω_r/ω_{LH}
3.0
4.0
5.0
6.0
7.0
8.0
9.0
10.0
$\frac{V_o}{V_i}$

Figure 3.

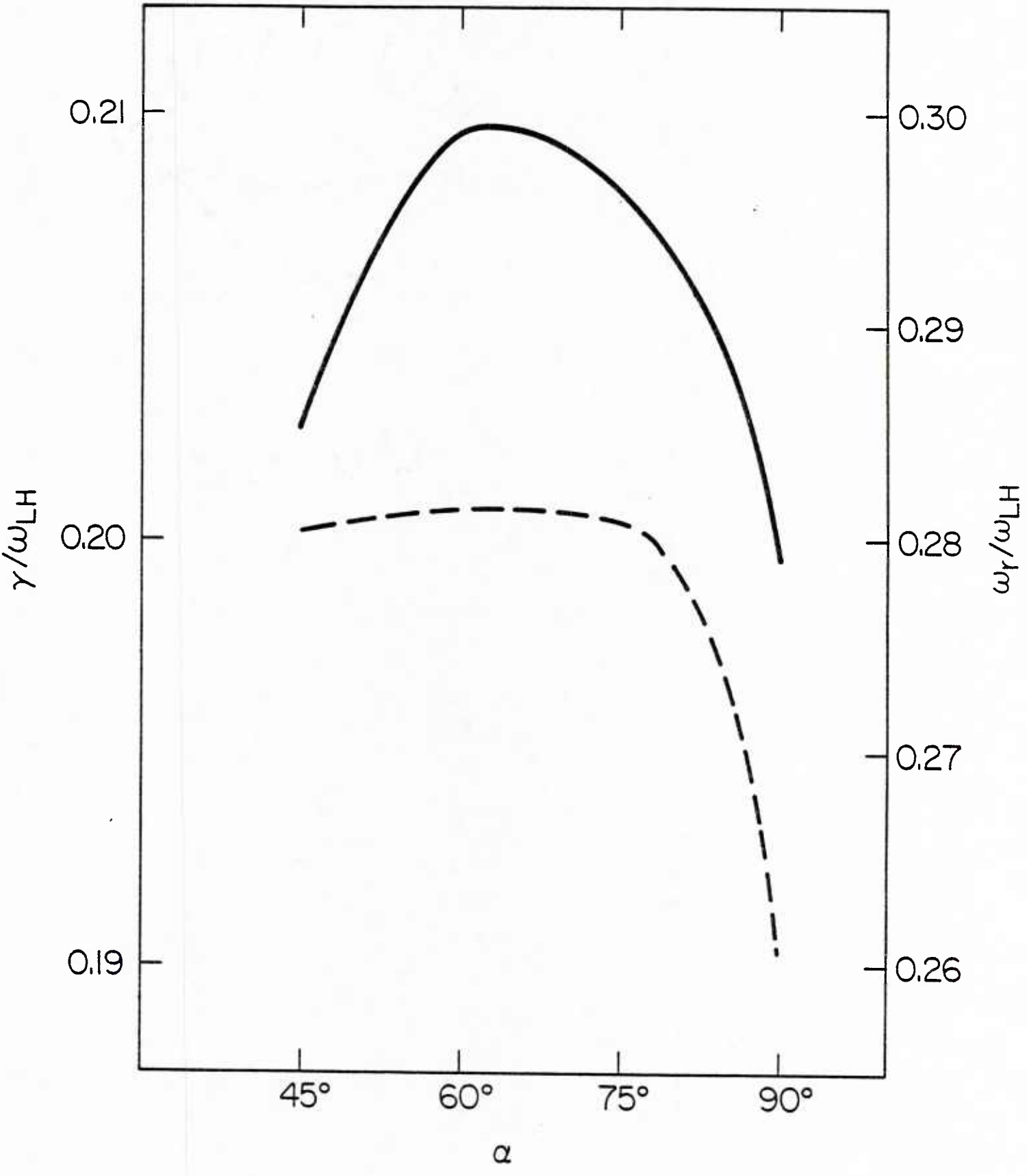
0.21
0.20
0.19
γ/ω_{LH}
0.30
0.29
0.28
0.27
0.26
ω_r/ω_{LH}
45°
60°
75°
90°
α

Figure 4.

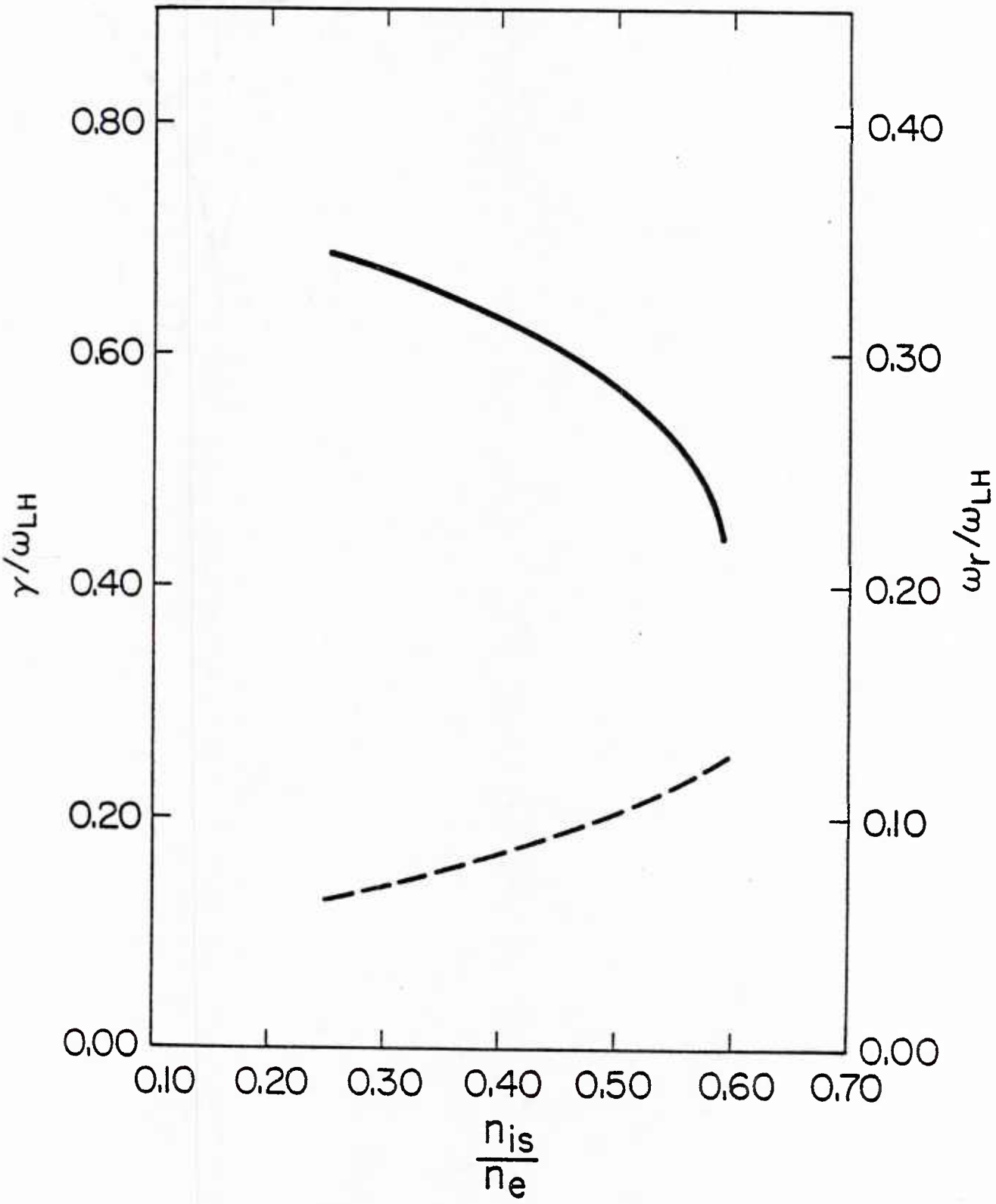
0.80
0.60
0.40
0.20
0.00
0.40
0.30
0.20
0.10
0.00
γ/ω_LH
ω_r/ω_LH
0.10
0.20
0.30
0.40
0.50
0.60
0.70
n_is / n_e

Figure 5.

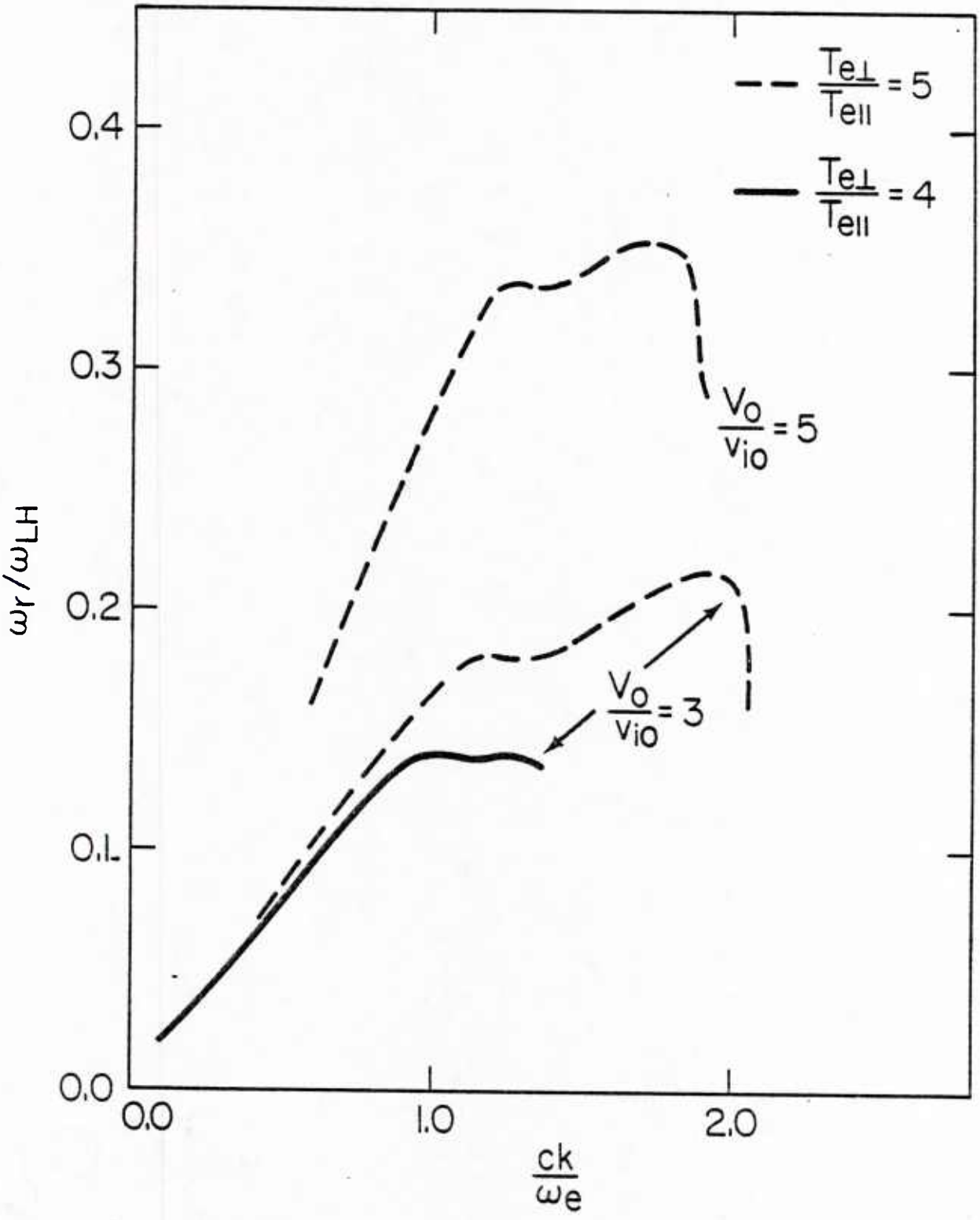
$\frac{T_{e\perp}}{T_{e\parallel}} = 5$
$\frac{T_{e\perp}}{T_{e\parallel}} = 4$
$\frac{V_o}{v_{io}} = 5$
$\frac{V_o}{v_{io}} = 3$
ω_r/ω_{LH}
0.0
0.1
0.2
0.3
0.4
0.0
1.0
2.0
$\frac{ck}{\omega_e}$

Figure 6.

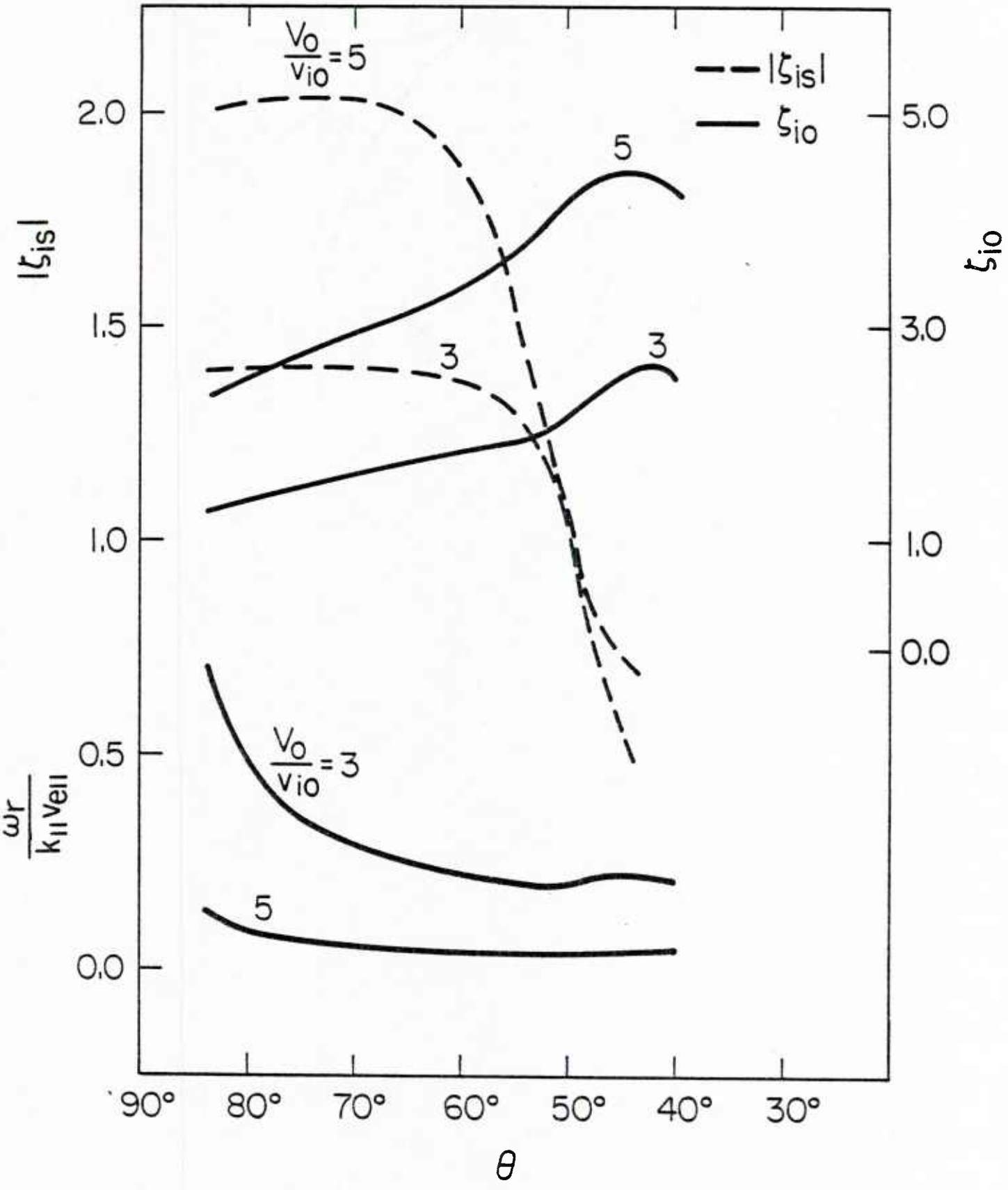
$\frac{V_o}{v_{io}}=5$
$|\zeta_{is}|$
ζ_{io}
5
3
3
$\frac{V_o}{v_{io}}=3$
5
2.0
1.5
1.0
0.5
0.0
5.0
3.0
1.0
0.0
$|\zeta_{is}|$
ζ_{io}
$\frac{\omega_r}{k_{||}v_{e||}}$
90°
80°
70°
60°
50°
40°
30°
θ

Figure 7.

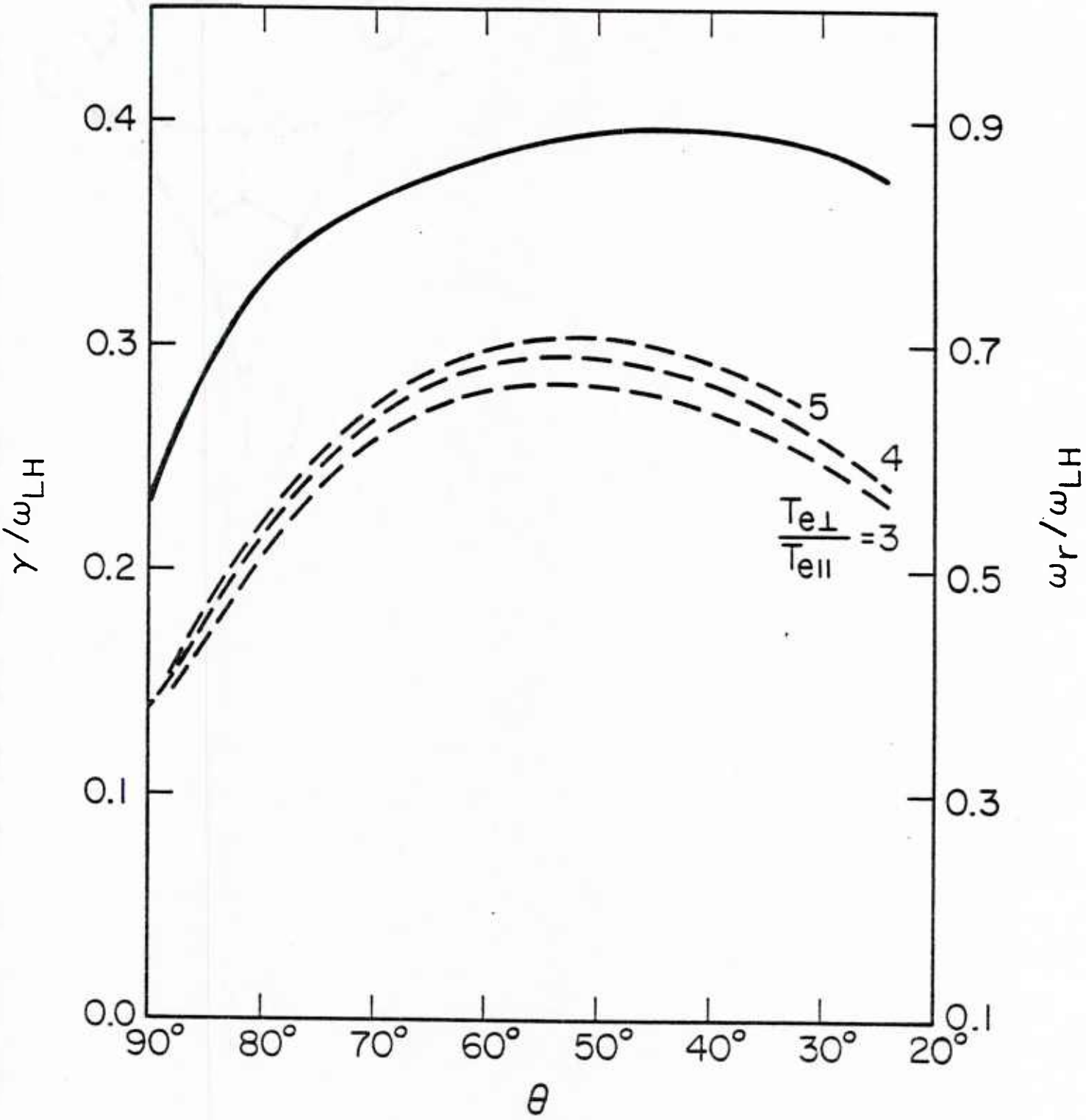
0.4
0.3
0.2
0.1
0.0
0.9
0.7
0.5
0.3
0.1
γ/ω_{LH}
ω_r/ω_{LH}
5
4
$\frac{T_{e\perp}}{T_{e\parallel}}$ =3
90°
80°
70°
60°
50°
40°
30°
20°
θ

Figure 8.

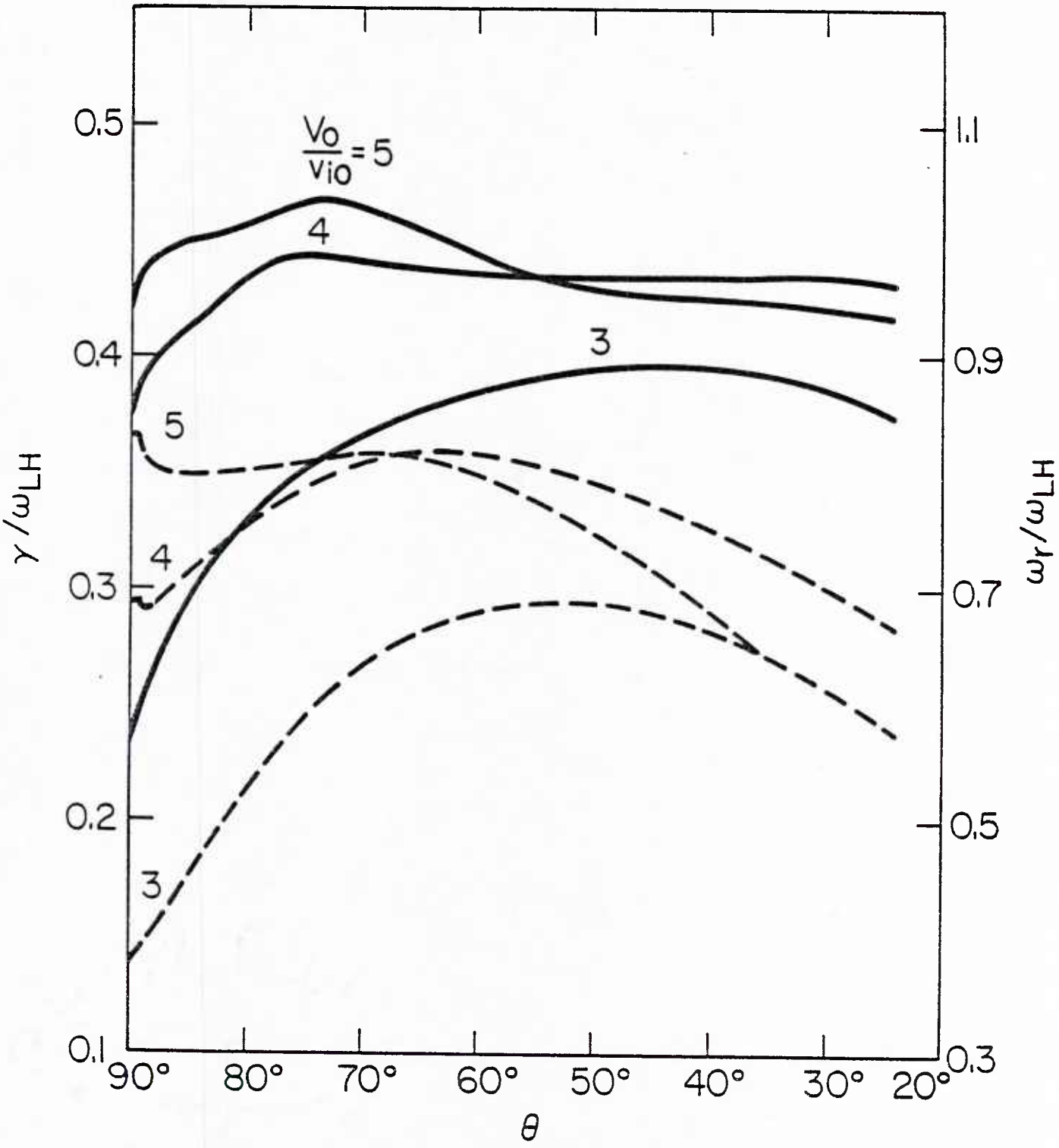
0.5
0.4
0.3
0.2
0.1
$\frac{V_o}{v_{io}} = 5$
4
3
5
4
3
γ/ω_{LH}
1.1
0.9
0.7
0.5
0.3
ω_r/ω_{LH}
90°
80°
70°
60°
50°
40°
30°
20°
θ

Figure 9.

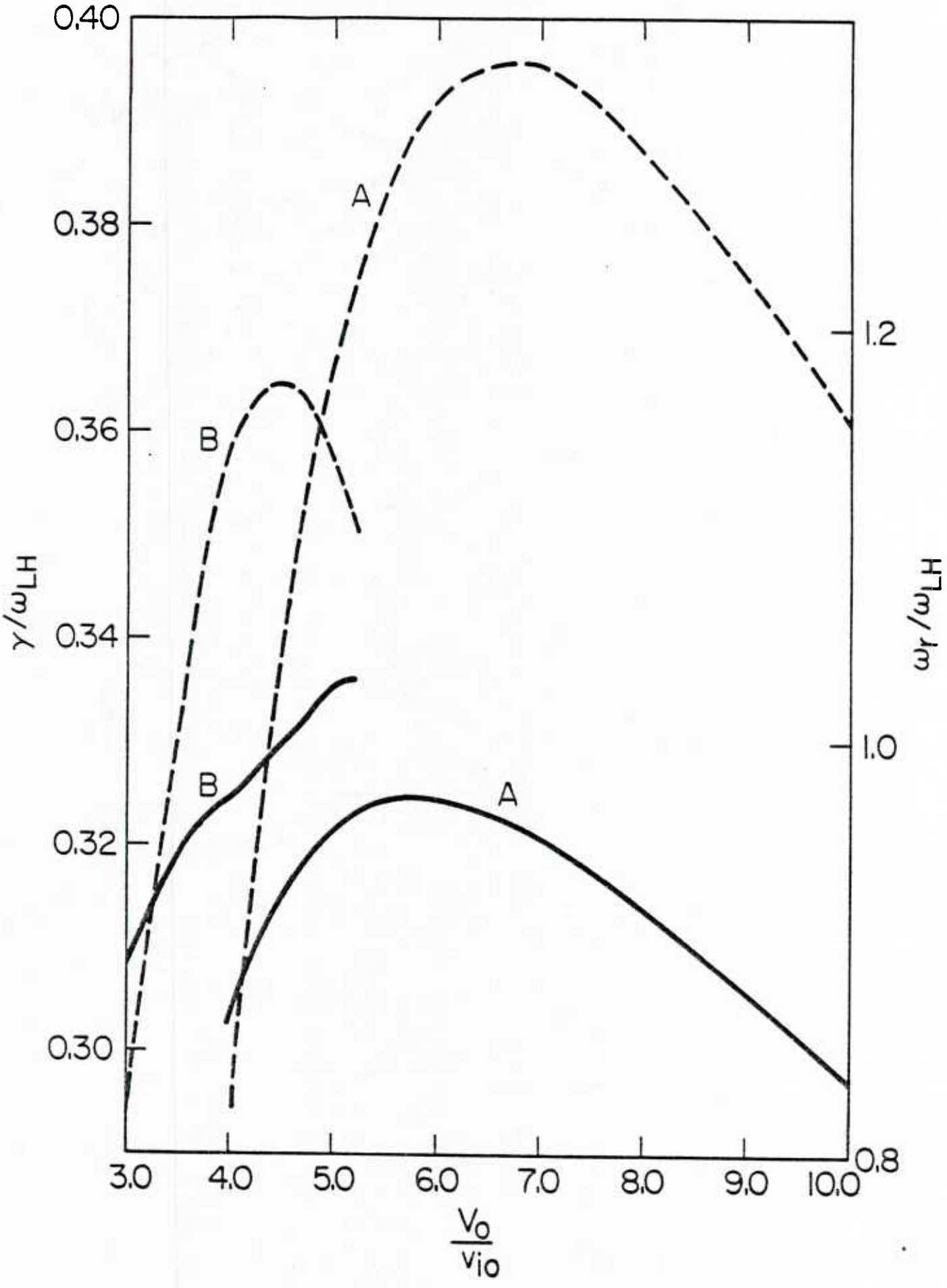
0.40
0.38
0.36
0.34
0.32
0.30
γ/ω_LH
A
B
B
A
1.2
1.0
0.8
ω_r/ω_LH
3.0
4.0
5.0
6.0
7.0
8.0
9.0
10.0
V_o / V_io

Figure 10.

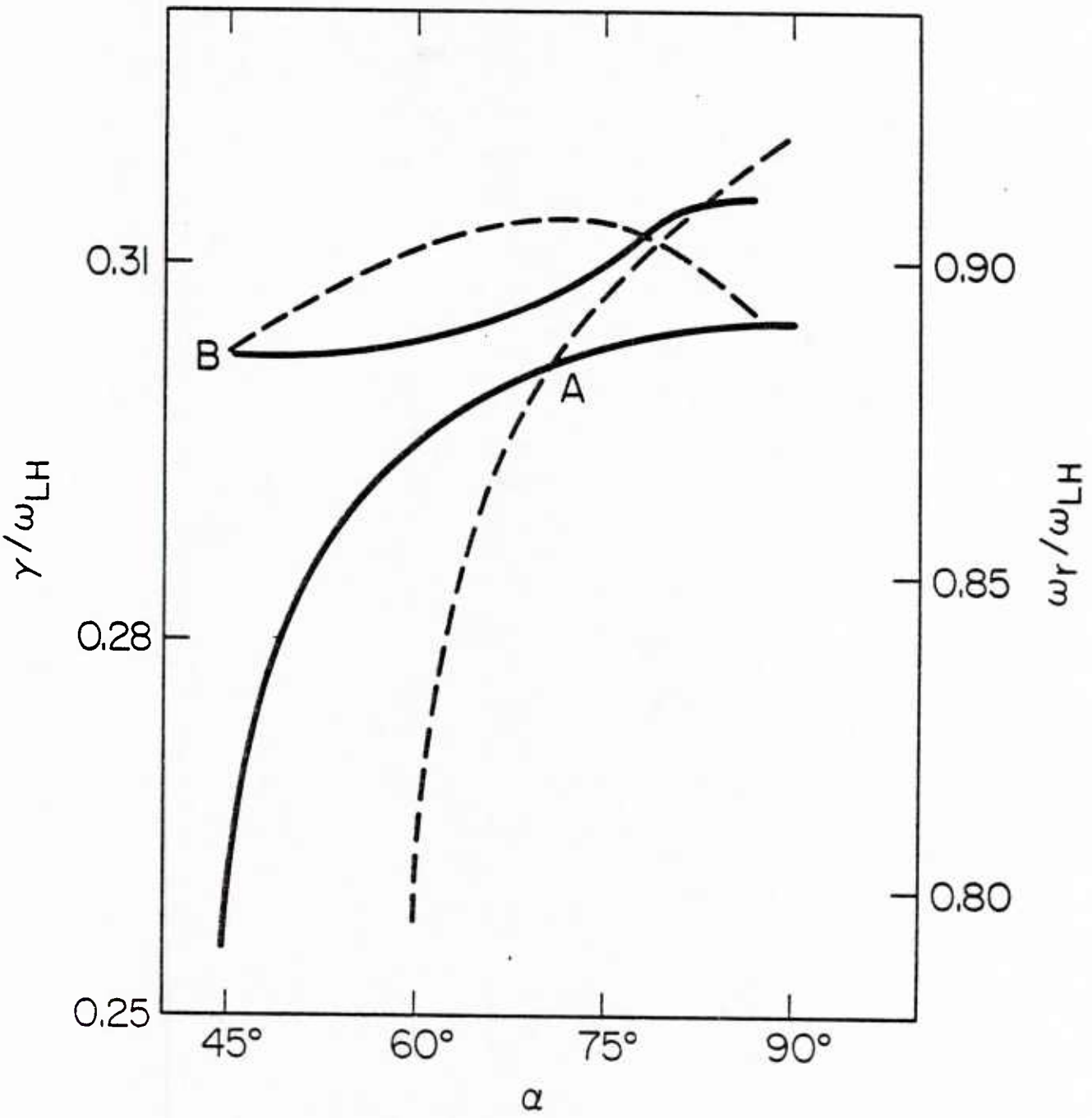

Figure 11.

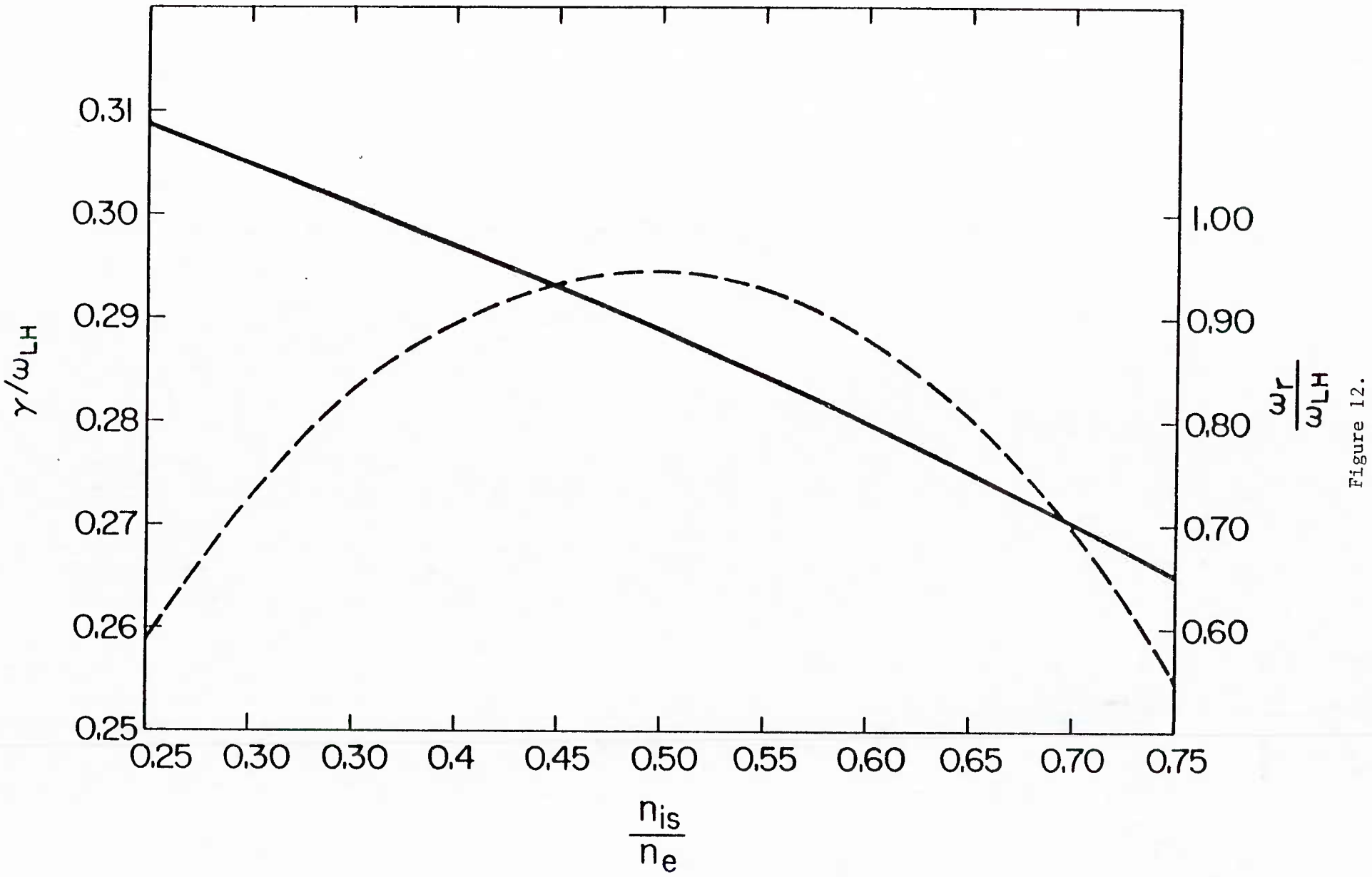
0.31
0.30
0.29
0.28
0.27
0.26
0.25
γ/ω_LH
1.00
0.90
0.80
0.70
0.60
ω_r/ω_LH
0.25 0.30 0.30 0.4 0.45 0.50 0.55 0.60 0.65 0.70 0.75
n_is/n_e

Figure 12.

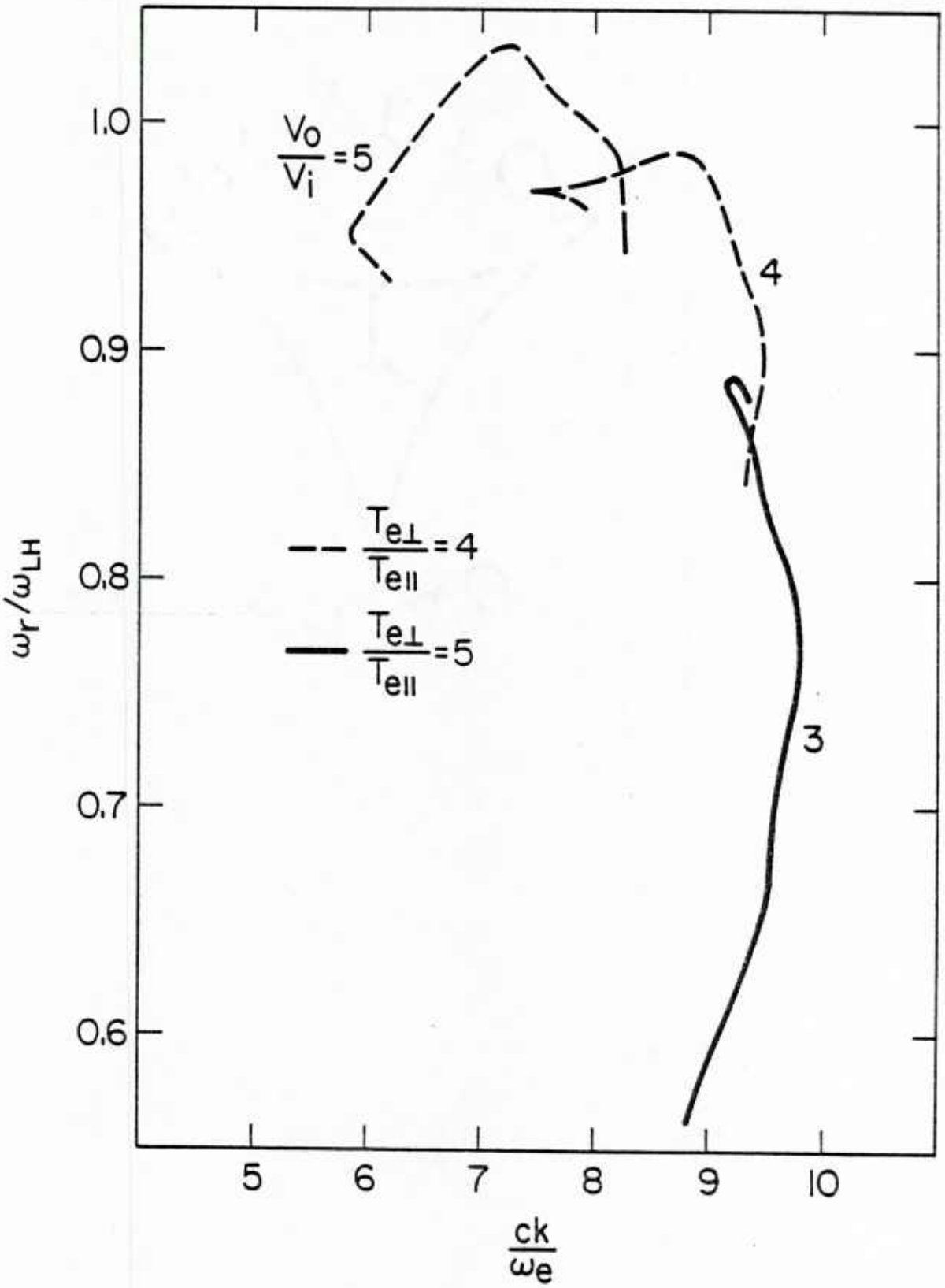
1.0
0.9
0.8
0.7
0.6
ω_r/ω_{LH}
$\frac{V_0}{V_i}=5$
4
2
3
$\frac{T_{e\perp}}{T_{e\parallel}}=4$
$\frac{T_{e\perp}}{T_{e\parallel}}=5$
5
6
7
8
9
10
$\frac{ck}{\omega_e}$

Figure 13.

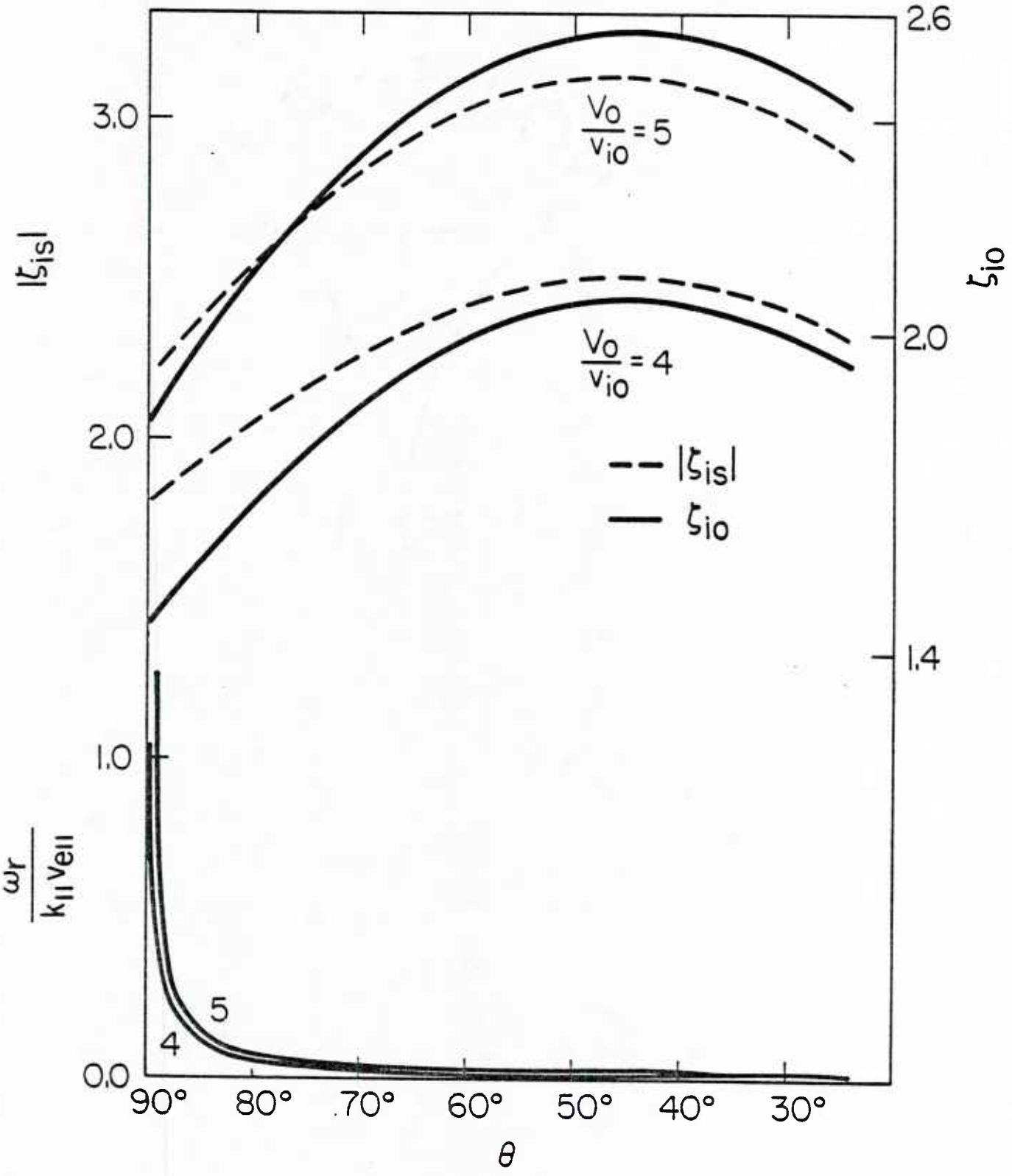
2.6
3.0
2.0
1.4
1.0
0.0
$|\zeta_{is}|$
ζ_{io}
$\frac{V_o}{v_{io}} = 5$
$\frac{V_o}{v_{io}} = 4$
$|\zeta_{is}|$
ζ_{io}
$\frac{\omega_r}{k_{\parallel} v_{e\parallel}}$
5
4
90°
80°
70°
60°
50°
40°
30°
θ

Figure 14.

EFFECT OF ELECTRON THERMAL ANISOTROPY ON THE KINETIC CROSS-FIELD STREAMING INSTABILITY

S.T. Tsai*, M. Tanaka, J.D. Gaffey, Jr., E.H. da Jornada† and C.S. Wu

Institute for Physical Science and Technology,

University of Maryland,

College Park, Maryland 20742

and

L.F. Ziebell

Instituto de Fisica

Universidade Federal do Rio Grande do Sul,

90.000 Porto Alegre, R.S.,

BRASIL

*Permanent address: Institute of Physics
Chinese Academy of Sciences
Beijing, China

†Permanent address: Instituto de Fisica
Universidade Federal do Rio Grande do Sul
90.000 Porto Alegre, R.S. Brasil

ABSTRACT

The investigation of the kinetic cross-field streaming instability, which is motivated by the research of collisionless shock waves and studied by Wu et al. (1983), is discussed more fully in the present work. Since in the ramp region of a quasiperpendicular shock electrons can be preferentially heated in the direction transverse to the ambient magnetic field, the inclusion of the effect of the thermal anisotropy on the instability associated with a shock is both desirable and necessary. The present study has found that $T_{e\perp} > T_{e\parallel}$ can significantly enhance the peak growth rate of the cross-field streaming instability when the electron beta is sufficiently high. Furthermore, the present analysis also improves the analytical and numerical solutions obtained from the earlier theory by Wu et al. (1983).

I. INTRODUCTION

In a previous article (Wu et al., 1983) it has been reported that the relative electron-ion cross-field drift in a perpendicular shock wave can result in a kinetic instability which has the following essential features: (1) the characteristic real frequency of the unstable waves is of the order of the lower-hybrid frequency, (2) the unstable waves are basically whistlers and have mixed electrostatic and electromagnetic polarization, (3) the instability is highly kinetic, and (4) unlike the usual modified two-stream instability (McBride et al., 1972; McBride and Ott, 1972) this instability is not suppressed by electromagnetic effects when the relative electron-ion drift exceeds the Alfven speed of the plasma. Since the free energy which drives the instability is associated with the relative cross-field drift, the unstable whistlers must inherently have oblique or nearly perpendicular propagation. It is anticipated that the growth rate should diminish for waves with wave vectors nearly parallel to the ambient magnetic field B_0. The fact that whistlers can be amplified by streaming ions was first pointed out by Ross (1970).

The instability theory is motivated by the research of collisionless shock waves. The basic physical situation is described and discussed in a review article by Wu et al. (1984). In view of the fact that in a shock front electrons can be heated preferentially in the direction transverse to the ambient magnetic field, it is anticipated that in this region the perpendicular electron temperature, $T_{e\perp}$, may exceed the parallel electron temperature, $T_{e\parallel}$, as evidenced by in situ spacecraft observations (Scudder et al., 1983). Consequently such a thermal anisotropy can provide an additional source of free energy. The pertinent question is how does the anisotropy affect the cross-field streaming instability. With this in mind we feel that the preceding analysis by

Wu et al. (1983) needs to be generalized to include the effect of $T_{e\perp} > T_{e\parallel}$ so that the stability theory can be improved.

In passing we remark that in the preceding work by Wu et al. (1983) we have imposed an approximation. That is, in the dispersion equation we have only retained electron terms associated with $n = 0$ (where n is the cyclotron harmonic number). The justification is that we are only interested in waves with frequencies $\omega << \Omega_e$ and with wavelengths such that $k_\perp^2 v_{e\perp}^2/\Omega_e^2 << 1$. However, numerical solutions of the dispersion equation show that the unstable waves can have wave-numbers $k_\perp \lesssim \omega_e/c$. This implies that for the case $\beta_e \sim 1$ we have $k_\perp v_{e\perp}/\Omega_e \lesssim 1$, which is inconsistent with the postulate. As a result, it appears that in order to improve the numerical solutions we need to consider terms associated with $n \neq 0$. This task is carried out in the present paper in addition to the investigation of the effect of the thermal anisotropy on the instability.

The organization of the paper is described as follows: In Sec. II the basic considerations are introduced. In this section the physical model and assumptions are described, the dispersion tensor is discussed and the plasma parameters for the problem of interest are listed. In Sec. III a numerical analysis of the complete dispersion equation in presented and the treatment of the kinetic cross-field streaming instability of Wu et al. (1983) is generalized to include the effects of electron temperature anisotropy. The discussion is given in Sec. IV. Finally, the summary and conclusions are provided in Sec. V. An alternative form of the dispersion tensor is derived in Appendix A and approximate analytical expressions are obtained in Appendix B.

II. BASIC CONSIDERATIONS

a. Physical Model and Assumptions

In the present study the physical model under consideration is the same as that described by Wu et al. (1983, 1984). In addition to the cross-field ion drift, the electron thermal anisotropy is included in the discussion of this paper. It may be helpful to comment on the assumptions and to describe the model briefly so that the subsequent discussion is self-contained. We consider a one dimensional perpendicular shock. To facilitate our discussion we introduce the following coordinate system. We choose the z axis to be parallel to the ambient magnetic field $\underset{\sim}{B}_0$. All macroscopic quantities vary in the x direction normal to the shock. It is anticipated that a cross-field current can occur in the shock front region because of two principal causes: first, the presence of the electrostatic potential barrier and the diamagnetic effects on the electrons; and, second, the reflection of a small population of ions. In general, the relative drift between electrons and ions can occur in both the x and y directions. The relative drift in the y direction may be attributed to both effects just mentioned, whereas the relative drift in the x direction is only caused by the transmitted and reflected ions. The important point is that there exists a cross-field current in the y direction, but the plasma remains current free in the x direction within the context of the present model, as shown in Fig. 1 of Wu et al. (1983). Thus, in principle, the plasma density inhomogeneity may be significant for the stability of waves propagating in the y-z plane (Wu et al., 1984; Zhou et al., 1983). In the subsequent discussion, the effects of plasma inhomogeneity are neglected. Obviously for waves propagating in the x-z plane,

this assumption is generally justified (Wu et al., 1983; 1984). Moreover, if the $\underset{\sim}{E}_0 \times \underset{\sim}{B}_0$ drift prevails over the diamagnetic drift, the gradient of density and temperature may be of secondary importance in the stability analysis, even for waves propagating in the y-z plane.

We postulate that the unstable waves have frequencies and growth rates much higher than the ion gyrofrequency so that ions may be treated as unmagnetized. This assumption will be checked a posteriori. In the electron frame the reflected ions and the transmitted ions have opposite drift-velocities (Leroy et al., 1981; 1982). Thus, it is expected that there may exist two types of unstable waves; one is excited by the reflected ions and the other by the transmitted ions. Hence, without loss of generality, we only need to consider one ion species in the stability analysis because only one ion species can be in resonance with the wave, since the transmitted and reflected ions have oppositely directed drift relocation in the electron frame. Of course, this leaves out an ion-ion instability, which may not occur in a high Mach number shock wave anyway (Wu et al., 1984).

b. Comments on High Beta Effects

Whistlers with oblique propagation have been discussed in the literature. However, in most discussions it is implicitly assumed that the electron beta of the plasma is very low (i.e. $\beta_e << 1$) . Because the subtlety of this point may not be appreciated at first, an explanation appears to be not only instructive but also rather desirable.

It is usually argued that to study whistlers with oblique propagation, one may approximate and simplify the dispersion tensor by neglecting the electric field perturbation along the magnetic field, δE_z . [Readers are referred to the discussion given on pages 97 and 103 of the review article by Mikhailovskii (1975)]. The point is that for whistlers the

dielectric tensor element ε_{zz}, which is of order ω_e^2/ω^2, where $\omega_e^2 = 4\pi ne^2/m_e$, is large in comparison with the other elements of the dispersion tensor, which are of order k^2c^2/ω^2. This is so for whistlers because the condition

$$\omega_e^2 >> k^2c^2$$

is satisfied. However, it should be pointed out that $\varepsilon_{zz} \sim 0(\omega_e^2/\omega^2)$ is true only when $\omega/k_\parallel > v_e$, where v_e is the electron thermal speed and $k_\parallel$ denotes the component of wave vector $\underset{\sim}{k}$ parallel to the ambient magnetic field. Considering the usual whistler dispersion relation

$$\omega = \frac{c^2k^2}{\omega_e^2}\,\Omega_e \cos\theta \quad , \tag{1}$$

where $\Omega_e = |eB_0/m_ec|$ is the electron cyclotron frequency and $\cos\theta = \underset{\sim}{k}\cdot\underset{\sim}{B}_0/kB_0$, we find

$$\frac{\omega}{k_\parallel v_e} = \frac{ck}{\omega_e}\frac{c\Omega_e}{\omega_e v_e} = \frac{ck}{\omega_e}\frac{1}{\beta_e^{1/2}} \quad . \tag{2}$$

For $\beta_e \simeq 1$, the parallel phase velocity $\omega/k_\parallel$ is apparently smaller than the thermal speed v_e. In this case the aforementioned argument becomes invalid because ε_{zz} is no longer of $0(\omega_e^2/\omega^2)$. In fact, one can readily show that in this case

$$\varepsilon_{zz} = \frac{1}{k_\parallel^2\lambda_e^2} = \frac{2\omega_{pe}^2}{k_\parallel^2 v_e^2} \quad , \tag{3}$$

where λ_e is the electron Debye length. From Eqs. (1) and (3) we find

$$\varepsilon_{zz} \frac{\omega^2}{c^2k^2} = 2 \frac{c^2\Omega_e^2}{v_e^2\omega_e^2} = \frac{2}{\beta_e} \quad . \tag{4}$$

This result implies that if $\beta_e \simeq 1$, ε_{zz} is also of $0(c^2k^2/\omega^2)$. Evidently the approximation of neglecting δE_z is unjustified and the complete 3 x 3 dispersion matrix must be considered for a high-beta plasma. This is the task which we carry out in the present investigation.

c. Dispersion Tensor D_{ij} for an Anisotropic Plasma

To proceed with our discussion we first obtain the expressions for the dispersion tensor elements. In doing so we choose to work in the electron frame of reference, in which the ions are considered to have a cross-field drift $\underset{\sim}{V}_0$. For convenience we assume $\underset{\sim}{k}\cdot\underset{\sim}{V}_0 = k_\perp V_0$, where the wavevector $\vec{k}$ lies in the x-z plane. Because ions are massive their contributions to the electromagnetic perturbations are neglected. Moreover, as mentioned earlier, they are treated as unmagnetized. In the following, the ions and electrons are described by the model distribution functions

$$F_i = \frac{n_i}{\pi^{3/2} v_i^3} \exp\left[- \frac{v_\parallel^2}{v_i^2} - \frac{(v_x - V_0)^2}{v_i^2} - \frac{(v_y - v_d)^2}{v_i^2} \right] , \tag{5}$$

$$F_e = \frac{n_e}{\pi^{3/2} v_{e\parallel} v_{e\perp}^2} \exp\left[- \frac{v_\parallel^2}{v_{e\parallel}^2} - \frac{v_\perp^2}{v_{e\perp}^2} \right] , \tag{6}$$

where v_i , $v_{e\parallel}$ and $v_{e\perp}$ are the ion and the parallel and perpendicular electron thermal velocities, $v_j^2 = 2T_j/m_j$ and v_d represents the $\vec{E} \times \vec{B}$ and diagmagnetic drifts. Waves propagating in the x-z plane are not affected by v_d.

The expression for the dispersion tensor D_{ij} of interest for the present case can be found in the literature (Stix, 1962; Tsai et al., 1981) and are evaluated in Appendix A for the distribution functions (5) and (6).

Hereafter, we shall restrict our discussion to waves which have the following properties:

$$\frac{k_\perp^2 v_{e\perp}^2}{2\Omega_e^2} \lesssim 1 \quad \text{and} \quad \Omega_i << \omega << \Omega_e \tag{7}$$

$$\left| \frac{\omega \pm \Omega_e}{k_\parallel v_{e\parallel}} \right| > 1 \tag{8}$$

$$\frac{\omega}{k_\parallel v_{e\parallel}} < 1 \tag{9}$$

and

$$N^2 = \frac{c^2 k^2}{\omega^2} \sim 0\left(\frac{\omega_e^2}{\omega\Omega_e}\right) . \tag{10}$$

Based on these assumptions we can estimate the order of magnitude of various terms in the dispersion equation. We shall return to this point in Appendix B.

d. Basic Plasma Parameters

Since the present study is mainly motivated by the research of the earth's bow shock, the physical parameters under consideration should be compatible with those of the solar wind, particularly at the bow shock region. Thus, we shall consider:

$$\beta_e \simeq \beta_i = 1$$

$$\frac{\omega_e}{\Omega_e} = 150$$

$$B_0 \cong 7 \quad \gamma$$

$$1 \leq \frac{T_{e\perp}}{T_{e\parallel}} \leq 2$$

$5v_A \leq V_0 \leq 20v_A$ (v_A is the Alfven speed)

$n_e \simeq 10\ cm^{-3}$ (n_e is the electron density) .

The magnitude of the cross-field drift V_0 depends upon its nature and direction. The range given here is based on recent in situ observations by spacecraft (Paschmann et al., 1982) and computer simulation (Leroy et al., 1981 and 1982). Discussion along this line is also presented in Wu et al. (1984).

III. NUMERICAL ANALYSIS OF THE COMPLETE DISPERSION EQUATION

In this section we present a numerical treatment of the complete dispersion equation, which is given in Appendix A. In Fig. 1 the growth rate, maximized over wavenumber, and the real part of the frequency are plotted as a function of the angle of propagation θ for several values of the ion drift velocity. These curves have general features which are similar to those obtained by Wu et al. (1983) for the same values of the parameters, $\beta_e = \beta_i = 1$, $T_{e\perp}/T_{e\parallel} = 1$, and $\omega_e/\Omega_e = 150$. It is seen that increasing the ion drift velocity to several times the Alfven velocity does not suppress the instability, but rather shifts the direction of propagation more nearly parallel to the magnetic field. This result may be attributed to retaining the electromagnetic terms in the dispersion equation. A significant difference between Fig. 1 and Figs. 2 and 3 of Wu et al. (1983) is that the peak growth rate in Fig. 1 in this paper is a slowly decreasing function of the drift velocity for $V_0/v_A > 7.5$ whereas in the figures of Wu et al. it is an increasing function of V_0/v_A up to $V_0/v_A = 20$. This discrepancy occurs because in the present calculation we have retained the sum of electron cyclotron harmonic terms with $n \neq 0$. In general, we find that the terms associated with the cyclotron harmonics $n = \pm 1$ in the dispersion equation must be retained. These terms give rise to a significant modification of the growth rate, as shown. Moreover, terms with $|n| \geq 2$ result in a correction of order 20 %.

The combined effects of electron temperature anisotropy and ion drift are illustrated in Fig. 2. This plot is the same as Fig. 1, except that the electron temperature ratio $T_{e\perp}/T_{e\parallel} = 1.5$ in this case. It is seen that the electron temperature anisotropy reduces the real frequency.

However, the temperature anisotropy significantly increases the peak growth rate and shifts the corresponding direction of propagation to slightly larger angles. These effects are illustrated more clearly in Fig. 3. Here the growth rate is plotted as a function of θ for $V_0/v_A = 10$ and $T_{e\perp}/T_{e\parallel} = 1.0$, 1.5 and 2.0. Decreasing β at constant V_0/v_i greatly increases the growth rate (Wu et al., 1983); however, increasing the temperature ratio $T_{e\perp}/T_{e\parallel}$ results in only a very small increase in the growth rate when $\beta << 1$.

In Fig. 4 the growth rate and real frequency are plotted as functions of the ion drift velocity for the same parameters as in Figs. 1 and 2 Both the growth rate and the real frequency increase rapidly with increasing drift velocity, reach a peak, and then decrease rather slowly after the peak. It is particularly important to note that the peak value of the growth rate occurs for $V_0/v_A \approx 7.5$. Increasing the temperature ratio $T_{e\perp}/T_{e\parallel}$ increases the growth rate for all values of V_0/v_A, but increasing the temperature ratio does not change the value $V_0/v_A \approx 7.5$ where the peak growth rate occurs. It is also seen that the assumptions $\omega_r > \gamma > \Omega_i$ are satisfied.

The real frequency $\omega_r(k)$ corresponding to the maximum growth rate is plotted as a function of the wavevector k in Fig. 5. It is seen that the assumption $ck/\omega_e << 1$ is not satisfied in many cases and the terms of order c^2k^2/ω_e^2 must be retained in the dispersion equation, as discussed in Wu et al. (1983) and Appendix B.

The arguments of the plasma dispersion function $z_0 = \omega_r/k_\parallel v_{e\parallel}$ and $|\zeta_i| = |(\omega_r - k_\perp V_0)/kv_i|$ corresponding to maximum growth rate are plotted in Fig. 6 as a function of the angle of propagation. The following two conditions,

$$\frac{\omega_r}{k_{\parallel}v_{e\parallel}} \lesssim 1 \quad \text{and} \quad \frac{|\omega_r - k_{\perp}V_0|}{kv_i} \gtrsim 1$$

are satisfied over the entire range of θ. This is a further indication of the kinetic nature of the instability studied in this paper. For the maximum growth rate

$$\frac{\omega_r}{k_{\parallel}v_{e\parallel}} \approx 0.5 \quad \text{and} \quad \frac{|\omega_r - k_{\perp}V_0|}{kv_i} \approx 1.6 \ ,$$

and the assumption (9), $\omega_r/k_{\parallel}v_{e\parallel} < 1$ is only marginally satisfied. Because of the highly kinetic nature of the instability and the importance of the terms c^2k^2/ω_e^2, it is not possible to treat this instability accurately in a simple way. However, the discussion in Sec. IV helps to illustrate the physics of this instability.

Another important characteristic of the instability is that it has mixed polarization, with electromagnetic as well as electrostatic components. The ratio of electromagnetic to electrostatic electric field energy density is plotted in Fig. 7 as a function of θ for V_0/v_A = 5,10, 15,20 and $T_{e\perp}/T_{e\parallel}$ = 1.0 and 1.5. For smaller values of V_0/v_A, the mode propagates more nearly perpendicular to the magnetic field, and the polarization is predominantly electrostatic. For larger values of V_0/v_A the mode propagates more obliquely, and the electromagnetic component of the electric field becomes comparable to the electrostatic component. The ratio of the electromagnetic to electrostatic field energy density increases with increasing drift velocity. Increasing the temperature ratio $T_{e\perp}/T_{e\parallel}$ increases $|\delta E_{em}|^2/|\delta E_{es}|^2$ slightly. Although the ratio of electromagnetic to electrostatic electric field energy density is less than one in all cases, the ratio of fluctuating magnetic field energy density to electrostatic electric field energy density can be

very large, since

$$\frac{|\delta B_{em}|^2}{|\delta E_{es}|^2} = \frac{c^2 k^2}{|\omega|^2} \frac{|\delta E_{em}|^2}{|\delta E_{es}|^2} \quad ,$$

from Ampere's law and $c^2k^2/|\omega|^2$ is very large because the phase velocity of the waves is small (Lemons and Gary 1977).

IV. DISCUSSION

The numerical analysis in the previous section shows that an electron temperature anistoropy $T_{e\perp} > T_{e\parallel}$ results in a substantial increase of the peak growth rate and a decrease of the real frequency for large angles of propagation. However, the fundamental nature of the unstable waves is essentially the same as in the isotropic case; that is, they are basically obliquely propagating whistlers. This suggests that the graphs in Sec. III may be qualitatively interpreted using the theory for the isotropic case.

Before proceeding, a significant point should be also mentioned. That is, the ion dynamics influence the wave dispersion even when the relative electron-ion cross-field drift is small and negligible. This can occur in the case of the solar wind, for which the ion plasma frequency is comparable to the electron cyclotron frequency. In the following we write the dispersion equation, including the ion dynamics (Wu et al. 1983), as

$$\frac{\omega_r^2}{\omega_0^2} = \frac{A}{A - \sin^2\theta} \quad , \tag{11}$$

where

$$A = \beta_i / \mathrm{Re}Z'(\zeta_i^0) - \beta_e/2 \quad ,$$

$$\zeta_i^0 = \frac{\omega_0 - k_\perp V_0}{k\bar{v}_A \beta_i^{\frac{1}{2}}} \quad ,$$

$$\omega_0 = \frac{c^2 k^2}{\omega_e^2} \Omega_e \cos\theta \quad .$$

Since the curves in the previous section were calculated for the maximum growth rate, we use the ion resonant condition $\omega_r = k_\perp V_0$ to obtain

$$\frac{\omega_r}{\omega_{LH}} = \frac{ck}{\omega_e}\frac{V_0}{v_A}\sin\theta \ , \tag{12}$$

which is an increasing function of the wavenumber, of the drift velocity and of the angle of propagation. This equation describes how the real frequency changes as a function of $(V_0/v_A)\sin\theta$, for the value of k that maximizes the growth rate. If we now substitute the resonant condition into Eq. (11), neglecting the effect of the ions for simplicity, we obtain

$$\frac{V_0}{v_A}\sin\theta = \left(\frac{m_i}{m_e}\right)^{\frac{1}{2}}\frac{ck}{\omega_e}\cos\theta \ . \tag{13}$$

The set of equations (12) and (13) are convenient to describe the nature of Figs. 1 to 6. From Eq. (13) we infer that $(V_0/v_A)\sin\theta$ and V_0/v_A , for the value of k that maximizes the growth rate, are both decreasing functions of the propagation angle. Therefore, the real frequency is an increasing function of the drift velocity. In Fig. 5, the larger the ratio V_0/v_A , the bigger the value of the frequency. Since ω_r/ω_{LH} increases linearly with k , as shown in Eq. (12), our qualitative estimate is in good agreement with Fig. 5, as well as with Fig. 4 when V_0/v_A is not too large. Furthermore, from Eq. (13) we also deduce that, at sufficiently small propagation angles, the drift velocity assumes large values and the increase of the parameter V_0/v_A dominates the increase of $(V_0/v_A)\sin\theta$ as we decrease the angle of propagation. Therefore, when the drift velocity is large, a small decrease in θ can produce a significant variation in V_0/v_A , without

changing the value of $(V_0/v_A)\sin\theta$. In this way, the flat region of the real frequency for large values of the drift velocity shown in Fig. 4 can also be qualitatively described.

In Figs. 1, 2 and 3, the real frequency is plotted as a function of the propagation angle, for several values of the drift velocity. Since each point on these curves has a different value of k , which approximately satisfies Eq. (12), it is convenient to combine Eqs.(12) and (13) to eliminate k . This gives

$$\frac{\omega_r}{\omega_{LH}} = \left(\frac{m_e}{m_i}\right)^{\frac{1}{2}} \frac{V_0^2}{v_A^2} \sin\theta \tan\theta \ , \tag{14}$$

which increases very rapidly with angle at a fixed V_0/v_A , as shown in Figs. 1, 2 and 3, and increases with V_0/v_A at fixed angle, as shown in Figs. 1 and 2.

In Fig. 6 it is seen that $|\omega_r - k_\perp V_0|/kv_i$ is of order unity, even though ω_r/kv_i and V_0/v_i are large. This shows that the ion resonant condition is nearly satisfied in all cases, which justifies the use of Eq. (12) in this discussion. The quantity $\omega_r/k_\parallel v_{e\parallel}$ is also of order unity when the drift velocity or the propagation angle is large. The results $|\omega_r - k_\perp v_0|/kv_i \gtrsim 1$ and $\omega_r/k_\parallel v_{e\parallel} \lesssim 1$ clearly indicate the kinetic nature of the cross-field streaming instability. Similar results were obtained in the previous study of Wu et al. (1983). Based on the arguments presented at the beginning of this section, we could have anticipated that the inclusion of the electron thermal anisotropy results only in minor modifications of the curves, as shown in Fig. 6.

Although it is difficult to obtain quantitatively accurate expressions for the growth rates because they are sensitive to small changes of the variables, the qualitative shape of the graphs of the growth

rates can be understood easily. For very small angles, the mode is stable because the nearly parallel propagating wave is unable to interact efficiently with the perpendicular ion drift. As the angle increases, the ion growth initially increases faster than the electron damping and an instability develops. Eventually, the growth rate curve turns over and decreases with increasing angle when the electron damping increases faster than the ion growth. Finally, the mode becomes stable at an angle less than 90°. These effects are shown clearly in Fig. 1, 2 and 3. Furthermore, because the qualitative analysis for the maximum growth rate has demonstrated that the ratio V_0/v_A is a decreasing function of θ, we expect the peak growth rate to move toward the region of increasing propagation angle, as the drift velocity decreases, in agreement with Figs. 1 and 2.

In Fig. 4 the growth rates increase initially with the drift velocity because the free energy which feeds the instability is proportional to $\frac{1}{2} m_i V_0^2$. The growth rates reach a maximum at $V_0/v_A \simeq 7.5$, and then decrease with increasing drift velocity because the angle at which the growth rate peaks decreases, which increases $k_\parallel$ and the electron Landau damping.

In short, this discussion qualitatively explains the essential features of the numerical analysis of the kinetic cross-field streaming instability presented in Sec. III. The most important results are that the unstable waves have been identified as whistlers, and that the growth rate is largest for oblique angles of propagation.

V. SUMMARY AND CONCLUSIONS

We have investigated both analytically and numerically the kinetic instability produced by a relative electron-ion cross-field drift and an electron temperature anisotropy $T_{e\perp}/T_{e\parallel} > 1$. The unstable waves have been shown to be whistlers as discussed in Sec. IV. The instability is not suppressed by electromagnetic effects when $V_0/v_A > 1$ and $\beta \sim 1$. This agrees with the results of Lemons and Gary (1977). As can be seen in the numerical results in Sec. III, the effect of increasing V_0/v_A is to shift the direction of propagation more nearly parallel to the magnetic field. The effect of increasing the electron temperature ratio $T_{e\perp}/T_{e\parallel}$ is to increase the growth rate and to shift the direction of propagation more nearly perpendicular to the magnetic field. The mode has mixed electrostatic and electromagnetic polarization. However, for $\beta \sim 1$ and for nearly perpendicular propagation the mode is predominantly electrostatic, whereas for more oblique propagation, the electromagnetic and electrostatic components are nearly equal. Finally for β small, the mode becomes the well known modified two-stream instability (Wu et al., 1983).

In summary we have studied the plasma instability resulting from a cross-field ion drift and an electron temperature anisotropy, $T_{e\perp}/T_{e\parallel} > 1$. We find that both effects significantly affect the instability. In particular, the present study has led to the following major conclusions:

1. A relative electron-ion cross-field drift can cause instability, even if $V_0/v_A > 1$.

2. An electron temperature anisotropy $T_{e\perp}/T_{e\parallel} > 1$ significantly enhances the peak growth rate.

3. The unstable waves have both electrostatic and electromagnetic components in general. For $\beta \sim 1$ and nearly parallel propagation,

the electrostatic and electromagnetic components are comparable and the polarization is mixed.

4. The instability is highly kinetic for high $\beta \sim 1$. From numerical solutions of the dispersion equation we find that

$$\frac{\omega_r}{k_{\parallel} v_{e\parallel}} \lesssim 1 \quad \text{and} \quad \frac{|\omega_r - k_{\perp} v_0|}{k v_i} \gtrsim 1$$

over the entire range of angles of propagation. In addition, electromagnetic effects, high order electron cyclotron harmonics, and ion terms all affect the dispersion equation significantly and therefore it is difficult to treat the dispersion equation accurately by analytic techniques.

Since the instability is driven by an ion - wave resonance, the growth rate is proportional to the number density of the resonant ions. Thus, if one wants to apply the results to the instability associated with the reflected ions, he must bear in mind that the growth rate should be reduced by a factor n_r/n_0. If $n_r/n_0 \lesssim 0.2$, such an approximate estimate should be sufficient. Correspondingly, for transmitted ions the growth is modified by a factor n_t/n_0 which is of order unity. However, in other situations, the real frequency as well as the growth rate may be significantly modified by the densities of the two ion species (Gaffey, da Jornada, Winske, and Wu, 1984).

In addition to the obliquely propagating kinetic cross-field streaming instability, there is also a quasi-parallel propagating whistler instability which can be excited by an electron temperature anisotropy $T_{e\perp}/T_{e\parallel} > 1$ (Kennel and Petschek, 1966; Sharer and Trivelpiece, 1967; Mikhailovskii, 1975). The maximum growth rate occurs for exactly parallel propagation, and

the growth rate decreases very rapidly as the angle of propagation increases. This mode is insensitive to ion streaming, and it does not couple to the cross-field streaming instability. The application of the parallel whistler to the earth's shock is discussed in a recent article (Wu et al., 1984).

ACKNOWLEDGMENTS

The authors thank Dr. D. Winske and Dr. H.K. Wong for useful discussions. The present research was supported in part by the U.S. Office of Naval Research under grant N00014-82-K-0208, in part by the National Aeronautics and Space Administration under grant NAGW-81, and in part by the Conselho Nacional de Desenvolvimento Científico e Tecnológico and the Financiadora de Estudo e Projetos, of Brazil.

REFERENCES

Gaffey, Jr., J. D., da Jornada, E. H., Winske, D., Wu, C. S., 1984, Phys. Fluids 25 (to be submitted)

Hsia, J.B., Chiu, S.M., Hsia, M.F., Chou, R.L., and Wu, C.S., 1979, Phys. Fluids, 22, 1737.

Kennel, C.F. and Petschek, H.E., 1966, J. Geophys. Res. 71, 1.

Lemons, D.S., Gary, S.P., 1977, J. Geophys. Res., 82, 2337.

Leroy, M.M., Goodrich, C.C., Winske, D., Wu, C.S., and Papadopoulos, K. 1981, Geophys. Res. Lett., 8, 1269.

Leroy, M.M., Winske, D., Goodrich, C.C., Wu, C.S. and Papadopoulos, K., 1982, J. Geophys. Res., 87, 5081.

McBride, J.B. and Ott, E., 1972, Phys. Lett., 39A, 363.

McBride, J.B., Ott, E., Boris, J.P., and Orens, J.H., 1972, Phys. Fluids, 15, 2367.

Mikhailovskii, A.B., 1975, Reviews of Plasma Physics, Vol. 6, ed. M.A. Leontovich, Consultants Bureau, New York.

Paschmann, G., Sckopke, N., Bame, S.J. and Gosling, J.T., 1982, Geophys. Res. Lett., 9, 881.

Ross, D.W., 1970, Phys. Fluids, 12, 764.

Scudder, J.D., Mangeney, A., Gosling, J.T., Paschmann, G., Wu, C.S., Russell, C.R., Rodriguez, P., Anderson, R.R., Bame, S.J., Filzenreiter, R.J., Harvey, C., Hoppe, M., Lacombe, J., Ogilvie, K.W., and Sckopke, N., 1983, J. Geophys. Res., 88, (to be submitted).

Sharer, J.R. and Trivelpiece, A.W. 1967, Phys. Fluids, 10, 591.

Stix, T.H., 1962, The Theory of Plasma Waves, McGraw-Hill, New York.

Tsai, S.T., Wu, C.S., Wang, Y.D., and Kang, S.W., 1981, Phys. Fluids 24, 2186.

Wu, C.S., Zhou, Y.M., Tsai, S.T., Guo, S.C., Winske, D. and Papadopoulos, K., 1983, Phys. Fluids, 26, 1259.

Wu, C.S., Winske, D., Zhou, Y.M., Tsai, S.T., Rodriguez, P., Tanaka, M., Papadopoulos, K., Akimoto, K., Lin, C.S., Leroy, M.M., and Goodrich, C.C., 1984, Space Science Review, 36, (in press).

Zhou, Y. M., Wong, H. K., Wu, C. S., and Winske, D., 1983, J. Geophys. Res. 88, 3026.

APPENDIX A

In this appendix we derive an alternative form of the dispersion tensor, including the ion terms and the electron temperature anisotropy, in a representation based on the electrostatic and electromagnetic potentials $\delta\phi,\delta\underset{\sim}{A}$, rather than the electric field $\delta\underset{\sim}{E}$. We do this for two reasons; first, to make contact with and generalize our previous analysis of the kinetic cross-field streaming instability (Wu et al., 1983), which is based on an earlier paper (Hsia et al., 1979), and second, for the greater algebraic simplicity inherent in the $\delta\phi,\delta\underset{\sim}{A}$ representation. This point will be discussed further below.

Since $\delta\underset{\sim}{E} = -ik\delta\phi + i(\omega/c)\delta\underset{\sim}{A}$ and $\underset{\sim}{k}\cdot\delta\underset{\sim}{A} = 0$ (Coulomb gauge), we can write

$$\begin{pmatrix} \delta E_x \\ \delta E_y \\ \delta E_z \end{pmatrix} = \frac{i\omega}{c} \begin{pmatrix} -\frac{k_\perp}{k} & 0 & -\frac{k_\parallel}{k_\perp} \\ 0 & 1 & 0 \\ -\frac{k_\parallel}{k} & 0 & 1 \end{pmatrix} \begin{pmatrix} N\delta\phi \\ \delta A_y \\ \delta A_z \end{pmatrix} , \qquad \text{(A1)}$$

where we have taken $\underset{\sim}{k} = (k_\perp, 0, k_\parallel)$ and $N = ck/\omega$. In the following we define the dispersion matrix $||D_{ij}||$ in the $\delta\underset{\sim}{E}$ and $\delta\phi,\delta\underset{\sim}{A}$ representations such that Maxwell's equations become

$$\begin{pmatrix} D_{xx} & D_{xy} & D_{xz} \\ D_{yx} & D_{yy} & D_{yz} \\ D_{zx} & D_{zy} & D_{zz} \end{pmatrix} \begin{pmatrix} \delta E_x \\ \delta E_y \\ \delta E_z \end{pmatrix} = 0$$

and

$$\begin{pmatrix} D_{11} & D_{12} & D_{13} \\ D_{21} & D_{22} & D_{23} \\ D_{31} & D_{32} & D_{33} \end{pmatrix} \begin{pmatrix} N\delta\phi \\ \delta A_y \\ \delta A_z \end{pmatrix} = 0 \qquad \text{(A2)}$$

One can readily show from (A1) and (A2) that

$$
\begin{aligned}
D_{11} &= \frac{k_\perp^2}{k^2} D_{xx} + \frac{2k_\perp k_\parallel}{k^2} D_{xz} + \frac{k_\parallel^2}{k^2} D_{zz} \\
D_{12} &= -D_{21} = -\left(\frac{k_\perp}{k} D_{xy} - \frac{k_\parallel}{k} D_{yz}\right) \\
D_{13} &= \frac{k^2}{k_\perp^2} D_{31} = \frac{k}{k_\perp}\left[\frac{k_\perp k_\parallel}{k^2}(D_{xx}-D_{zz}) - \frac{(k_\perp^2-k_\parallel^2)}{k^2} D_{xz}\right] \\
D_{22} &= D_{yy} \\
D_{23} &= -\frac{k^2}{k_\perp^2} D_{32} = \frac{k}{k_\perp}\left(\frac{k_\parallel}{k} D_{xy} + \frac{k_\perp}{k} D_{yz}\right) \\
D_{33} &= \frac{k_\parallel^2}{k^2} D_{xx} - \frac{2k_\perp k_\parallel}{k^2} D_{xz} + \frac{k_\perp^2}{k^2} D_{zz} \quad .
\end{aligned}
\tag{A3}
$$

The expressions for $D_{ij}(i,j = x,y,z)$ in the $\delta\underset{\sim}{E}$ representation can be written in terms of the dielectric tensor ε_{ij} such that

$$
D_{ij} = N^2\left(\frac{k_i k_j}{k^2} - \delta_{ij}\right) + \varepsilon_{ij}(\underset{\sim}{k},\omega) \quad . \tag{A4}
$$

The electron contribution to ε_{ij} may be found in the literature. For the bi-Maxwellian distribution function given in Eq. (5) with $T_{e\perp} \neq T_{e\parallel}$ $\varepsilon_{ij}^{(e)}$ has been derived by Stix (1962) and recently by Tsai et al. (1981), including relativistic effects. Making use of the approximations that the ions may be treated as unmagnetized and neglecting the electromagnetic ion terms one finds

$$
D_{xx}=1-N^2\cos^2\theta + \frac{\omega_e^2}{\omega^2}\left[\left(\frac{T_{e\perp}}{T_{e\parallel}}-1\right)+\frac{T_{e\perp}}{T_{e\parallel}}\frac{e^{-\mu}}{\mu}\sum_{n=-\infty}^{\infty} n^2 I_n(\mu)\bar{z}_n Z(z_n)\right]+\varepsilon^{(i)}\sin^2\theta
$$

$$
D_{xy}=-D_{yx}=\frac{i\omega_e^2}{\omega^2}\frac{T_{e\perp}}{T_{e\parallel}} e^{-\mu}\sum_{n=-\infty}^{\infty} n[I_n(\mu)-I_n'(\mu)]\bar{z}_n Z(z_n)
$$

$$D_{yy}=1-N^2+\frac{\omega_e^2}{\omega^2}\left(\left(\frac{T_{e\perp}}{T_{e\parallel}}-1\right)+\frac{T_{e\perp}}{T_{e\parallel}}e^{-\mu}\mu\sum_{n=-\infty}^{\infty}\left\{\frac{n^2}{\mu^2}I_n(\mu)+2[I_n(\mu)-I_n'(\mu)]\right\}\bar{z}_n Z(z_n)\right)$$

$$D_{xz}=D_{zx}=N^2\sin\theta\cos\theta+\frac{\omega_e^2}{\omega^2}\left[-\frac{k_\perp}{k_\parallel}\left(\frac{T_{e\perp}}{T_{e\parallel}}-1\right)+\frac{2\Omega_e}{k_\perp v_{e\parallel}}e^{-\mu}\sum_{n=-\infty}^{\infty}nI_n(\mu)\bar{z}_n z_n Z(z_n)\right]+\varepsilon^{(i)}\sin\theta\cos\theta$$

$$D_{yz}=-D_{zy}=-\frac{i2\omega_e^2}{\omega^2}\frac{\Omega_e}{k_\perp v_{e\parallel}}e^{-\mu}\mu\sum_{n=-\infty}^{\infty}[I_n(\mu)-I_n'(\mu)]\bar{z}_n z_n Z(z_n) \qquad \text{(A5)}$$

$$D_{zz}=1-N^2\sin^2\theta+\frac{\omega_e^2}{\omega^2}\left[\frac{k_\perp^2}{k_\parallel^2}\left(\frac{T_{e\perp}}{T_{e\parallel}}-1\right)+2z_0^2+2e^{-\mu}\sum_{n=-\infty}^{\infty}I_n(\mu)\bar{z}_n z_n^2 Z(z_n)\right]+\varepsilon^{(i)}\cos^2\theta$$

where

$$\varepsilon^{(i)}=\frac{2\omega_i^2}{k^2v_i^2}\left[1+\zeta_i Z(\zeta_i)\right] \quad ,$$

I_n is a modified Bessel function, Z is the plasma dispersion function, and the following definitions have been introduced:

$$\omega_j^2=\frac{4\pi ne^2}{m_j} \quad , \quad \Omega_j=\left|\frac{e_j B_0}{m_j c}\right| \quad , \quad v_j^2=\frac{2T_j}{m_j} \quad ,$$

$$\mu=\frac{k_\perp^2 v_{e\perp}^2}{2\Omega_e^2} \quad , \quad z_n=\frac{(\omega-n\Omega_e)}{k_\parallel v_{e\parallel}} \quad , \quad \bar{z}_n=\frac{[\omega-n\Omega_e(1-\frac{T_{e\parallel}}{T_{e\perp}})]}{k_\parallel v_{e\parallel}} \quad , \text{ and } \zeta_i=\frac{(\omega-k_\perp V_0)}{kv_i} \quad .$$

Substituting (A5) into (A3) yields

$$D_{11}=1+\frac{2\omega_e^2}{\omega^2}\frac{k_\parallel^2}{k^2}z_0^2[1+e^{-\mu}\sum_{n=-\infty}^{\infty}I_n(\mu)\bar{z}_n Z(z_n)]+\frac{2\omega_i^2}{k^2v_i^2}[1+\zeta_i Z(\zeta_i)]$$

$$D_{12}=-D_{21}=-\frac{i\omega_e^2}{\omega\Omega_e}\frac{k_\perp}{k}\frac{T_{e\perp}}{T_{e\parallel}}e^{-\mu}\sum_{n=-\infty}^{\infty}[I_n(\mu)-I_n'(\mu)]\bar{z}_n Z(z_n)$$

$$D_{13}=\frac{k^2}{k_\perp^2}D_{31}=-\frac{2\omega_e^2}{\omega^2}\frac{k_\parallel}{k}z_0^2[1+e^{-\mu}\sum_{n=-\infty}^{\infty}I_n(\mu)(1-\frac{n\Omega_e}{\omega}\frac{k^2}{k_\perp^2})\bar{z}_n Z(z_n)]$$

$$D_{22}=1-N^2+\frac{\omega_e^2}{\omega^2}\left(\left(\frac{T_{e\perp}}{T_{e\parallel}}-1\right)+\frac{T_{e\perp}}{T_{e\parallel}}e^{-\mu}\mu\sum_{n=-\infty}^{\infty}\left\{\frac{n^2}{\mu^2}I_n(\mu)+2[I_n(\mu)-I_n'(\mu)]\right\}\bar{z}_n Z(z_n)\right) \qquad (A6)$$

$$D_{23}=-\frac{k_\perp^2}{k_\perp^2}D_{32}=-\frac{i\omega_e^2}{\omega\Omega_e}\frac{k_\perp}{k_\parallel}\frac{T_{e\perp}}{T_{e\parallel}}e^{-\mu}\sum_{n=-\infty}^{\infty}[I_n(\mu)-I_n'(\mu)]\left(1-n\frac{\Omega_e}{\omega}\frac{k_\perp^2}{k_\perp^2}\right)\bar{z}_n Z(z_n)$$

$$D_{33}=1-N^2+\frac{\omega_e^2}{\omega^2}\frac{k_\perp^2}{k^2}\left[\frac{k^4}{k_\parallel^2 k_\perp^2}\left(\frac{T_{e\perp}}{T_{e\parallel}}-1\right)+2z_0^2+2z_0^2e^{-\mu}\sum_{n=-\infty}^{\infty}I_n(\mu)\left(1-n\frac{\Omega_e}{\omega}\frac{k_\perp^2}{k_\perp^2}\right)^2\bar{z}_n Z(z_n)\right]$$

Obviously in the $\delta\phi,\delta\underset{\sim}{A}$ representation, the dispersion equation reduces to $D_{11}=0$ if electromagnetic effects are ignored. In other words, the advantage of writing the dispersion equation in terms of $D_{11},D_{22}\ldots.$ (in the $\delta\phi,\delta\underset{\sim}{A}$ representation) is that it greatly facilitates the discussion of electromagnetic effects because it simplifies the separation of the electrostatic and electromagnetic perturbations.

APPENDIX B

In this appendix we present an approximate analytical treatment of the kinetic cross-field streaming instability.

To facilitate our discussion we introduce a quantity ω_0 which is the usual whistler frequency for $\beta_e \ll 1$, without including the ion dynamics. That is,

$$\omega_0 = \frac{c^2k^2}{\omega_e^2}\Omega_e \cos\theta \quad . \tag{B1}$$

Obviously, it is convenient to normalize the frequency ω to ω_0. It not only provides a direct comparison, but also results in considerable algebraic simplification, as will be seen later. In the following we list the expressions for the elements of the dispersion matrix D_{ij} in which the index of refraction $N(= ck/\omega)$ and the propagation angle $\theta[= \cos^{-1}(\underset{\sim}{k}\cdot\underset{\sim}{B}_0/kB_0)]$ are introduced. If we retain only the terms of order unity, it is found that

$$D_{xx}=N^2\{-\cos^2\theta+\frac{\omega^2}{\omega_0^2}\frac{c^2k^2}{\omega_e^2}\cos^2\theta-\frac{1}{2}(\beta_{e\perp}-\beta_{e\parallel})\cos^2\theta+ig_1+\frac{2}{\beta_i}\frac{\omega^2}{\omega_0^2}[1+\zeta_i Z(\zeta_i)]\sin^2\theta\cos^2\theta\}$$

$$D_{yy}=N^2\{-1+\frac{\omega^2}{\omega_0^2}\frac{c^2k^2}{\omega_e^2}\cos^2\theta+\beta_{e\perp}[(\frac{T_{e\perp}}{T_{e\parallel}}-1)+\frac{T_{e\perp}}{T_{e\parallel}}z_0Z(z_0)]\sin^2\theta-\frac{1}{2}(\beta_{e\perp}-\beta_{e\parallel})\cos^2\theta+ig_1\}$$

$$D_{zz}=N^2\{-\sin^2\theta+\frac{2}{\beta_{e\parallel}}\frac{\omega^2}{\omega_0^2}[1+z_0Z(z_0)]-\frac{1}{2}(\beta_{e\perp}-\beta_{e\parallel})\sin^2\theta+ig_3\tan^2\theta+\frac{2\omega^2}{\beta_i\omega_0^2}[1+\zeta_iZ(\zeta_i)]\cos^4\theta\}$$

$$D_{xy}=-D_{yx}=-iN^2(\frac{\omega}{\omega_0}\cos\theta+if_1) \qquad \text{(B2)}$$

$$D_{xz}=D_{zx}=N^2\{\sin\theta\cos\theta+\frac{1}{2}(\beta_{e\perp}-\beta_{e\parallel})\sin\theta\cos\theta-ig_2\tan\theta+\frac{2\omega^2}{\beta_i\omega_0^2}[1+\zeta_iZ(\zeta_i)]\sin\theta\cos^3\theta\}$$

$$D_{yz}=-D_{zy}=-iN^2\{\frac{\omega}{\omega_0}\frac{T_{e\perp}}{T_{e\parallel}}[1+z_0Z(z_0)]\sin\theta+if_2\tan\theta\}$$

where

$$f_j=\frac{\pi^{\frac{1}{2}}\omega\omega_e}{2\beta_{e\parallel}^{\frac{1}{2}}\omega_0ck}\{[j(\frac{T_{e\perp}}{T_{e\parallel}}-1)+1]\Phi_- -\frac{\Omega_e}{\omega}(\frac{T_{e\perp}}{T_{e\parallel}}-1)\Phi_+\} \qquad \text{(B3)}$$

$$g_j=\frac{\pi^{\frac{1}{2}}\omega\omega_e}{2\beta_{e\parallel}^{\frac{1}{2}}\omega_0ck}\{[j(\frac{T_{e\perp}}{T_{e\parallel}}-1)+1]\Phi_+ -\frac{\Omega_e}{\omega}(\frac{T_{e\perp}}{T_{e\parallel}}-1)\Phi_-\}$$

$$\Phi_\pm=\exp[-\frac{(\omega-\Omega_e)^2}{k_\parallel^2v_{e\parallel}^2}]\pm\exp[-\frac{(\omega+\Omega_e)^2}{k_\parallel^2v_{e\parallel}^2}] \quad ,$$

and the index $j = 1,2,3$. In these expressions we have defined:

$$T_{e\perp}=m_ev_{e\perp}^2/2 \ , \quad T_{e\parallel}=m_ev_{e\parallel}^2/2 \ , \quad z_0=\omega/k_\parallel v_{e\parallel} \ , \quad \zeta_i=(\omega-k_\perp V_0)/kv_i \ , T_i=m_iv_i^2/2$$

and $Z(\eta)$ is the usual plasma dispersion function.

Equation (B2) is obtained from Eq. (A5) by assuming $\mu\equiv k_\perp^2v_{e\perp}^2/2\Omega_e^2 \ll 1$ and keeping only the terms associated with $n = 0$ and ± 1. However, we should bear in mind that since

$$\mu=\frac{k_\perp^2v_{e\perp}^2}{2\Omega_e^2}=\frac{\beta_{e\perp}}{2}\frac{c^2k^2}{\omega_e^2}\sin^2\theta \quad , \qquad \text{(B4)}$$

the postulate becomes unjustified when $\beta_{e\perp}$, ck/ω_e and $\sin\theta$ are all

of order unity. Moreover, in Eq. (B2) we have also made use of the assumption

$$\omega << \Omega_e \quad .$$

We remind the reader that Eq. (B2) was derived for $\beta_e \sim 0(1)$. For the case $\beta_e << 1$, the term $(2N^2\omega^2/\beta_e\omega_0^2)[1 + z_0 Z(z_0)]$ in D_{zz} becomes large compared to the other elements. As a result, the dispersion equation may be reduced to a 2×2 determinant (Mikhailovskii, 1975). In short, the discussion in Sec. IIb shows that for $\beta_e \sim 1$ we must treat the 3×3 determinant in order to derive the appropriate dispersion equation. This is the principal task of this Appendix.

In the following we write $\omega = \omega_r + i\gamma$ and postulate that $\omega_r >> \gamma$. Furthermore, since we assume $\omega << \Omega_e$ and

$$\frac{c^2k^2}{\omega_e^2} >> \frac{\omega^2}{\Omega_e^2} \quad , \tag{B5}$$

as usual, the term $\omega^2c^2k^2/\omega_0^2\omega_e^2$ which appears in D_{xx} and D_{yy} may be considered to be negligible. Such an approximation is commonly made in the literature when the dispersion equation for whistlers is discussed (Mikhailovskii, 1975). Making this approximation, we find by setting the real part of the determinant of D_{ij} to zero that

$$\frac{\omega_r^2}{\omega_0^2} = \frac{B}{A} \tag{B6}$$

where

$$A= 1+[1+ \frac{2}{\beta_{e\parallel}}\sin^2\theta-\sin^4\theta(\frac{T_{e\perp}}{T_{e\parallel}}-1)^2 + 3\sin^2\theta\cos^2\theta(\frac{T_{e\perp}}{T_{e\parallel}}-1)] \frac{T_{e\parallel}}{T_i}[1+\zeta_i^0 ReZ(\zeta_i^0)]$$

$$B=(1+ \frac{\beta_{e\perp}}{2}-\frac{\beta_{e\parallel}}{2})\{\frac{\beta_{e\parallel}}{2}(\frac{T_{e\perp}}{T_{e\parallel}}-1)^2\sin^2\theta+[1-\beta_{e\perp}(\frac{T_{e\perp}}{T_{e\parallel}}-1)\sin^2\theta+(\frac{\beta_{e\perp}}{2}-\frac{\beta_{e\parallel}}{2})\cos^2\theta] \times$$

$$\times (1 + \frac{T_{e\parallel}}{T_i}[1 + \zeta_i^0 ReZ(\zeta_i^0)])\}$$

and

$$\zeta_i^0 = (\omega_0 - k_\perp V_0)/kv_i \ .$$

From this expression it can be shown that increasing the electron temperature anisotropy $T_{e\perp} > T_{e\parallel}$ decreases the real frequency when the angle of propagation is large. This effect may be seen by comparing Fig. 1 to Fig. 2 and is also shown in Fig. 3.

For the case of isotropic electrons, Eq. (B6) may be simplified,

$$\frac{\omega_r^2}{\omega_0^2} = 1 - \frac{2\sin^2\theta[1 + \zeta_i^0 ReZ(\zeta_i^0)]}{\beta_i + (\beta_e+2\sin^2\theta)[1 + \zeta_i^0 ReZ(\zeta_i^0)]} \ . \qquad (B7)$$

The ion dynamics influence the wave dispersion even when the relative electron-ion cross-field drift is small. The effect of the ions is is greater when the angle is larger.

Next, the imaginary part of ω is calculated by the standard approach.

$$\gamma = - \frac{ImD}{\frac{\partial ReD}{\partial \omega}}$$

However, at this point a remark is necessary. As mentioned earlier, in deriving Eq. (B6) we have neglected the term $N^2c^2k^2\omega^2/\omega_0^2\omega_e^2$ in D_{xx} and D_{yy}. However, we have found that this approximation should be avoided in deriving the imaginary part of D, the determinant of D_{ij}, because a careful study has shown that these terms can qualitatively modify the growth rate at sufficiently large θ. The reason is explained above and in Wu et al. (1983).

In the following we write

$$\gamma = \gamma_i + \gamma_e + \gamma_{ce} \qquad (B8)$$

where γ_i denotes the ion contribution to the growth rate, γ_e is the electron Landau damping decrement, and γ_{ce} is the part of the growth rate due to the cyclotron resonance. We find the ion term for $T_{e\perp} = T_{e\parallel}$

$$\gamma_i = \frac{\pi^{\frac{1}{2}}}{\Lambda}\frac{T_e}{T_i}\zeta_i e^{-\zeta_i^2}\{1-\beta_e z_0 Z(z_0)\sin^2\theta - \frac{\omega_r^2}{\omega_0^2}\{1+\frac{2}{\beta_e}[1+(1+\beta_e\cos^2\theta)z_0 ReZ(z_0)]\sin^2\theta -$$

$$-[z_0 ReZ(z_0)]^2\sin^4\theta + \frac{c^2k^2}{\omega_e^2}[1+\cos^2\theta-\beta_e z_0 ReZ(z_0)\sin^2\theta\cos^2\theta]\cos^2\theta\}+$$

$$+\frac{\omega_r^4}{\omega_0^4}\frac{c^2k^2}{\omega_e^2}\frac{2}{\beta_e}[1+z_0 ReZ(z_0)]\sin^2\theta\cos^2\theta\} \qquad \text{(B9)}$$

and the electron Landau term for $T_{e\perp} = T_{e\parallel}$

$$\gamma_e = \frac{\pi^{\frac{1}{2}}}{\Lambda} z_0 e^{-z_0^2}\{1-\beta_e[1+z_0 ReZ(z_0)+\frac{\beta_e}{2}\frac{c^2k^2}{\omega_e^2}\sin^2\theta+\frac{T_e}{T_i}\{1+\zeta_i ReZ(\zeta_i)\}]\sin^2\theta -$$

$$-\frac{\omega_r^2}{\omega_0^2}\{1+\frac{c^2k^2}{\omega_e^2}[1+\cos^2\theta-\beta_e z_0 ReZ(z_0)\sin^2\theta]+\frac{2}{\beta_e}[1+\beta_e\{\cos^2\theta-z_0 ReZ(z_0)\sin^2\theta-$$

$$-\frac{\beta_e}{2}\frac{c^2k^2}{\omega_e^2}\cos^4\theta\}]\frac{T_e}{T_i}[1+\zeta_i ReZ(\zeta_i)]\sin^2\theta\}+\frac{\omega_r^4}{\omega_0^4}\frac{c^2k^2}{\omega_e^2}\frac{2}{\beta_e}\frac{T_e}{T_i}[1+\zeta_i ReZ(\zeta_i)]\sin^2\theta\cos^2\theta\}\ . \qquad \text{(B10)}$$

Taking $f_1 = f_2$ and $g_1 = g_2 = g_3$ for the case $T_{e\perp} = T_{e\parallel}$ and suppressing the index j, the electron cyclotron resonance term is

$$\gamma_{ce} = -\frac{2f}{\Lambda\cos\theta}\frac{\omega_r}{\omega_0}\{[1+z_0 ReZ(z_0)][1+\frac{\beta_e}{2}\frac{c^2k^2}{\omega_e^2}\sin^2\theta+\frac{T_e}{T_i}\{1+\zeta_i ReZ(\zeta_i)\}\sin^2\theta] +$$

$$+\frac{T_e}{T_i}[1+\zeta_i ReZ(\zeta_i)]\cos^2\theta\}-\frac{g}{\Lambda\cos^2\theta}\{[1+\cos^2\theta-\beta_e z_0 ReZ(z_0)\sin^2\theta]\times$$

$$\times\left(1+\ z_0 ReZ(z_0)+\frac{\beta_e}{2}\frac{c^2k^2}{\omega_e^2}\sin^2\theta+\frac{T_e}{T_i}[1+\zeta_i ReZ(\zeta_i)]\right)+\frac{\beta_e}{2}[z_0 ReZ(z_0)]^2\sin^2\theta-$$

$$-\frac{\omega_r^2}{\omega_0^2}\cos^2\theta\left[2\ \frac{c^2k^2}{\omega_e^2}\ \{1+z_0 ReZ(z_0)\}+\left(\frac{2}{\beta_e}[1+z_0 ReZ(z_0)]\sin^2\theta+\frac{c^2k^2}{\omega_e^2}[1+\cos^4\theta]\right)\times\right.$$

$$\left.\times\frac{T_e}{T_i}\{1+\zeta_i ReZ(\zeta_i)\}\right]\}\ . \qquad \text{(B11)}$$

The expression for ω_r is given in Eq. (B6) and the function $\Lambda(k,\omega,\theta)$ for $T_{e\perp} = T_{e\parallel}$ is defined as

$$\Lambda = -\frac{1}{2}\frac{\beta_e}{N^6}\frac{\omega_0^2}{\omega_r^2}\frac{1}{\cos^2\theta}\ \frac{\partial ReD}{\partial\omega_r} = \frac{2\omega_r A}{\omega_0^2}+\frac{\omega_r^2}{\omega_0^2}\frac{\partial A}{\partial\omega_r}-\frac{\partial B}{\partial\omega_r} =$$

$$= \frac{2\omega_r}{\omega_0^2}\{1+(1+\frac{2}{\beta_e}\sin^2\theta)\frac{T_e}{T_i}[1+\zeta_i ReZ(\zeta_i)]\}+[\frac{\omega_r^2}{\omega_0^2}(1+\frac{2}{\beta_e}\sin^2\theta)-1]\frac{T_e}{T_i}\frac{\partial}{\partial\omega_r}[\zeta_i ReZ(\zeta_i)]. \qquad \text{(B12)}$$

It is easy to see that one of the reasons the electron temperature anisotropy substantially increases the growth rate γ is because the functions f_j and g_j given in Eq. (B3) are much greater for $T_{e\perp} > T_{e\parallel}$ than for $T_{e\perp} = T_{e\parallel}$. This conclusion is in agreement with the numerical solutions of the complete dispersion equation, which are shown in Figs. 1, 2, and 3.

FIGURE CAPTIONS

Figure 1. Growth rate (dashed curve) maximized over wavenumber and real part of the frequency (solid curve) as a function of propagation angle θ for several values of the relative electron-ion drift velocity $V_0/v_A = 5,10,15,20$, $T_{e\perp}/T_{e\parallel} = 1.0$, $\beta_e = \beta_i = 1$, $\omega_e/\Omega_e = 150$. The lower-hybrid frequency $\omega_{LH} \simeq (\Omega_e\Omega_i)^{\frac{1}{2}}$.

Figure 2. Growth rate (dashed curve) maximized over wavenumber and real part of the frequency (solid curve) as a function of propagation angle θ for several values of the relative electron-ion drift velocity $V_0/v_A = 5,10,20$, $T_{e\perp}/T_{e\parallel} = 1.5$, $\beta_{e\parallel} = \beta_i = 1$, and $\omega_e/\Omega_i = 150$.

Figure 3. Maximum growth rate (dashed curve) and real part of the frequency (solid curve) versus propagation angle for several values of the electron temperature anisotropy $T_{e\perp}/T_{e\parallel} = 1, 1.5, 2$ and the parameters $\beta_{e\parallel} = \beta_i = 1.0$, $\omega_e/\Omega_e = 150$, and $V_0/v_A = 10$.

Figure 4. Maximum growth rate (dashed curve) and real part of the frequency (solid curve) versus relative electron-ion drift velocity V_0/v_A for $T_{e\perp}/T_{e\parallel} = 1.0$ and 1.5, $\beta_{e\parallel} = \beta_i = 1$, and $\omega_e/\Omega_e = 150$.

Figure 5. Real part of the frequency versus wavenumber ck/ω_e corresponding to maximum growth for several values of V_0/v_A, $T_{e\perp}/T_{e\parallel} = 1$ (solid curve), $T_{e\perp}/T_{e\parallel} = 1.5$ (dashed curve), $\beta_{e\parallel} = \beta_i = 1$, and $\omega_e/\Omega_e = 150$.

Figure 6. Values of $|\omega_r - k_\perp V_0|/kv_i$ and $\omega_r/k_\parallel v_{e\parallel}$ corresponding to maximum growth versus angle of propagation θ for several values of V_0/v_A, $T_{e\perp}/T_e = 1$ (solid curve), $T_{e\perp}/T_{e\parallel} = 1.5$ (dashed curve), $\beta_{e\parallel} = \beta_i = 1$, and $\omega_e/\Omega_e = 150$.

Figure 7. Ratio of electromagnetic to electrostatic electric field energy density $|\delta E_{em}|^2/|\delta E_{es}|^2$ for the most unstable mode versus angle of propagation θ for various values of V_0/v_A, $T_{e\perp}/T_{e\parallel} = 1$ (solid curve), $T_{e\perp}/T_{e\parallel} = 1.5$ (dashed curve), $\beta_{e\parallel} = \beta_i = 1$, and $\omega_e/\Omega_e = 150$.

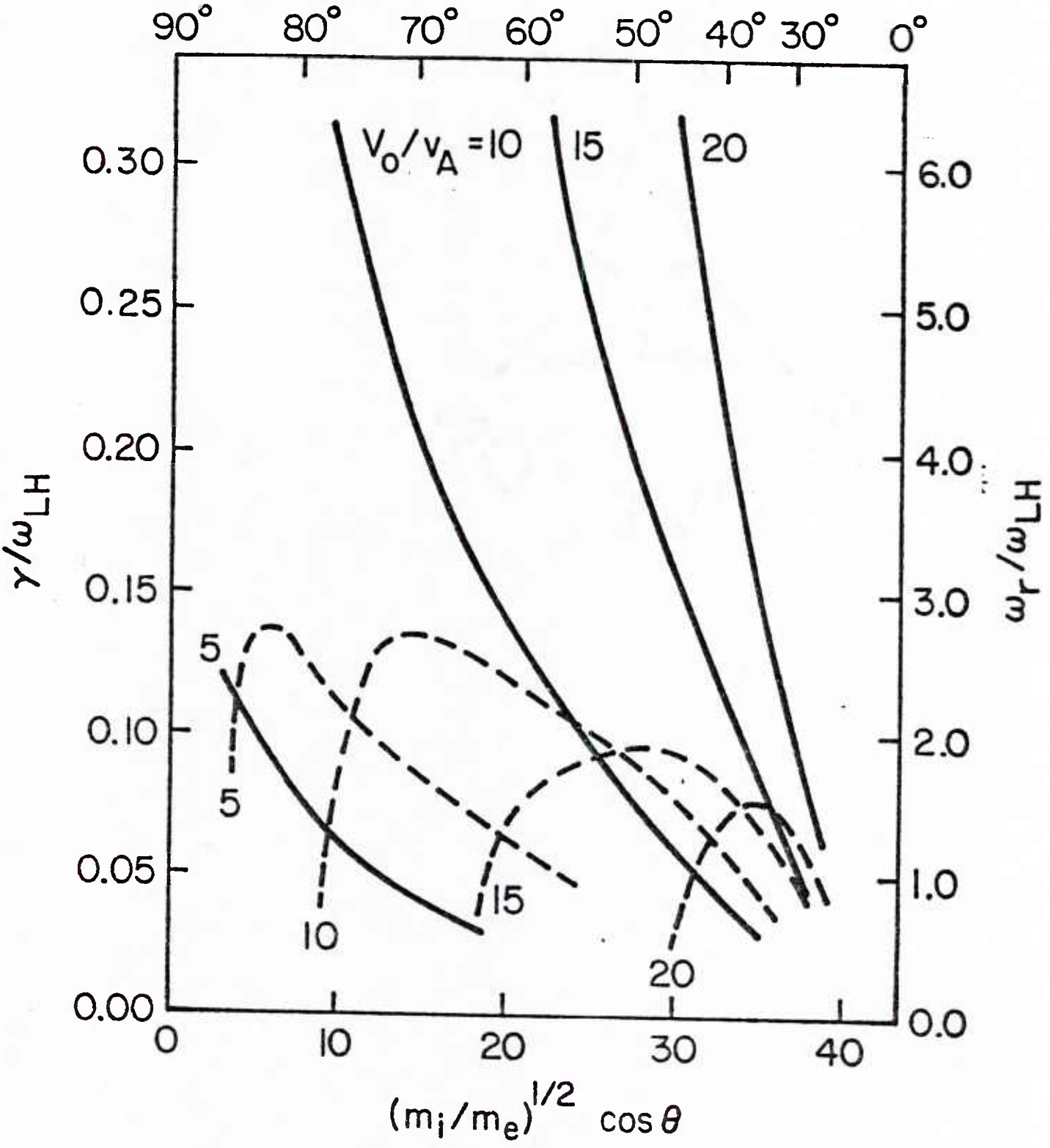
90°
80°
70°
60°
50°
40°
30°
0°
V_o/v_A =10
15
20
0.30
0.25
0.20
0.15
0.10
0.05
0.00
6.0
5.0
4.0
3.0
2.0
1.0
0.0
γ/ω_{LH}
ω_r/ω_{LH}
5
5
10
15
20
0
10
20
30
40
$(m_i/m_e)^{1/2}$ cos θ

Figure 1

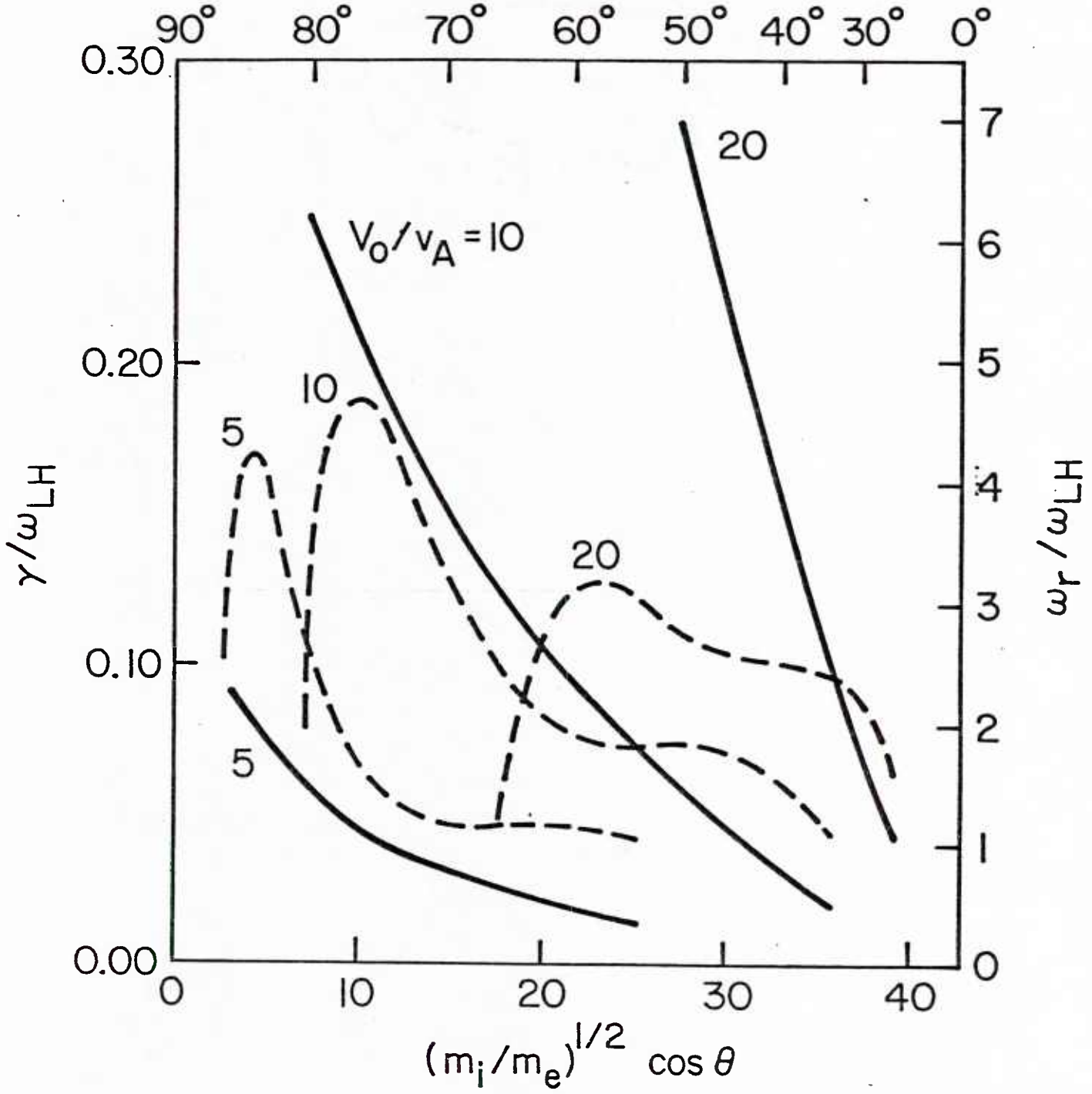
90°
80°
70°
60°
50°
40°
30°
0°
0.30
0.20
0.10
0.00
0
10
20
30
40
7
6
5
4
3
2
1
0
20
$V_0/v_A = 10$
10
5
20
5
γ/ω_{LH}
ω_r/ω_{LH}
$(m_i/m_e)^{1/2} \cos\theta$

Figure 2

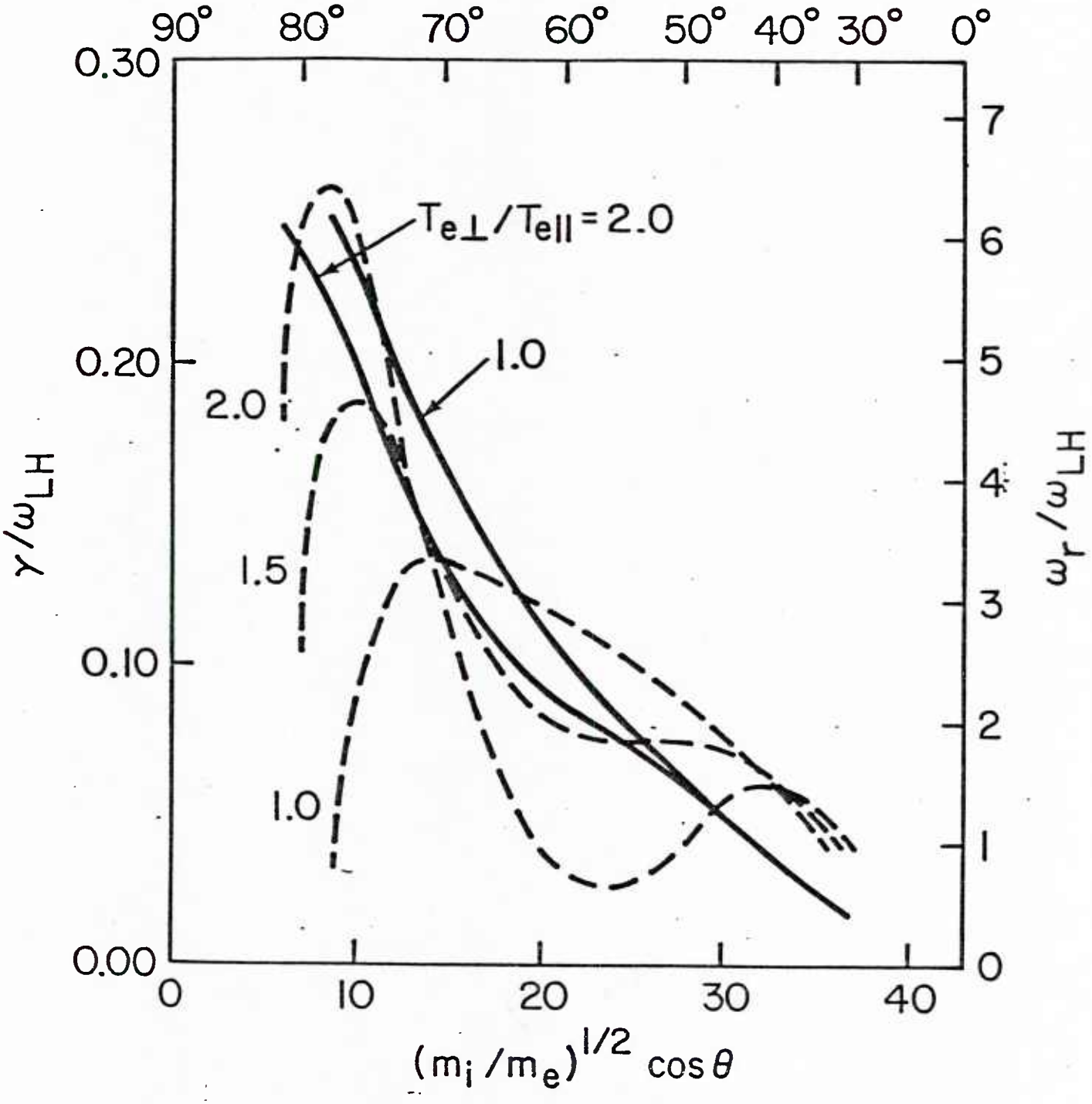
90°
80°
70°
60°
50°
40°
30°
0°
0.30
0.20
0.10
0.00
0
10
20
30
40
7
6
5
4
3
2
1
0
$T_{e\perp}/T_{e\parallel} = 2.0$
1.0
2.0
1.5
1.0
γ/ω_{LH}
ω_r/ω_{LH}
$(m_i/m_e)^{1/2} \cos\theta$

Figure 3

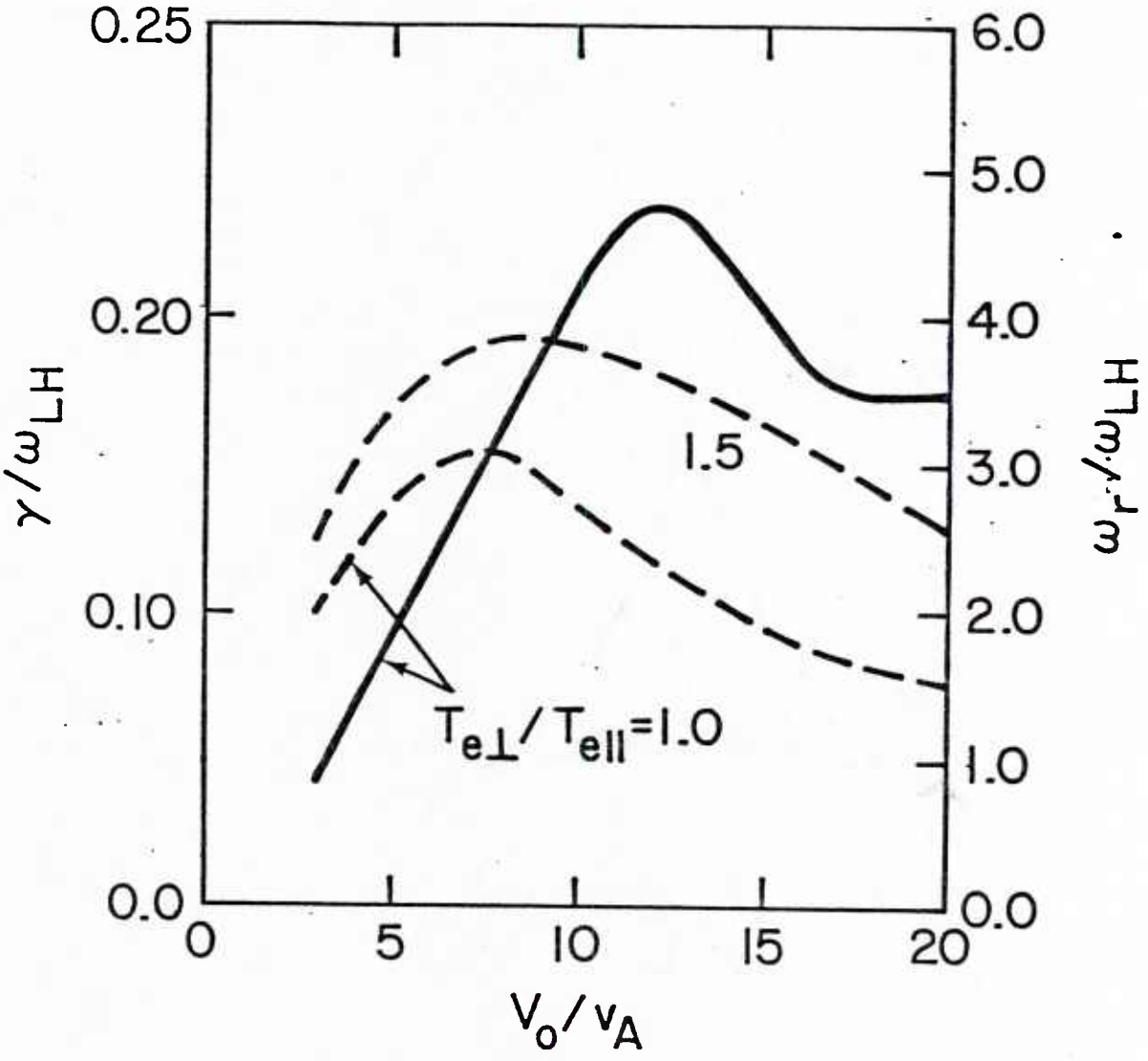
0.25
0.20
0.10
0.0
6.0
5.0
4.0
3.0
2.0
1.0
0.0
0
5
10
15
20
γ/ω_{LH}
ω_r/ω_{LH}
V_o/v_A
1.5
$T_{e\perp}/T_{e\parallel}=1.0$

Figure 4

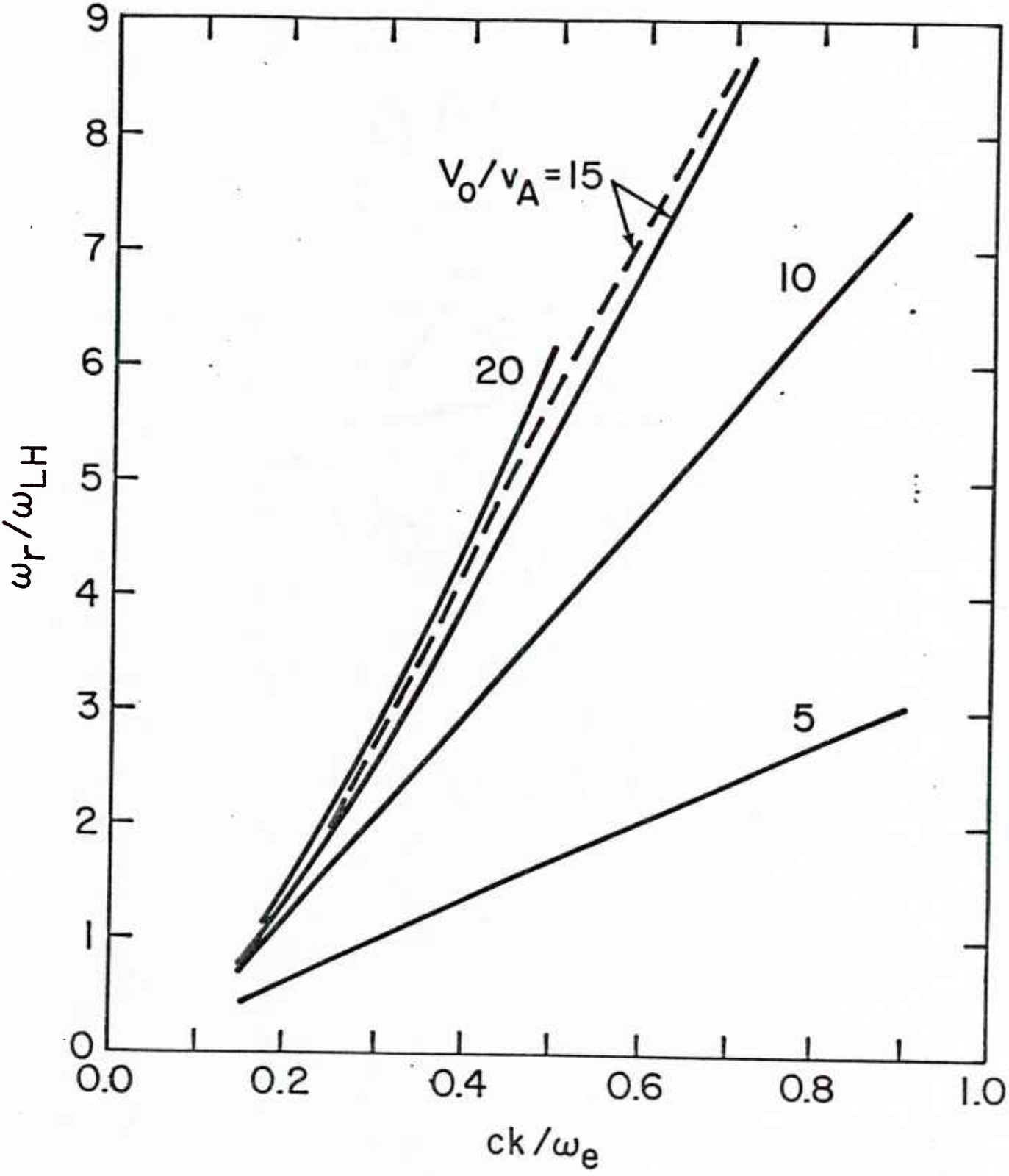
9
8
7
6
5
4
3
2
1
0
0.0
0.2
0.4
0.6
0.8
1.0
ω_r/ω_{LH}
ck/ω_e
$V_0/v_A = 15$
20
10
5

Figure 5

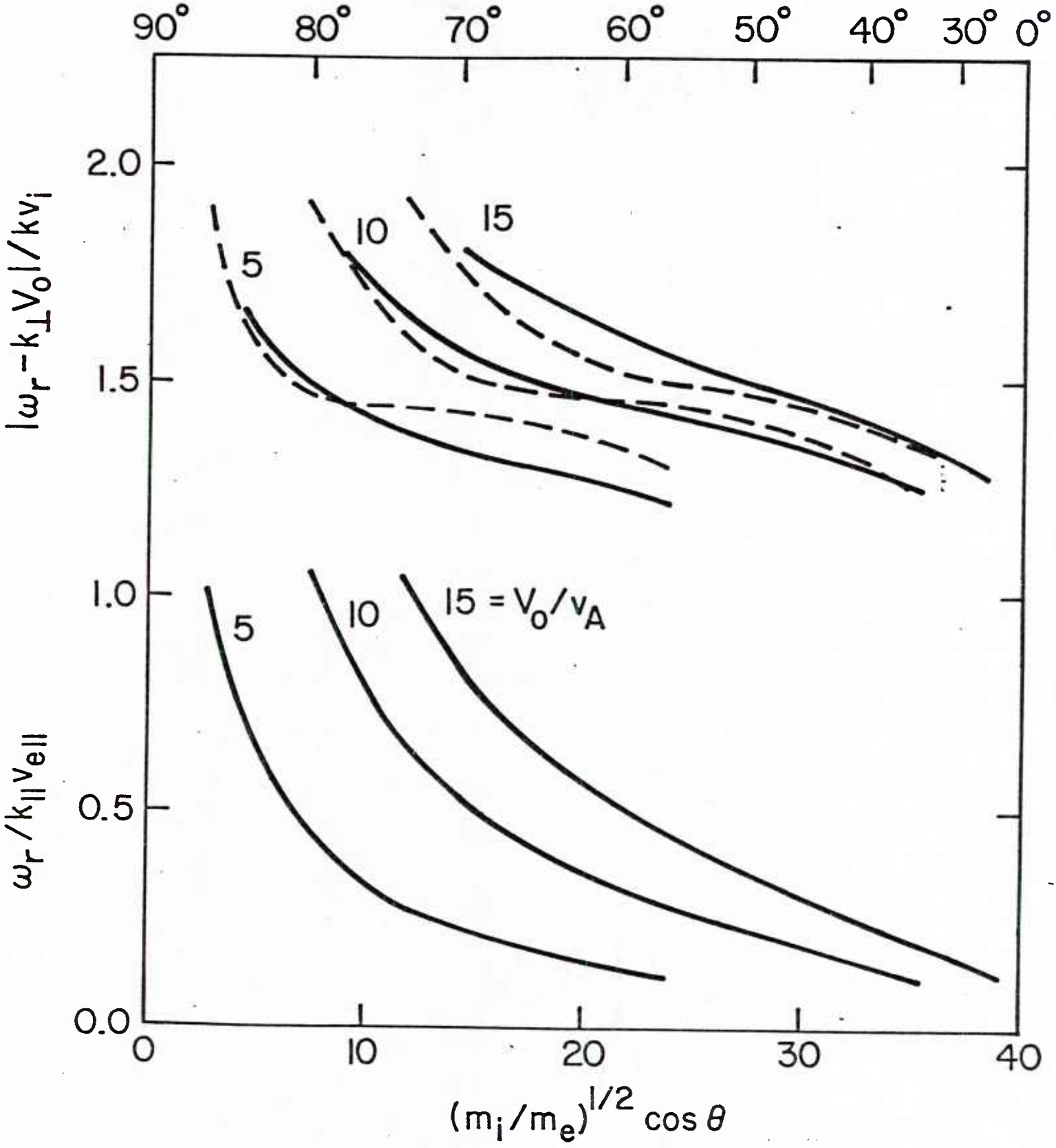
90°
80°
70°
60°
50°
40°
30°
0°
2.0
1.5
1.0
0.5
0.0
$|\omega_r - k_\perp V_o| / k v_i$
$\omega_r / k_{||} v_{e||}$
5
10
15
5
10
15 = V_o / v_A
0
10
20
30
40
$(m_i/m_e)^{1/2} \cos\theta$

Figure 6

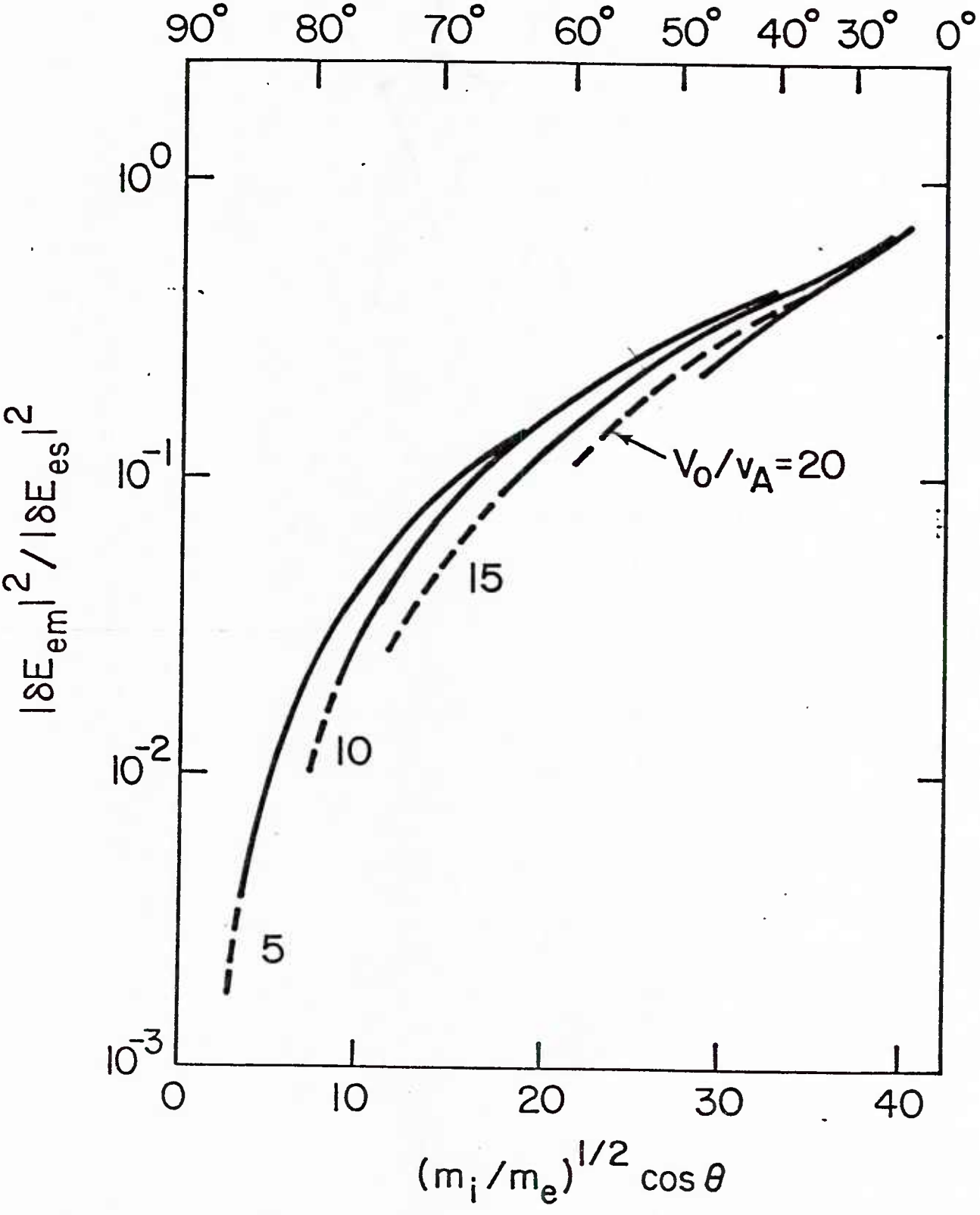
90°
80°
70°
60°
50°
40°
30°
0°
10^0
10^{-1}
10^{-2}
10^{-3}
$|\delta E_{em}|^2 / |\delta E_{es}|^2$
$V_0/v_A=20$
15
10
5
0
10
20
30
40
$(m_i/m_e)^{1/2} \cos\theta$

Figure 7

ACCELERATION OF AURORAL ELECTRONS BY LOWER-HYBRID TURBULENCE AND A QUASISTATIC PARALLEL ELECTRIC FIELD[†]

J. D. Gaffey, Jr., Z. X. Liu[*] and S.C. Guo[**]

Institute for Physical Science and Technology,

University of Maryland.

College Park, Maryland 20742

[*]Present address: Institute of Space Physics, Chinese Academy of Sciences, Beijing, China

[**]Present address: Institute of Physics, Chinese Academy of Sciences, Beijing, China

[†]Work supported by ONR and NASA

ABSTRACT

The acceleration of electrons along the auroral magnetic field by large amplitude lower-hybrid turbulence and a quasistatic parallel electric field is discussed. Perturbations are excited by a cross-field current due to a relative electron-ion drift. The fluctuating electric field is primarily electrostatic and propagates nearly perpendicularly to the auroral magnetic field. It is assumed that the instability saturates rapidly. The time evolution of the energy of an individual test electron is calculated. The quasilinear diffusion equation, with a power law spectral energy density, is solved using a Green's function method. The time evolution of an initial Maxwellian distribution is given, and the average electron energy is obtained for various cases. It is found that turbulent acceleration and electric field acceleration are comparable in some cases.

I. INTRODUCTION

One of the most important problems in auroral physics is the acceleration of auroral electrons to high energies. Experimental measurements of the energy spectra of the precipitating auroral electrons have been made by the ISIS-1 and S3-3 satellites which have orbits passing through the auroral region at 2000 and 8000 km, respectively. These data suggest that electrons from the plasma sheet are injected into the auroral region with energies of order 1 keV and are subsequently accelerated to energies of order 10 keV before precipitating. The results from the S3-3 satellite indicate that the energization of auroral electrons along the auroral magnetic field lines seems to occur at altitudes between 4000 km and 8000 km (Sharp et al., 1980). Furthermore, the presence of precipitating electrons with energies in excess of 10 keV at low altitudes in the auroral zones during disturbed times has been known long before the S3-3 measurements.

Recent electric field measurements by the S3-3 satellite indicate the presence of a quasistatic electric field parallel to the auroral magnetic field (Mozer et al., 1977, 1979, 1980; Torbert and Mozer, 1978; Cladis et al., 1979; Sharp et al., 1979; Mizera et al., 1980). Such an electric field may provide the field aligned acceleration process required to explain the observations of energetic precipitating auroral electrons. Although the origin of the parallel electric field is still not completely understood, theoretical discussions have given by several authors (Chiu and Schulz , 1978; Kan et al., 1979; Shawhan et al., 1979).

In addition, wave measurements by the instruments onboard the Hawkeye and IMP6 satellites have observed that electrostatic plasma turbulence is generated in the region where the quasistatic parallel electric fields

occur (Gurnett and Frank, 1972; 1977). Observations by the S3-3 satellite also confirm the existence of ion cyclotron and lower-hybrid waves in this same region (Kintner et al., 1978; 1979; Temerin, 1978, 1979; Mozer et al., 1979, 1980; Temerin et al., 1979). The lower-hybrid waves are generally broad band and the wave intensity is relatively high.

In the literature, several schools of thought have been proposed to explain the acceleration of auroral electrons. A brief summary of these models is given below.

(1) The acceleration may result from the presence of a parallel electric field (Hoffman and Evans, 1968; Gurnett, 1972; Paschmann et al., 1972; Whalen and McDiarmid, 1972; Hall and Bryant, 1974; Kaufmann et al., 1976; Bryant et al., 1978; Whalen and Daly, 1979; Fridman and Lemair, 1980).

(2) The acceleration may be associated with electrostatic shock waves (Swift, 1970; Kan, 1975; Hudson and Mozer, 1978).

(3) The acceleration may result from electrostatic plasma waves (Gary et al., 1968; Laval and Pellat, 1970; Swift, 1970).

The fundamental question is what is the principal mechanism responsible for the acceleration of auroral electrons. Most of the dicussions described above are qualitative and emphasize only the basic physical concepts. No detailed analysis of the characteristic time scale of a specific acceleration process has been performed.

The purpose of the present paper is to give a detailed discussion of the acceleration of auroral electrons due to the presence of both a quasistatic parallel electric field and enhanced electrostatic plasma turbulence. We are primarily interested in the time scale which characterizes the rate of change of the electron energy in the aforementioned situation. The following discussion is primarily based on an individual test particle approach, although a kinetic-theoretical analysis is also

considered. It is found that the results are qualitatively the same.

The rest of the paper is organized as follows: In section II, the basic assumptions and the physical model are described and the mathematical problem is formulated. In section III, the electron velocity and kinetic energy are calculated for an individual test particle. A Green's function technique is used in section IV to obtain the electron velocity and kinetic energy, and the time evolution of an initial Maxwellian distribution is given. Finally, the discussion and conclusions are given in section V. The Green's functions used in section IVC are derived in the Appendix.

II. GENERAL CONSIDERATIONS AND THE PHYSICAL MODEL

A. The Quasistatic Parallel Electric Field

The measurements by the S3-3 satellite at altitudes of approximately one earth radius indicate that occasionally the maximum value of the parallel electric field can be as large as 200 mV/m to 400 mV/m (Mozer et al., 1977). The average value of the parallel electric field is typically less than 10 mV/m (Temerin et al.,1982). However, the subject remains controversial.

A number of authors have used the S3-3 measurements of the electron energy spectrum and pitch angle distribution to estimate the potential difference along the auroral magnetic field lines (Sharp et al., 1979; Cladis et al., 1979). It is found from the plasma data that the signature of an electrostatic potential drop exists over a broad altitude range, from approximately 4000 km to 8000 km. The peak value of the total potential difference is estimated to be between 4 kilovolts and 5 kilovolts.

B. The Quasilinear Diffusion Equation

The electric field and plasma turbulence measurements outlined above suggest that in the acceleration region, the electrons are energgized under the combined influence of both a quasistatic parallel electric field and large amplitude electrostatic plasma turbulence. A theoretical study of the collective instability mechanism of electron acceleration is essential not only for the understanding of the anomalous energization of auroral electrons, but is also important in the context of fundamental plasma physics. The statistical acceleration of electrons and ions in turbulent plasmas has been discussed by many authors and comprehensive reviews have been given in the literature

(Tsytovich 1966, 1977). Recently the linear and nonlinear evolution of plasma instabilities driven by cross-field currents and the resulting anomalous heating of electrons and ions have been studied analytically and numerically (Davidson and Krall, 1977). These works show that statistical acceleration processes can play an important role in space plasmas and laboratory plasmas.

The physical situation which is treated in this paper may be described briefly as follows. We consider a plasma that can support an instability that amplifies perturbations excited by a cross-field current, due to a relative electron-ion drift. Among the instabilities driven by a cross-field current, the modified two-stream instability and the lower-hybrid-drift instability are the most important. A rather complete description of the literature of cross-field instabilities is contained in a recent paper (Hsia, et al., 1979), which gives a unified theory of the lower-hybrid-drift and modified two-stream instabilities. These modes with frequencies in the range of the lower-hybrid frequency can interact simultaneously with both the electrons and the ions, and thus can transfer energy from the ions to the electrons. The fluctuating electric field of the lower-hybrid waves is primarily electrostatic and propagates nearly perpendicularly to the auroral magnetic field. It is assumed that the instability saturates rapidly. In this paper we are not concerned with the details of the saturation mechanism but rather with the acceleration of the electrons by plasma turbulence that has already reached the saturation level. Recently, some laboratory experiments have demonstrated that the combined effects of a parallel electric field and plasma turbulence is particularly effective in producing energetic electrons (Yamamoto et al., 1980). This phenomenon has been observed in a tokamak, and we expect that the physical mechanism should

be operative in the auroral region also. It is based on this notion that we are motivated to proceed with the present study. The approach consists of two parts; one is the study of a test particle problem, and the other is the investigation of the time evolution of the distribution function. The latter is based on a quasilinear kinetic equation.

Our discussion starts with the quasilinear kinetic equation for a magnetized plasma (Davidson, 1972; Kennel and Engelmann, 1966), including the quasistatic parallel electric field. Since the plasma turbulence has a characteristic frequency, $\omega \approx \omega_{LH} << \Omega_e$, and since we only consider long wavelengths, $k_\perp v_{eth} < \Omega_e$ (v_{eth} is the electron thermal velocity), the most important diffusion process is associated with the $n = 0$ term. In this case, the quasilinear equation reduces to

$$\frac{\partial F_e}{\partial t} - \frac{|e|}{m_e} E_\parallel \frac{\partial F_e}{\partial v_\parallel} = \frac{\partial}{\partial v_\parallel} D_\parallel(v_\parallel) \frac{\partial F_e}{\partial v_\parallel} \quad , \tag{1}$$

where

$$D_\parallel(v_\parallel) = \frac{8\pi^2 e^2}{m_e^2} \int d^3k \; \varepsilon_{\vec{k}} \frac{k_\parallel^2}{k^2} \delta(\omega - k_\parallel v_\parallel) \quad . \tag{2}$$

In Eqs. (1) and (2) F_e is the electron distribution function, and the spectral energy density $\varepsilon_{\vec{k}} = \langle |\vec{E}_{\vec{k}}|^2 \rangle / 8\pi$, where $\vec{E}_{\vec{k}}$ is the fluctuating field.

To facilitate our discussion we adopt a coordinate system in which the z axis is parallel to the ambient magnetic field and the turbulence is excited by a cross-field drift v_d parallel to the y axis. For a given unstable mode, the frequency ω and the wavevector $\vec{k}$ are related by

$$\omega \simeq \vec{k} \cdot \vec{v}_d = k_y v_d \; . \tag{3}$$

We further assume spectral energy density has the form

$$\varepsilon_{\vec{k}} = \psi(\vec{k}_\perp)\phi(k_\parallel) \quad , \tag{4}$$

where $\phi(k_\parallel)$ is the power-law spectrum discussed recently by Wu, Gaffey and Liberman (1981),

$$\phi(k_\parallel) = \begin{cases} \dfrac{\alpha-1}{2k_m}\left|\dfrac{k_m}{k_\parallel}\right|^\alpha & \text{for } |k_\parallel| > k_m \\ 0 & \text{for } |k_\parallel| < k_m \end{cases} \tag{5}$$

The spectral index α is considered to be a parameter, and ϕ is normalized such that $\int_{-\infty}^{\infty} dk\ \phi(k_\parallel) = 1$, for $\alpha > 1$. The saturation wave energy

$$\bar{W}_s = \int d^3k\ \varepsilon_{\vec{k}} = \int d^2k_\perp\ \psi(\vec{k}_\perp) \tag{6}$$

is discussed in Section IIC. In the following we further assume that

$$\frac{\partial\omega}{\partial k_\parallel} \ll v_\parallel \quad \text{and} \quad k_y^2 \gg k_x^2\ ,\ k_\parallel^2 \quad .$$

The diffusion coefficient (2) can be simplified using Eqs.(4), (5) and (6).

$$D_\parallel(v_\parallel) = D\left|\frac{v_\parallel}{v_{the}}\right|^{\alpha-3} \quad , \tag{7}$$

where

$$D = \pi(\alpha-1)\frac{\omega_{pe}^2 \bar{W}_s v_d^2}{\omega n_e m_e v_{the}^2}\left(\frac{k_m v_{the}}{\omega}\right)^{\alpha-1} \quad . \tag{8}$$

The electron plasma frequency $\omega_{pe} = (4\pi n_e e^2/m_e)^{\frac{1}{2}}$ and $v_{the} = (2T_e/m_e)^{\frac{1}{2}}$ is the electron thermal velocity.

It is convenient to introduce the dimensionless parameter,

$$E = \frac{|e|E_{||}v_{the}}{m_e D} \tag{9}$$

and the dimensionless variables,

$$u = \frac{v_{||}}{v_{the}} \quad , \tag{10}$$

$$t = \frac{1}{v_{the}^2} \int_0^t dt' D(t') \quad . \tag{11}$$

If v_d and $\bar{W}_s$ can be taken to be approximately time-independent, Eq. (11) simplifies to

$$\tau = \frac{D}{v_{the}^2} t \quad . \tag{11a}$$

In terms of these variables, the diffusion equation (1) can be written as

$$\frac{\partial F_e}{\partial \tau} = \frac{\partial}{\partial u} |u|^{\alpha-3} \frac{\partial F_e}{\partial u} + E \frac{\partial F_e}{\partial u} \quad . \tag{12}$$

C. The Physical Model of the Acceleration Region

Since the present study is primarily motivated by the observations of precipitating energetic auroral electrons, we now discuss the model of the acceleration region, which was mentioned previously in Section IIB. In this region, where the quasi-static parallel electric fields occur, the Hawkeye and IMP 6 satellites have measured large amplitude electrostatic plasma turbulence at the lower-hybrid and ion cyclotron frequencies (Gurnett and Frank, 1972, 1977). We expect that the turbulence at the lower-hybrid frequency is a manifestation of the lower-hybrid-drift instability, which is excited by a cross-field current due to a relative electron-ion drift (Hsia et al., 1979; and references therein). The sources of free energy available in the acceleration region to drive the lower-hybrid-drift instability are the $\vec{E} \times \vec{B}$ drift and the plasma density inhomogeneity. In this region there is a rather strong electric field perpendicular to the ambient magnetic field, $E_\perp \approx 400$ mV/m. This large perpendicular electric field can generate quite a large relative cross-field drift between the electrons and the ions. In the large electric field region, the low energy particles are expelled and there is a strong density gradient at the boundary of this region. These ideas are supported by the observations of Whalen and Daley (1979) that the most intense energetic electron precipitation occurs at the edge of the auroral arcs. The lower-hybrid waves, which are generated at the edge can propagate into the center of the regions, and thus the waves are able to accelerate electrons in regions of large spatial extent.

The cross-field electron drift velocity is

$$v_{oe} = v_E + v_{De} = - c \frac{E_\perp}{B} - \frac{T_e}{m_e \Omega_e} \frac{\partial}{\partial x} \ell n \, n_e \, , \qquad (13)$$

and the cross-field ion drift velocity is

$$v_{oi} = v_{Di} = \frac{T_i}{M_i \Omega_i} \frac{\partial \ell n}{\partial x} n_i \ . \tag{14}$$

where v_E is the $\vec{E} \times \vec{B}$ drift velocity, v_{De} and v_{Di} are the electron and ion diamagnetic drift velocities, T_e and T_i are the electron and ion temperatures in the acceleration region and the electron and ion cyclotron frequencies are $\Omega_e = |e|B_0/m_e c$ and $\Omega_i = |e|B_0/M_i c$. The ions are not able to $\vec{E} \times \vec{B}$ drift because the ion gyroradius is comparable to the length scale of the acceleration region, i. e.,

$$r_i = v_{Di}/\Omega_i \approx L_n = (\partial \ell n \ n/\partial x)^{-1} \ .$$

Recent research results indicate that ion diamagnetic drift energy provides the free energy reservoir which drives the lower-hybrid-drift instability (Hsia et al., 1979). The saturation electrostatic turbulent energy density, given in Eq. (8), may be expressed as,

$$\bar{W}_s = \gamma(\tfrac{1}{2} n_e m_e v_{oe}^2 + \tfrac{1}{2} n_i M_i v_{Di}) \approx \tfrac{1}{2}\gamma n_i M_i v_{Di}^2 \ , \tag{15}$$

where γ is the energy conversion efficiency coefficient.

III. TEST PARTICLE PROBLEM

The time evolution of the velocity and of the energy may be obtained by taking moments of the diffusion equation (12) and integrating by parts. For a test particle we take the distribution function to be

$$F_e(u,\tau) = \delta[u - u(\tau)] \quad , \tag{16}$$

and obtain

$$\frac{du}{d\tau} = (\alpha-3)|u|^{\alpha-4}\,\mathrm{sgn}\ u - E \quad , \tag{17}$$

and

$$\frac{d\varepsilon}{d\tau} = 2(\alpha-2)\ |u|^{\alpha-3} - 2Eu \quad . \tag{18}$$

In Eq. (18) the dimensionless energy $\varepsilon = u^2$. This expression is similar to a criterion for statistical acceleration that has been used frequently (Melrose 1968, 1969) but includes the effect of the parallel electric field. We caution the reader that some care must be taken when using the expressions (17) and (18). As was pointed out in a recent paper (Wu, Gaffey and Liberman, 1981), these equations are valid only when the terms that were integrated by parts are well behaved functions that are integrable over the entire range. For the problem considered in this paper, $\alpha > 2$ is required.

In the following subsections we give solutions to Eqs. (17) and (18) for various cases so that a comparison may be made.

A. Electric Field Only

Under the influence of the electric field alone, without diffusion, the velocity is

$$u(\tau) = -E\tau + u(0) \ , \tag{19}$$

where the initial velocity at time $\tau = 0$ is $u(0)$, and the energy is

$$\varepsilon(\tau) = E^2\tau^2 - 2u(0)E\tau + \varepsilon(0) \quad , \tag{20}$$

where the initial energy at time $\tau = 0$ is $\varepsilon(0) = u^2(0)$.

B. $\alpha = 3$ case

The velocity is

$$u(\tau) = - E\tau + u(0) \quad . \tag{21}$$

If the electric field is zero, the energy is

$$\varepsilon(\tau) = 2\tau + \varepsilon(0) \quad , \quad \text{for} \quad E = 0 \quad . \tag{22}$$

If the electric field is nonzero, Eq. (18) may be integrated to obtain

$$\sqrt{\varepsilon(\tau)} = - E\tau \ \text{sgn}\, u - \frac{\text{sgn}\, u}{E} \ell n\left(\frac{E\sqrt{\varepsilon(\tau)}\,\text{sgn}\ u-1}{E\sqrt{\varepsilon(0)}\,\text{sgn}\ u-1}\right) + \sqrt{\varepsilon(0)}, \ \text{for} \ E \neq 0 \ , \tag{23}$$

where $\text{sgn}\, u$ is the sign of the velocity. For E small, the logarithm may be expanded, and to second order Eq. (22) is recovered. For E large, the logarithm term is small, and we iterate to obtain

$$\varepsilon(\tau) \approx E^2\tau^2 + 2\tau \ \ell n \left(\frac{E\tau}{\sqrt{\varepsilon(0)}}\right) , \tag{23a}$$

where $\text{sgn}\ u = - 1$ has been used.

C. $\alpha = 4$ case

The velocity is

$$u(\tau) = - (E - \text{sgn}\ u\ )\tau + u(0) \quad , \tag{24a}$$

and the energy is

$$\varepsilon(\tau)=(2-E\ \mathrm{sgn}\ u)^2\tau^2 + 2\sqrt{\varepsilon(0)}(2-E\ \mathrm{sgn}\ u)\,\tau + \varepsilon(0) \quad . \tag{25a}$$

For $E > 1$, all particles are eventually accelerated to negative velocities,

$$u(\tau) = -(E+1)\tau + u(0) \quad , \tag{24b}$$

and the energy becomes

$$\varepsilon(\tau) = (E+2)^2\tau^2 + 2\sqrt{\varepsilon(0)}(E+2)\tau + \varepsilon(0) \quad . \tag{25b}$$

D. Averaged moments

For many purposes it is useful to have the moments averaged over the distribution of initial values, which we take to be a Maxwellian. We define the average value of a quantity A to be

$$\langle A\rangle \equiv \frac{1}{\sqrt{\pi}} \int_{-\infty}^{\infty} A e^{-u^2(0)} du(0) \quad . \tag{26}$$

For the case with only the electric field, the average velocity is

$$\langle u(t)\rangle = -E\tau \quad . \tag{27}$$

The average energy is

$$\langle \varepsilon(\tau)\rangle = E^2\tau^2 + \frac{1}{2} \quad . \tag{28}$$

The mean velocity squared is

$$\langle (\Delta u)^2\rangle \equiv \langle u^2\rangle - \langle u\rangle^2 = \frac{1}{2} \quad . \tag{29}$$

For the case $\alpha = 3$, the average velocity is

$$\langle u(\tau)\rangle = -E\tau \quad . \tag{30}$$

If the electric is zero, the average energy from Eq. (22) is

$$<\varepsilon(\tau)> = 2\tau + \frac{1}{2} \quad , \tag{31}$$

and the mean velocity squared is

$$<(\Delta u)^2> = 2\tau + \frac{1}{2} \quad . \tag{32}$$

If the electric field is large, the average energy from Eq. (23a) is

$$<\varepsilon(\tau)> \simeq E^2\tau^2 + 2\tau \ell n(E\tau) + (2\ell n2 + c) \quad , \tag{33}$$

where Euler's constant c is defined as

$$c \equiv \lim_{n\to\infty} \left(\sum_{m=1}^{n} \frac{1}{m} - \ell n\, n \right) = 0.577... \tag{34}$$

(Gradsteyn and Ryzhik, 1965). The mean velocity squared is

$$<(\Delta u)^2> = 2\tau \ell n(E\tau) + \tau(2\ell n2 + c) \quad . \tag{35}$$

For the case $\alpha = 4$, for $E < 1$, the average velocity is

$$<u(\tau)> = - E\tau \quad , \tag{36a}$$

the average energy from Eq. (25a) is

$$<\varepsilon(\tau)> = (E^2+4)\tau + \frac{4}{\sqrt{\pi}} \tau + \frac{1}{2} \quad , \tag{37a}$$

and the mean velocity squared is

$$<(\Delta u)^2> = 4\tau^2 + \frac{4}{\sqrt{\pi}} \tau + \frac{1}{2} \quad . \tag{38a}$$

For $E > 1$, the average velocity is

$$<u(\tau)> = - (E+1)\tau \quad , \tag{36b}$$

the average energy from Eq. (25b) is

$$\langle \varepsilon(\tau) \rangle = (E+2)^2 \tau^2 + \frac{2}{\sqrt{\pi}} (E+2)\tau + \frac{1}{2} \quad , \tag{37b}$$

and the mean velocity squared is

$$\langle (\Delta u)^2 \rangle = (2E+3)\tau^2 + \frac{2}{\sqrt{\pi}}(E+2)\tau + \frac{1}{2} \quad . \tag{38b}$$

IV. KINETIC THEORY

In this section we obtain solutions to the diffusion equation (12) for the electron Green's function and distribution function, and for moments of the Green's function and distribution function. Before proceeding we mention three points.

First, in order to conserve particle number density the functions

$$|u|^{\alpha-3}\frac{\partial F_e}{\partial u} \text{ and } F_e \text{ must be continuous} \qquad (39)$$

and vanish at the endpoints. This can be seen by integrating the diffusion equation (12) over the range of velocity.

Second, the wave-particle resonance, $k_{\|}v_{\|} = \omega$, is not expected to be satisfied for very small velocities because lower-hybrid waves usually have $k_{\|} \lesssim k(m_e/M_i)^{\frac{1}{2}}$. However, since the diffusion coefficient is proportional to the spectral energy density $\mathcal{E}_{\vec{k}}$ which varies as $k_{\|}^{-\alpha}$, the resonant electrons with small parallel velocities will diffuse very little.

Third, in Section III it was pointed out that the spectral index α must be > 2. Furthermore, α must be < 5 so that the diffusion process does not "runaway" to infinite velocities. In the following we shall find solutions for $\alpha = 3$ and 4 so that a comparison can be made.

We solve the diffusion equation (12) by using the method of Laplace transforms. The Laplace transform of (12) is

$$\frac{\partial}{\partial u} |u|^{\alpha-3} \frac{\partial f}{\partial u} + E \frac{\partial f}{\partial u} - sf = - f_0 \quad , \tag{40}$$

where the initial value $f_0(u) = F_e(u,0)$. We first construct a (41)
Green's function $g(u,u';s)$ which statisfies

$$\frac{\partial}{\partial u} |u|^{\alpha-3} \frac{\partial g}{\partial u} + E \frac{\partial g}{\partial u} - sg = - \delta(u-u') \quad . \tag{42}$$

Then $G(u,u';\tau)$, the inverse Laplace transform of $g(u,u';s)$, is calculated, and the time evolution of the distribution function is given by

$$F_e(u,\tau) = \int_{-\infty}^{\infty} du' \; G(u,u';\tau) f_0(u') \quad . \tag{43}$$

The Green's function $G(u,u';\tau)$ is somewhat analogous to the test particle distribution (16), and the velocity and energy moments of $G(u,u';\tau)$ are calculated and compared to the velocity and energy moments calculated for the test particle problem in section III.

In the next subsections we carry out the solution procedure for various cases, as we did in section III, so that a comparison may be made.

A Electric Field Only

Under the influence of the electric field alone, without diffusion,

the Vlasov equation is

$$\frac{\partial F_e}{\partial \tau} - E \frac{\partial F_e}{\partial u} = 0 \quad , \tag{44}$$

which is satified by any function $F_e(u,\tau) = F_e(u + E\tau)$. The Green's function is

$$G(u,u';\tau) = \delta(u-u' + E\tau) \ . \tag{45}$$

For an initial Maxwellian,

$$F_e(u,0) = \frac{1}{\sqrt{\pi}} e^{-u^2} \quad , \tag{46}$$

the distribution function is

$$F_e(u,\tau) = \frac{1}{\sqrt{\pi}} e^{-(u+E\tau)^2} \ . \tag{47}$$

The velocity moment of the Green's function (45) is

$$u(\tau) = - E\tau + u' \quad , \tag{48}$$

and the energy moment of Eq. (45) is

$$\varepsilon(\tau) = E^2\tau^2 - 2u'E\tau + \varepsilon' \ . \tag{49}$$

The velocity moment of the distribution function (47) is

$$\langle u(\tau) \rangle = - E\tau \quad , \tag{50}$$

the energy moment of (47) is

$$\langle \varepsilon(\tau) \rangle = E^2\tau^2 + \frac{1}{2} \quad , \tag{51}$$

and the mean velocity squared is

$$\langle(\Delta u)^2\rangle = \frac{1}{2} \quad . \tag{52}$$

B. Solution for the case $\alpha = 3$

For the case of the spectral index $\alpha = 3$, the diffusion equation (42) is particularly simple,

$$\frac{\partial^2 g}{\partial u^2} + E\frac{\partial g}{\partial u} - sg = -\delta(u-u') \quad . \tag{53}$$

The solutions of the associated homgeneous differential equation are

$$g_{\pm}(u) = e^{-\gamma_{\pm}u} \quad , \tag{54}$$

where

$$\gamma_{\pm} = \frac{E \pm (E^2 + 4s)^{\frac{1}{2}}}{2} \quad . \tag{55}$$

We note that $\gamma_- < 0 < \gamma_+$ for $E \geq 0$.

Because $g_-(u \to -\infty) = 0$ and $g_+(u \to \infty) = 0$, we look for a solution to Eq. (53) of the form,

$$g(u,u';s) = Ae^{-(\gamma_- u + \gamma_+ u')}U(u'-u) + Ae^{-(\gamma_+ u + \gamma_- u')}U(u-u') \quad . \tag{56}$$

where A is a function of u' and s , U is a Heaviside step function, and we have required that g be continuous at $u = u'$.

The coefficient A is determined by substituting Eq. (56) into Eq. (53). The desired solution has

$$A = \frac{1}{\gamma_+ - \gamma_-} e^{(\gamma_+ + \gamma_-)u'} \quad , \tag{57}$$

and thus,

$$g(u,u';s) = \frac{1}{2\sqrt{s + \tfrac{1}{4}E^2}} e^{-\frac{1}{2}E(u-u')} e^{-\sqrt{s+\frac{1}{4}E^2}\,|u-u'|} , \tag{58}$$

The inverse Laplace transform is well known (Abramowitz and Stegun 1964, Erdelyi 1954). Thus,

$$G(u,u',\tau) = \frac{1}{2\sqrt{\pi\tau}} e^{-(u-u'+E\tau)^2/4\tau} . \tag{59}$$

The distribution function is obtained from Eq. (43), using the Green's function (59) and the initial condition (46).

$$F_e(u,\tau) = \frac{1}{\sqrt{(4\tau+1)\pi}} e^{-(u+E\tau)^2/(4\tau+1)} . \tag{60}$$

If the electric field is zero, then the Green's function is

$$G(u,u';\tau) = \frac{1}{2\sqrt{\pi\tau}} e^{-(u-u')^2/4\tau} , \tag{59a}$$

which is the well known solution to the heat equation (Morse and Feshbach, 1953), and the distribution function is

$$F_e(u,\tau) = \frac{1}{\sqrt{\pi(4\tau+1)}} e^{-u^2/(4\tau+1)} , \tag{60a}$$

which was given by Wu, Gaffey and Liberman (1981).Note that the results in this paper differ by a normalization factor from those of Wu, Gaffey and Liberman.

The velocity moment of the Green's function (59) is

$$u(\tau) = - E\tau + u' , \tag{61}$$

and the energy moment of Eq. (59) is

$$\varepsilon(\tau) = E^2\tau^2 + 2(1-u'E)\tau + \varepsilon' . \tag{62}$$

The velocity moment of the distribution function (60) is

$$\langle u(\tau)\rangle = - E\tau \quad , \tag{63}$$

the energy moment of Eq. (60) is

$$\langle \varepsilon(\tau)\rangle = E^2\tau^2 + 2\tau + \frac{1}{2} \quad , \tag{64}$$

and the mean velocity squared is

$$\langle (\Delta u)^2\rangle = 2\tau + \frac{1}{2} \quad . \tag{65}$$

C. Solution for the case $\alpha = 4$

For the case of the spectral index $\alpha = 4$, the diffusion equation (42) is

$$\frac{\partial}{\partial u} |u| \frac{\partial g}{\partial u} + E \frac{\partial g}{\partial u} - sg = - \delta(u-u') \quad . \tag{66}$$

Changing variables to $z = 2\sqrt{|u|}$ yields,

$$\frac{\partial^2 g_{\pm}}{\partial z^2} + \frac{(1\pm 2E)}{z} \frac{\partial g_{\pm}}{\partial z} - sg_{\pm} = - \frac{1}{z'} \delta(z-z') \quad , \tag{67}$$

where the $\pm$ signs are for $u \gtrless 0$. Without loss of generality we have taken $E \geq 0$.

C.1 Solution for $u > 0$

The Green's function for $u > 0$ is derived in Appendix A.1. From Eq. (A5)

$$G_+(u,u';\tau) = \frac{1}{2\tau} \left(\frac{u'}{u}\right)^{E/2} e^{-\frac{(u+u')}{\tau}} I_E\left(\frac{2\sqrt{u\,u'}}{\tau}\right) \quad . \tag{68}$$

This expression is rather complicated. In many situations, the long time asymptotic behavior is of more interest. Using the small argument expansion of the Bessel function,

$$G_+(u,u';\tau) = \frac{u'^{E}}{2\Gamma(1+E)\tau^{(1+E)}} e^{-\frac{(u+u')}{\tau}} . \tag{69}$$

The distribution function is obtained from Eq. (43), using Eqs. (69) and (46). Using the small argument expansion of the parabolic cylinder function and the duplication formula for the gamma function (Abramowitz and Stegun 1964), $\Gamma(1+E) = \pi^{-\frac{1}{2}}2^{E}\Gamma(\frac{1+E}{2})\Gamma(\frac{2+E}{2})$, we find

$$F_+(u,\tau) = \frac{e^{-\frac{u}{\tau}}}{\Gamma(\frac{2+E}{2})(2\tau)^{(1+E)}} . \tag{70}$$

We note that Eq. (70) satisfies (12) exactly for $\alpha = 4$.

C.2. Solution for $u < 0$

The Green's function for $u < 0$ is derived in Appendix A.2. From Eqs. (A13) and (A15)

$$G_-(u,u';\tau) = \frac{1}{2\tau}\left|\frac{u}{u'}\right|^{\frac{E}{2}} e^{-\frac{(|u|+|u'|)}{\tau}} I_E\left(\frac{2\sqrt{|uu'|}}{\tau}\right) +$$

$$+ \frac{|uu'|^{E}}{2\Gamma(E)\Gamma(1+E)} \int_0^{\tau} \frac{d\lambda}{[\lambda(\tau-\lambda)]^{(1+E)}} e^{-\left(\frac{|u|}{\tau-\lambda}+\frac{|u'|}{\lambda}\right)} . \tag{71}$$

The long-time asymptotic behavior, for $\tau > 2\sqrt{|uu'|}$, is found by using the small argument expansion of the Bessel function in the first term.

$$G_-(u,u',\tau) = \frac{|u|^E}{2\Gamma(1+E)\tau^{(1+E)}} e^{-\frac{(|u|+|u'|)}{\tau}} +$$

$$+ \frac{|uu'|^E}{2\Gamma(E)\Gamma(1+E)} \int_0^\tau \frac{d\lambda}{[\lambda(\tau-\lambda)]^{(1+E)}} e^{-(\frac{|u|}{\tau-\lambda} + \frac{|u'|}{\lambda})} \quad . \tag{72}$$

The distribution function is obtained from Eq. (43) using Eqs. (72) and (46).

$$F_-(u,\tau) = \frac{|u|^E}{2\Gamma(1+E)\tau^{(1+E)}} e^{-\frac{|u|}{\tau}} e^{\frac{1}{4\tau^2}} \operatorname{erfc}(\frac{1}{2\tau}) +$$

$$+ \frac{|u|^E}{\sqrt{\pi}2^{\frac{(1+E)}{2}}\Gamma(E)} \int_0^\tau \frac{d\lambda}{[\lambda(\tau-\lambda)]^{(1+E)}} e^{-\frac{|u|}{\tau-\lambda}} e^{\frac{1}{8\lambda^2}} D_{-(1+E)}(\frac{1}{\sqrt{2}\lambda}) \quad , \tag{73}$$

where erfc is a complementary error function and $D_{-(1+E)}$ is a parabolic cylinder function.

For $\tau > \frac{1}{2}$, the first term can be expanded to give

$$F_-(u,\tau) = \frac{|u|^E}{2\Gamma(1+E)\tau^{(1+E)}} e^{-\frac{|u|}{\tau}} +$$

$$+ \frac{|u|}{\sqrt{\pi}2(\frac{1+E}{2})\Gamma(E)} \int_0^\tau \frac{d\lambda}{[\lambda(\tau-\lambda)]^{(1+E)}} e^{-\frac{|u|}{\tau-\lambda}} e^{\frac{|u|}{8\lambda^2}} D_{-(1+E)}(\frac{1}{\sqrt{2}\lambda}) \quad . \tag{74}$$

We note that Eq. (74) satisfies Eq. (12) exactly for $\alpha = 4$.

If the electric field is zero, then the Green's function is

$$G(u,u';\tau) = \frac{1}{2\tau} e^{-\frac{(|u|+|u'|)}{\tau}} I_0(\frac{2}{\tau}\sqrt{|uu'|}) \quad . \tag{75}$$

The long-time asymptotic behavior is found by taking the small argument expansion of the Bessel function,

$$G(u,u';\tau) \approx \frac{1}{2\tau} e^{-\frac{(|u|+|u'|)}{\tau}} \quad . \tag{76}$$

The long-time asymptotic form for the distribution function is

$$F_e(u,\tau) = \frac{1}{2\tau} e^{-\frac{|u|}{\tau}} \quad . \tag{77}$$

These results were obtained recently by Wu, Gaffey and Liberman (1981). Note that the functions in this paper differ by a normalization factor from those in the previous paper.

The velocity moment of the exact Green's functions (71) and (68) is

$$u(\tau) = -\frac{1}{2}\tau\{(E+1)+\frac{|u'|}{\tau} + \frac{(E+1)}{\Gamma(E)}\left[\Gamma(E, \frac{|u'|}{\tau}) - \frac{|u'|}{\tau}\Gamma(E-1, \frac{|u'|}{\tau})\right] -$$

$$- \frac{1}{\Gamma(E+1)}\left(\frac{|u'|}{\tau}\right)^E \Phi(E-1,E+1; -\frac{|u'|}{\tau})\} \quad , \tag{78}$$

and the energy moment is

$$\varepsilon(\tau) = \tau^2\{\frac{1}{2}(E+2)(E+1) + (E+2)\frac{|u'|}{\tau} + \frac{u'^2}{2\tau^2} + \frac{(E+2)(E+1)}{2\Gamma(E)}[\Gamma(E, \frac{|u'|}{\tau}) -$$

$$- 2\frac{|u'|}{\tau}\Gamma(E-1,\frac{|u'|}{\tau}) + \frac{u'^2}{\tau^2}\Gamma(E-2,\frac{|u'|}{\tau})] + \frac{1}{\Gamma(E+1)}\left(\frac{|u'|}{\tau}\right)^E \Phi(E-2,E+1;-\frac{|u'|}{\tau})\} \tag{79}$$

where $\Gamma(a)$ is the gamma function, $\Gamma(a,x)$ is the incomplete gamma function and $\Phi(a,b;x)$ is the confluent hypergeometric function (Abramowitz and Stegun, 1964; Gradsteyn and Ryzhik, 1965). The first several terms of the long-time expansions of Eqs. (78) and (79) are

$$u(\tau) \cong -\tau\left[(E+1) - \frac{1}{(E-1)}\,\frac{|u'|}{\tau} + \ldots\right] , \quad \text{for} \quad E > 1 , \tag{78a}$$

and

$$\varepsilon(\tau) \cong \tau^2\left[(E+2)(E+1) - \frac{2(E+2)}{(E-1)}\,\frac{|u'|}{\tau} + \frac{(E^2+2)}{(E-2)(E-1)}\,\frac{u'^2}{\tau^2} + \ldots\right], \text{for } E > 2 , \tag{79a}$$

where $E > 1$ has been assumed in Eq. (78a) and $E > 2$ in Eq. (79a) to neglect terms of order $(|u'|/\tau)^E$.

The dominant terms of the velocity and energy moments of the approximate Green's functions (72) and (69) are

$$u(\tau) \cong -(E+1)\tau \tag{78b}$$

and

$$\varepsilon(\tau) \cong (E+2)(E+1)\tau^2 , \tag{79b}$$

which agree with the expansions (78a) and (79a) to leading order.

The first few terms of the velocity, energy and mean velocity squared moments of the exact distribution functions obtained by averaging Eqs. (78a) and (79a) over an initial Maxwellian distribution are

$$\langle u(\tau)\rangle = -(E+1)\tau + \frac{1}{\sqrt{\pi}(E-1)} + \ldots , \qquad \text{for } E > 1 \tag{80}$$

$$\langle \varepsilon(\tau)\rangle = (E+2)(E+1)\tau^2 - \frac{2(E+2)\tau}{\sqrt{\pi}(E-1)} + \frac{(E^2+2)}{2(E-2)(E-1)} + \ldots, \qquad \text{for } E > 2, \tag{81}$$

and

$$\langle (\Delta u)^2\rangle = (E+1)\tau^2 - \frac{2\tau}{\sqrt{\pi}(E-1)} + \frac{E^2+2}{2(E-2)(E-1)} - \frac{1}{\pi(E-1)^2} + \ldots, \text{for } E > 2. \tag{82}$$

The dominant terms of the velocity, energy and mean velocity squared moments of time asymptotic distribution functions (74) and (70) are

$$\langle u(\tau)\rangle \approx -(E+1)\tau , \tag{80a}$$

$$\langle \varepsilon(\tau) \rangle = (E+2)(E+1)\tau^2 \quad , \tag{81a}$$

and

$$\langle (\Delta u)^2 \rangle = (E+1)\tau^2 \quad , \tag{82a}$$

which agree with Eqs. (80), (81) and (82) to leading order.

If the electric field is zero, the moments (78) and (79) may be easily evaluated to obtain

$$u(\tau) = (\tau + |u'|)\operatorname{sgn} u \quad , \quad \text{for} \quad E = 0 \ , \tag{78c}$$

and

$$\varepsilon(\tau) = 2\tau^2 + 4|u'|\tau + u'^2 \ , \quad \text{for} \quad E = 0 \ . \tag{79c}$$

The moments averaged over a Maxwellian are

$$\langle u(\tau) \rangle = 0 \quad , \quad \text{for} \quad E = 0 \tag{80b}$$

$$\langle \varepsilon(\tau) \rangle = 2\tau^2 + \frac{4}{\sqrt{\pi}} + \frac{1}{2} \quad , \quad \text{for} \quad E = 0 \ , \tag{81b}$$

$$\langle (\Delta u)^2 \rangle = 2\tau^2 + \frac{4}{\sqrt{\pi}} + \frac{1}{2} \quad , \quad \text{for} \quad E = 0 \ . \tag{82b}$$

V. DISCUSSION AND SUMMARY

A summary of the results of the test particle moments calculated in Section III is given in Table 1. A summary of the kinetic theory moments calculated in Section IV is given in Table 2. The averaged test particle moments are given in Table 3 and the averaged kinetic theory moments are given in Table 4.

We remark that the energy $\varepsilon(\tau)$ varies linearly with time for a diffusion process, whereas $\varepsilon(\tau)$ varies quadratically with time for an acceleration process.

When the electric field is zero, under the influence of quasilinear effects alone, for the case $\alpha = 3$, the energy $\varepsilon(\tau) \sim \tau$, which is characteristic of a diffusion process, and for $\alpha = 4$, $\varepsilon(\tau) \sim \tau^2$ because the quasilinear kinetic equation (12) contains an acceleration term as well as a diffusion term for this case. Thus, the larger the spectral index α (the narrower the spectrum) the more effective the energization process. We further note that in the absence of an electric field, the quasilinear effects increase the electron energy symmetrically for electrons with positive and negative velocities, since in this case Eq. (12) depends only on the absolute value of the velocity. This results is in agreement with satellite observations of Sharp, Shelley, Johnson and Ghielmetti (1980).

When the electric field is large, $E > 1$, the long time asymptotic velocity $u(\tau) \approx - E\tau$ and the energy $\varepsilon(\tau) \approx E^2\tau^2$ in all cases. This is characteristic of an acceleration process. For $\alpha = 3$, the fact that the test particle moments and the kinetic theory moments are approximately comparable if $\ell n(E\tau) \sim 0(1)$ may be attributed to the diffusion being constant, independent of the velocity. For $\alpha = 4$, the more rapid increase with time of the test particle moments compared to the kinetic

theory moments may be attributed to the fact that the test particle distribution function (16) was assumed to remain a delta function whereas the Green's function spreads with time. The Green's functions for $\alpha = 3$ and 4 both have denominators in the exponentials that vary linearly with time, which gives the velocity spread which increases with time. However, for the case of electric field acceleration alone, the Green's function $G(u,u';\tau) = \delta(u - u' + E\tau)$, because the diffusion has been neglected.

An important difference between the various cases is the spread in velocity. For electric field acceleration only, the mean velocity squared $\langle(\Delta u)^2\rangle = \frac{1}{2}$, which is the thermal spread of the initial Maxwellian. For $\alpha = 3$, $\langle(\Delta u)^2\rangle \sim \tau$, which is characteristic of diffusion with a constant diffusion coefficient. For $\alpha = 4$, $\langle(\Delta u)^2\rangle \sim \tau^2$, which is characteristic of an acceleration process.

Another feature is that in all cases the leading term of the long time asymptotic moments is independent of the initial distribution. This may be attributed to the nature of the diffusion and acceleration processes.

The observations of precipitating energetic auroral electrons by rockets at low altitudes (Kaufmann et al., 1976; Lundin, 1976; Bryant et al., 1978) and by satellites at higher altitudes (Whalen and Daly, 1979; Sharp et al., 1980) have several features that cannot be accounted for simply by the model of laminar acceleration by a quasistatic parallel electric field alone. As discussed in Section IIA, the peak value of the potential difference along the auroral magnetic field lines is estimated to be about 4 or 5 kV, and therefore can provide only about one half of the observed energy, $\gtrsim$ 10 keV, of the precipitating electrons. The additional energy must be the result of some other energization process, such as turbulent acceleration by electrostatic plasma waves. If the electrons fall through a potential difference Φ , the resulting energy gain will be $e\Phi$, but the velocity spread will remain the same as that before the acceleration.

Also, in this case the electron disrtibution function will fall off rather abruptly with increasing energy above $e\phi$, whereas the observed electron distribution functions tend to be rather broad and fall off more slowly. Our model, which includes the combined effects of velocity diffusion and electric field acceleration agrees better with the observed electron distribution functions.

Because the electron acceleration occurs near the open auroral magnetic field lines, we assume a dipole magnetic field $B = B_0(1 + h/R_E)^3$, where B_0 is the magnetic field strength at the earth, h is the altitude above the earth, and R_E is the radius of the earth, to calculate the electron and ion cyclotron frequencies as a function of altitude. The numerical values are listed in Table 5. The values for the electron number density used to calculate the plasma frequencies, are also given in Table 5. The values taken for the physical quantities are $B_0 = 0.40$ Gauss, $T_e = 1$ keV and $T_i = 200$ eV, which give $v_{the} = 1.88.10^9$ cm/sec and $v_{di} \approx \frac{1}{2} v_{thi} = 9.79.10^6$ cm/sec.

As an example, we take the intermediate altitude h = 5000 km, $E_{\parallel} = 1$ mV/m and 5 mV/m, $E_{\perp} = 400$ mV/m, $\gamma \approx 10^{-3}$, $\omega/k_m v_{the} \sim 0(1)$, $T_e = 1$ keV and $T_i = 200$ eV. In Figure 1, we plot the electron energy as a function of time from Eq. (20) for acceleration by the parallel electric field alone, for $E_{\parallel} = 1$ mV/m and 5 mV/m and an initial energy of 1 keV. The larger electric field, of course, gives rise to a greater acceleration. In Figure 2, the electron energy is plotted as a function of time for acceleration by the plasma turbulence alone from Eq. (22) for $\alpha = 3$ and from Eq. (25a) for $\alpha = 4$ for an initial energy of 1 keV. The larger the spectral index α (the narrower the spectrum) the greater is the turbulent acceleration of the electrons. Comparing Figures 1 and 2, we find that the electric field acceleration for $E_{\parallel} = 1$ mV/m and the turbulent acceleration for $\alpha = 4$ are very nearly comparable at an alti-

tude of 5000 km. At higher altitudes the turbulent acceleration is greater, whereas the electric field acceleration is independent of altitude. In Figure 3, the electron energy is plotted as a function of time for acceleration under the combined influence of plasma turbulence and a parallel electric field of 1 mV/v and 5 mV/m using Eq. (23) for $\alpha = 3$ and Eq. (25a) for $\alpha = 4$ for an initial energy of 1 keV. As in Figure 2, the acceleration is greater for the larger value of α. Also, the difference between $\alpha = 4$ and $\alpha = 3$ is more pronounced for the smaller value of the electric field. Of course, when both acceleration mechanisms are operable, the acceleration is greater than when only one acceleration mechanism is operable.

In this paper we have investigated the acceleration of auroral electron by parallel electric fields and electrostatic plasma turbulence near the lower-hybrid frequency. We find that the combined effects of a parallel electric field and electrostatic plasma turbulence is especially effective in producing energetic electrons. In particular, the present study has led to the following major conclusions:

1. A larger electric field produces greater acceleration; however, acceleration by an electric field alone does not increase the velocity spread of the electron distribution function.

2. A larger spectral index, i.e. a narrower spectrum of waves, produces greater turbulent acceleration. Turbulent acceleration increases both the velocity spread and the average energy of the electron distribution function.

3. The turbulent acceleration mechanism is more effective at higher altitudes, whereas the electric field acceleration is independent of altitude.

4. For some values of the parameters which are typical of the auroral zones the turbulent acceleration and the electric field acceleration are comparable.

5. When both acceleration mechanisms are operable the acceleration is greater than when only one acceleration mechanism is operable.

ACKNOWLEDGMENTS

Informative discussions with Dr. C.S. Wu are gratefully acknowledged. This work was supported in part by the Office of Naval Research under contract N-00014-82-K-0208 and in part by the National Aeronautics and Space Administration under grant NGL 21-002-005.

REFERENCES

Abramowitz, M. and I.A. Stegun, Handbook of Mathematical Functions, National Bureau of Standards, Washington, D.C., 1964.

Bryant, D.A., D.S. Hall and D.R. Lepine, Electron acceleration in an array of auroral arcs, Planet. Space Sci., 26, 81, 1978.

Chiu, Y.T. and M. Schulz, Self-consistent particle and parallel electrostatic field in ion and electron distributions in velocity space, J. Geophys. Res., 83, 2701, 1978.

Cladis, J.B., G.T. Davidson, W.E. Francis, L.L. Newkirk, and M. Walt, Assessment of magnetospheric processes of importance to Hane, final report, contract DNA-78-C-0081, Lockheed Palo Alto Res. Lab., Palo Alto, California, Jan. 15, 1979.

Davidson, R.C., Methods in Nonlinear Plasma Theory, p. 166, Academic Press, New York, 1972.

Davidson, R.C. and N.A. Krall, Anomalous transport in high-temperature plasmas with applications to solenoidal fusion systems, Nuclear Fusion, 17, 1313, 1977.

Erdelyi, A., Table of Integral Transforms, vol. 1, McGraw-Hill, New York, 1954.

Fridman, M. and J. Lemaire, Relationships between auroral electron fluxes and field-aligned electric potential difference, J. Geophys. Res., 85, 664, 1980.

Gary, S.P., M.D. Montgomery, and D.W. Swift, Particle acceleration by electrostatic waves with spatially varying phase velocities, J. Geophys. Res. 73, 7524, 1968.

Gradsteyn, I.S. and I.W. Ryzhik, Table of Integrals Series and Products, Academic Press, New York, 1965.

Gurnett, D.A. Electric field and plasma observations in the magnetosphere, in Critical Problems of Magnetospheric Physics, edited by E.R. Dyer, p. 123, National Academy of Sciences, Washington, D.C. 1972.

Gurnett, D.A. and L.A. Frank, VLF hiss and related plasma observations in the polar magnetosphere, J. Geophys. Res., 77, 172, 1972.

Gurnett, D.A. and L.A. Frank, A region of intense plasma wave turbulence on auroral field lines, J. Geophys. Res., 82, 1031, 1977.

Hall, D.S. and D.A. Bryant, Collimation of auroral particles by time-varying acceleration, Nature, 251, 402, 1974.

Hoffman, R.A. and D.S. Evans, Field-aligned electron bursts at high latitudes observed by OGO 4,J. Geophys. Res., 73, 6201, 1968.

Hsia, J.B.,S.M. Chiu, M.F. Hsia, R.L. Chou and C.S. Wu, Generalized Lower-hybrid-drift instability, Phys. Fluids, 22, 1737, 1979.

Hudson, M.K. and F.S. Mozer, Electrostatic shocks, double layers, and anomalous resistivity in the magnetosphere, Geophys. Res. Lett., 5, 131, 1978.

Kan, J.R., Energization of auroral electrons by electrostatic shock waves, J. Geophys. Res., 80, 2089, 1975.

Kan, J.R., L.C. Lee, and S.I. Akasofu, Two dimensional potential double layers and descrete auroras, J. Geophys. Res., 84, 4305, 1979.

Kaufmann, R.L., D.N. Walker, and R.L. Arnoldy,Acceleration of auroral electrons in parallel electric fields, J. Geophys. Res., 81, 1673, 1976.

Kennel, C.F. and F. Engelmann, Velocity space diffusion from weak plasma turbulence in a magnetic field, Phys. Fluids, 9, 2377, 1966.

Kintner, P.M., M.C. Kelley, and F.S. Mozer, Electrostatic hydrogen cyclotron waves near one earth radius altitude in the polar magnetosphere, Geophys. Res. Lett., 5, 139, 1978,

Kintner, P.M., M.C. Kelley, R.D. Sharp, A.G. Ghielmetti, M. Temerin, C.A. Cattell and P. Mizera, Simultaneous observations of energetic (keV) upstreaming ions and EHC waves, J. Geophys. Res., 84, 7201, 1979.

Laval, G. and R. Pellat, Particle acceleration by electrostatic waves propagating in an inhomogeneous plasma, J. Geophys. Res., 75, 6324, 1970.

Lundin, R., Rocket observations of electron spectra and angular characteristics in an inverted-V event, Planet. Space Sci., 24, 499, 1976.

Melrose, D.B., The emission and absorption of waves by charged particles in magnetized plasmas, Astrophys. Space Sci., 2, 171, 1968.

Melrose, D.B., Resonant interaction of hydromagnetic waves with charged particles, Astrophys. Space Sci., 4, 143, 1969.

Mizera, P.F., J.F. Fennell, D.R. Croley, Jr., A.L. Vampola, F.S. Mozer, R.B. Torbert, M. Temerin, R.L. Lysak, M.K. Hudson, C.A. Cattell,, R.G. Johnson, R.D. Sharp, P.M. Kintner, and M.C. Kelley. The aurora inferred from S3-3 particles and fields, J. Geophys. Res., 86, 2329. 1981.

Morse, P.M. and H. Feshbach, Methods of Theoretical Physics, vol. I, p. 862, McGraw-Hill, New York, 1953.

Mozer, F.S., C.W. Carlson, M.K. Hudson, R.B. Torbert, B. Parady, J. Yatteau, and M.C. Kelley, Observations of paired electrostatic shocks in the polar magnetosphere, Phys. Rev. Lett., 38, 292, 1977.

Mozer, F.S., C.A. Cattell, M. Temerin, R.B. Torbert, S. Von Glinske, M. Woldorff, and J. Wygant, The DC and AC electric field, plasma density, plasma temperature, and field-aligned current experiments on the S3-3 satellite, J. Geophys. Res., 84, 5875, 1979.

Mozer, F.S., C.A. Cattell, M.K. Hudson, R.L. Lysak, M. Temerin, and R.B. Torbert, Satellite measurements and theories of auroral acceleration mechanisms, Space Sci. Rev. 24, 155, 1980.

Paschmann,G., R.G. Johnson, R.D. Sharp, and E.G. Shelley, Angular distributions of auroral electrons in the energy range 0.8-16 keV, J. Geo-Phys. Res., 77, 6111, 1972.

Sharp, R.D., R.G. Johnson, and E.G. Shelley, Energetic particle measurements from within ionospheric structures responsible for auroral acceleration processes, J. Geophys. Res., 84, 480, 1979.

Sharp, R.D., E.G. Shelley, R.G. Johnson, and A.G. Ghielmetti, Counter-streaming electron beams at altitudes of $\sim 1\ R_E$ over the auroral zone, J. Geophys. Res. 85, 92, 1980.

Shawhan, S.D. C.G. Fälthammer, and L.P. Block, On the nature of large auroral zone electric fields at 1 - R_E altitude, J. Geophys. Res., 83, 1049, 1978.

Swift, D.W., Particle acceleration by electrostatic waves, J. Geophys. Res., 75, 6324, 1975.

Swift, D.W., An equipotential model for auroral arcs; the theory of two-dimensional electrostatic shocks, J. Geophys. Res., 84, 6427, 1979.

Temerin, M., The polarization, frequency, and wavelengths of high latitude turbulence, J. Geophys. Res., 83, 2609, 1978.

Temerin, M.A., A comment on the source of VLF saucers, J. Geophys. Res., 84, 6691, 1979.

Temerin, M.A., M. Woldorff, and F.S. Mozer, Nonlinear steepening of the electrostatic ion cyclotron wave, Phys, Rev. Lett., 43, 1491, 1979.

Temerin, M., K. Cerny, W. Lotko, and F.S. Mozer, Observations of double layers and solitary waves in the auroral plasma, Phys. Rev. Lett., 48, 1175, 1982.

Torbert, R.B. and F.S. Mozer, Electrostatic shocks as the source of discrete auroral arcs, Geophys. Res. Lett., 5, 135, 1978.

Tsytovich, V.N., Statistical acceleration of particles in a turbulent plasma, Sov. Phys.Uspeckhi, 9, 370, 1977.

Tsytovich, V.N., Theory of Turbulent Plasmas, Chap. 5, Plenum New York, 1977.

Whalen, B.A. and I.B. McDiarmid, Observations of magnetic-field-aligned auroral electron precipitation, J. Geophys. Res., 77, 191, 1972.

Whalen, B.A. and P.W. Daley, Do field-aligned particle distributions imply acceleration by quasi-static parallel electric fields? J. Geophys. Res., 84, 4175, 1979.

Wu, C.S., J.D. Gaffey, Jr. and B. Liberman, Statistical acceleration of electrons by lower-hybrid turbulence, J. Plasma Phys., 25, 391, 1981.

Yamamoto, T., T. Imai, M. Shinada, N. Suzuki, M. Maeno, S. Konoshima, T. Fujii, K. Uehara, T. Nakashima, A. Funahashi, and N. Fujisawa, Experimental observation of the rf-driven current by the lower hybrid wave in a tokamak, Phys. Rev. Lett., 45, 716, 1980.

APPENDIX

In this appendix we derive the Green's function used in Section IVC.

A.1. Derivation of the Green's Function for $u > 0$

The homogeneous differential equation associated with Eq. (67) for $u > 0$ is

$$\frac{\partial^2 g}{\partial z^2} + \frac{(1+2E)}{z}\frac{\partial g_+}{\partial z} - s g_+ = 0 \ . \tag{A1}$$

The solutions are

$$g_+(z) = z^{-E} I_{\pm E}(z\sqrt{s}) \quad \text{and} \quad z^{-E} K_E(z\sqrt{s}) \ , \tag{A2}$$

where $I_{\pm E}$ and K_E are modified Bessel functions. Only $z^{-E}K_E(z\sqrt{s})$ is bounded as $z \to \infty$ and only $z^{-E} I_E(z\sqrt{s})$ is bounded as $z \to 0$. Furthermore,

$$|u| \frac{\partial g_+}{\partial |u|} = \frac{1}{2} z \frac{\partial g_+}{\partial z} = 0 \quad \text{at} \quad u = 0 \ \text{and} \ \infty \ , \ \text{so that Eq. (39) is satisfied.}$$

We look for a solution of the inhomogeneous differential equation (67) of the form

$$g_+(z,z';s) = C_+(zz')^{-E}[K_E(z'\sqrt{s})I_E(z\sqrt{s})U(z'-z) + I_E(z'\sqrt{s})K_E(z\sqrt{s})U(z-z')]. \tag{A3}$$

where the coefficient C_+ is a function of z', U is a Heaviside step function, and we have required that g_+ be continuous at $z = z'$.

The coefficient C_+ is determined by substituting Eq. (A3) into Eq. (67). The particular solution of Eq.(70), with $C_+ = z'^{2E}$, is

$$g_+(z,z';s) = \left(\frac{z'}{z}\right)^E [K_E(z'\sqrt{s})I_E(z\sqrt{s})U(z'-z)+I_E(z'\sqrt{s})K_E(z\sqrt{s})U(z-z')] \ . \qquad (A4)$$

The inverse Laplace transform of g_+ is (Erdelyi 1954)

$$G_+(z,z';\tau) = \frac{1}{2\tau}\left(\frac{z'}{z}\right)^E e^{-\left(\frac{z^2+z'^2}{4\tau}\right)} I_E\left(\frac{zz'}{2\tau}\right) \qquad (A5)$$

Returning to the original velocity variable $u = \frac{1}{4}z^2$, gives Eq. (68).

A.2 Derivation of the Green's Function for $u < 0$

The homogeneous equation associated with Eq. (67) for $u < 0$ is

$$\frac{\partial^2 g_-}{\partial z^2} + \frac{(1 - 2E)}{z} \frac{\partial g_-}{\partial z} - sg_- = 0 \ . \qquad (A6)$$

The solutions are

$$g_-(z) = z^E I_{\pm E}(z\sqrt{s}) \text{ and } z^E K_E(z\sqrt{s}) \ . \qquad (A7)$$

Only $z^E K_E(z\sqrt{s})$ is bounded as $z \to \infty$. Both $z^E I_{\pm E}(z\sqrt{s})$ are well behaved as $z \to 0$. Furthermore,

$|u|\frac{\partial g_-}{\partial |u|} = \frac{1}{2} z \frac{\partial g_-}{\partial z} = 0$ at $z = 0$ and ∞ , so that Eq. (39) is satisfied.

We look for a solution of the inhomogeneous equation (67) of the form

$$g_-(z,z';s) = (zz')^E\{[B_- I_E(z'\sqrt{s}) + C_- I_{-E}(z'\sqrt{s})]K_E(z\sqrt{s})U(z-z')$$

$$+ K_E(z'\sqrt{s})[B_- I_E(z\sqrt{s}) + C_- I_{-E}(z\sqrt{s})]U(z'-z)\} \ . \qquad (A8)$$

We will need two conditions to determine the two coefficients B_- and C_-. Continuity at $z = z'$ has been imposed.

Requiring that $\lim_{z\to 0} g_-(z,z';s) = \lim_{z\to 0} g_+(z,z';s)$ gives

$$C_- = \frac{\Gamma(1-E)}{\Gamma(1+E)} \left(\frac{s}{4}\right)^E \quad . \tag{A9}$$

The coefficient B_- is determined by substituting Eq. (A8) into Eq. (67),

$$B_- = z'^{-2E} - \frac{\Gamma(1-E)}{\Gamma(1+E)} \left(\frac{s}{4}\right)^E \quad . \tag{A10}$$

With the coefficients given in Eqs. (A10) and (A9), the Green's function (A8) becomes

$$g_-(z,z';s) = \left(\frac{z}{z'}\right)^E \{I_E(z'\sqrt{s}) + \frac{\Gamma(1-E)}{\Gamma(I+E)} \left(\frac{sz'^2}{4}\right)^E [I_{-E}(z'\sqrt{s}) - I_E(z'\sqrt{s})]\} K_E(z\sqrt{s}) U(z-z')$$
$$+ \left(\frac{z}{z'}\right)^E K_E(z'\sqrt{s}) \{I_E(z\sqrt{s}) + \frac{\Gamma(1-E)}{\Gamma(1+E)} \left(\frac{sz'^2}{4}\right)^E [I_{-E}(z\sqrt{s}) - I_E(z\sqrt{s})]\} U(z'-z) . \tag{A11}$$

Expressing $I_{-E} - I_E$ in terms of K_E and using the reflection formula for the gamma function (Abramowitz and Stegun 1964), $\Gamma(1-E) = \pi/\Gamma(E)\sin \pi E$, we separate the inhomogeneous and homogeneous terms in Eq. (A11).

$$g_-(z,z';s) = \left(\frac{z}{z'}\right)^E [I_E(z'\sqrt{s}) K_E(z\sqrt{s}) U(z-z') + K_E(z'\sqrt{s}) I_E(z\sqrt{s}) U(z'-z)] +$$
$$+ \frac{2}{\Gamma(E)\Gamma(1+E)} \left(\frac{szz'}{4}\right)^E K_E(z'\sqrt{s}) K_E(z\sqrt{s}) \quad . \tag{A12}$$

The inverse Laplace transform of the first term $g_{1-}(z,z';s)$ is

$$G_{1-}(z,z';\tau) = \frac{1}{2\tau} \left(\frac{z}{z'}\right)^E e^{-\left(\frac{z^2+z'^2}{4\tau}\right)} I_E\left(\frac{zz'}{2\tau}\right) \quad . \tag{A13}$$

The inverse Laplace transform of the second term $g_{2-}(z,z';s)$ is obtained from the formula (Erdelyi 1954)

$$L^{-1}[(\frac{s}{a})^{\frac{E}{2}} K_E(2\sqrt{as})] = \frac{1}{2\tau^{(1+E)}} e^{-\frac{a}{\tau}} . \qquad (A14)$$

Using the convolution formula, we find

$$G_{2-}(z,z';\tau) = \frac{1}{2\Gamma(E)\Gamma(1+E)} (\frac{zz'}{4})^{2E} \int_0^\tau \frac{d\lambda}{[\lambda(\tau-\lambda)]^{(1+E)}} e^{-[\frac{z^2}{4(\tau-\lambda)} + \frac{z'^2}{4\lambda}]} , \qquad (A15)$$

Returning to the original velocity variable $|u| = \frac{1}{4}z^2$, gives Eq. (71)

TABLE 1

Test particle moments for various cases

$u(\tau) = -E\tau = u(0)$	electric field only
$\varepsilon(\tau) = E^2\tau^2 - 2u(0)E\tau + \varepsilon(0)$	
$u(\tau) = u(0)$	$\alpha = 3$
$\varepsilon(\tau) = 2\tau + \varepsilon(0)$	diffusion only
$u(\tau) = \tau \operatorname{sgn} u(\tau) + u(0)$	$\alpha = 4$
$\varepsilon(\tau) = 4\tau^2 + 4\tau\sqrt{\varepsilon(0)} + \varepsilon(0)$	diffusion only
$u(\tau) = -E\tau + u(0)$	$\alpha = 3$, $E > 1$
$\varepsilon(\tau) \approx E^2\tau^2 + 2\tau\, \ell n(\frac{E\tau}{\sqrt{\varepsilon(0)}})$	diffusion and electric field
$u(\tau) = -(E+1)\tau + u(0)$	$\alpha = 4$, $E > 1$
$\varepsilon(\tau) = (E+2)^2\tau^2 + 2\sqrt{\varepsilon(0)}(E+2)\tau + \varepsilon(0)$	diffusion and electric field

Table 2

Kinetic theory moments for various cases

$u(\tau) = - E\tau + u'$	electric field only
$\varepsilon(\tau) = E^2\tau^2 - 2u'E\tau + \varepsilon'$	
$u(\tau) = u'$	$\alpha = 3$
$\varepsilon(\tau) = 2\tau + \varepsilon'$	diffusion only
$u(\tau) = (\tau + \lvert u' \rvert)\ \mathrm{sgn}\ u$	$\alpha = 4$,
$\varepsilon(\tau) = 2\tau^2 + 4\lvert u' \rvert \tau + \varepsilon'$	diffusion only
$u(\tau) = - E\tau + u'$	$\alpha = 3$
$\varepsilon(\tau) = E^2\tau^2 - 2(u'E-1)\tau + \varepsilon'$	diffusion and electric field
$u(\tau) \approx - (E+1)\tau$	$\alpha = 4$, $E > 2$
$\varepsilon(\tau) \approx (E+2)(E+1)\tau^2$	diffusion and electric field

TABLE 3

Averaged test particle moments for various cases

$\langle u(\tau)\rangle = -E\tau$	
$\langle \varepsilon(\tau)\rangle = E^2\tau^2 + \frac{1}{2}$	electric field only
$\langle (\Delta u)^2\rangle = \frac{1}{2}$	
$\langle u(\tau)\rangle = 0$	$\alpha = 3$
$\langle \varepsilon(\tau)\rangle = 2\tau + \frac{1}{2}$	diffusion only
$\langle (\Delta u)^2\rangle = 2\tau + \frac{1}{2}$	
$\langle u(\tau)\rangle = 0$	
$\langle \varepsilon(\tau)\rangle = 4\tau^2 + \frac{4}{\sqrt{\pi}}\tau + \frac{1}{2}$	$\alpha = 4$.
$\langle (\Delta u)^2\rangle = 4\tau^2 + \frac{4}{\sqrt{\pi}}\tau + \frac{1}{2}$	diffusion only
$\langle u(\tau)\rangle = -E\tau$	$\alpha = 3$, $E > 1$
$\langle \varepsilon(\tau)\rangle \approx E^2\tau^2 + 2\tau\, \ell n(E\tau)$	diffusion and electric field
$\langle (\Delta u)^2\rangle \approx 2\tau\, \ell n(E\tau)$	
$\langle u(\tau)\rangle = -(E+1)\tau$	$\alpha = 4$, $E > 1$
$\langle \varepsilon(\tau)\rangle = (E+2)^2\tau^2 + \frac{2}{\sqrt{\pi}}(E+2)\tau + \frac{1}{2}$	diffusion and electric field
$\langle (\Delta u)^2\rangle = (2E+3)\tau^2 + \frac{2}{\sqrt{\pi}}(E+2)\tau + \frac{1}{2}$	

TABLE 4

Averaged kinetic theory moments for various cases

$\langle u(\tau)\rangle = -E\tau$ $\langle \varepsilon(\tau)\rangle = E^2\tau^2 + \frac{1}{2}$ $\langle (\Delta u)^2\rangle = \frac{1}{2}$	electric field only
$\langle u(\tau)\rangle = 0$ $\langle \varepsilon(\tau)\rangle = 2\tau + \frac{1}{2}$ $\langle (\Delta u)^2\rangle = 2\tau + \frac{1}{2}$	$\alpha = 3$ diffusion only
$\langle u(\tau)\rangle = 0$ $\langle \varepsilon(\tau)\rangle = 2\tau^2 + \frac{4}{\sqrt{\pi}}\tau + \frac{1}{2}$ $\langle (\Delta u)^2\rangle = 2\tau^2 + \frac{4}{\sqrt{\pi}}\tau + \frac{1}{2}$	$\alpha = 4$ diffusion only
$\langle u(\tau)\rangle = -E\tau$ $\langle \varepsilon(\tau)\rangle = E^2\tau^2 + 2\tau + \frac{1}{2}$ $\langle (\Delta u)^2\rangle = 2\tau + \frac{1}{2}$	$\alpha = 3$ diffusion and electric field
$\langle u(\tau)\rangle \approx -(E+1)\tau$ $\langle \varepsilon(\tau)\rangle \approx (E+2)(E+1)\tau^2$ $\langle (\Delta u)^2\rangle \approx (E+1)\tau^2$	$\alpha = 4$, $E > 2$ diffusion and electric field

TABLE 5

Plasma parameters in the acceleration region

h(in km)	2000	3000	4000	5000	6000	7000	8000
B(in G)	0.2595	0.1837	0.1347	0.1016	0.0783	0.0615	0.0496
Ω_e(in rad/sec)	$4.57.10^6$	$3.23.10^6$	$2.37.10^6$	$1.79.10^6$	$1.38.10^6$	$1.08.10^6$	$8.73.10^5$
Ω_i(in rad/sec)	$2.49.10^3$	$1.76.10^3$	$1.29.10^3$	$9.73.10^2$	$7.50.10^2$	$5.89.10^2$	$4.75.10^2$
n(in cm^{-3})	80	50	30	15	10	5	5
ω_{pe}(in rad/sec)	$5.04.10^5$	$3.49.10^5$	$3.09.10^5$	$2.18.10^5$	$1.78.10^5$	$1.26.10^5$	$1.26.10^5$
ω_{pi}(in rad/sec)	$1.18.10^4$	$9.33.10^3$	$7.23.10^3$	$5.11.10^3$	$4.17.10^3$	$2.95.10^3$	$2.95.10^3$

FIGURE CAPTIONS

Figure 1 Electron energy (in keV) as a function of time (in sec) from Eq. (20) for acceleration by a parallel electric field only, for $E_{\parallel}$ = 1 mV/m and 5 mV/m.

Figure 2 Electron energy (in keV) as a function of time (in sec) from Eq. (22) for $\alpha = 3$ (dash dot curve) and Eq. (25a) for $\alpha = 4$ (solid curve) for acceleration by plasma turbulence only.

Figure 3 Electron energy (in keV) as a function of time (in sec) from Eq. (23) for $\alpha = 3$ (dash dot curve) and Eq. (25a) for $\alpha = 4$ (solid curve) for acceleration by plasma turbulence and a parallel electric field, for $E_{\parallel}$ = 1 mV/m and 5 mV/m.

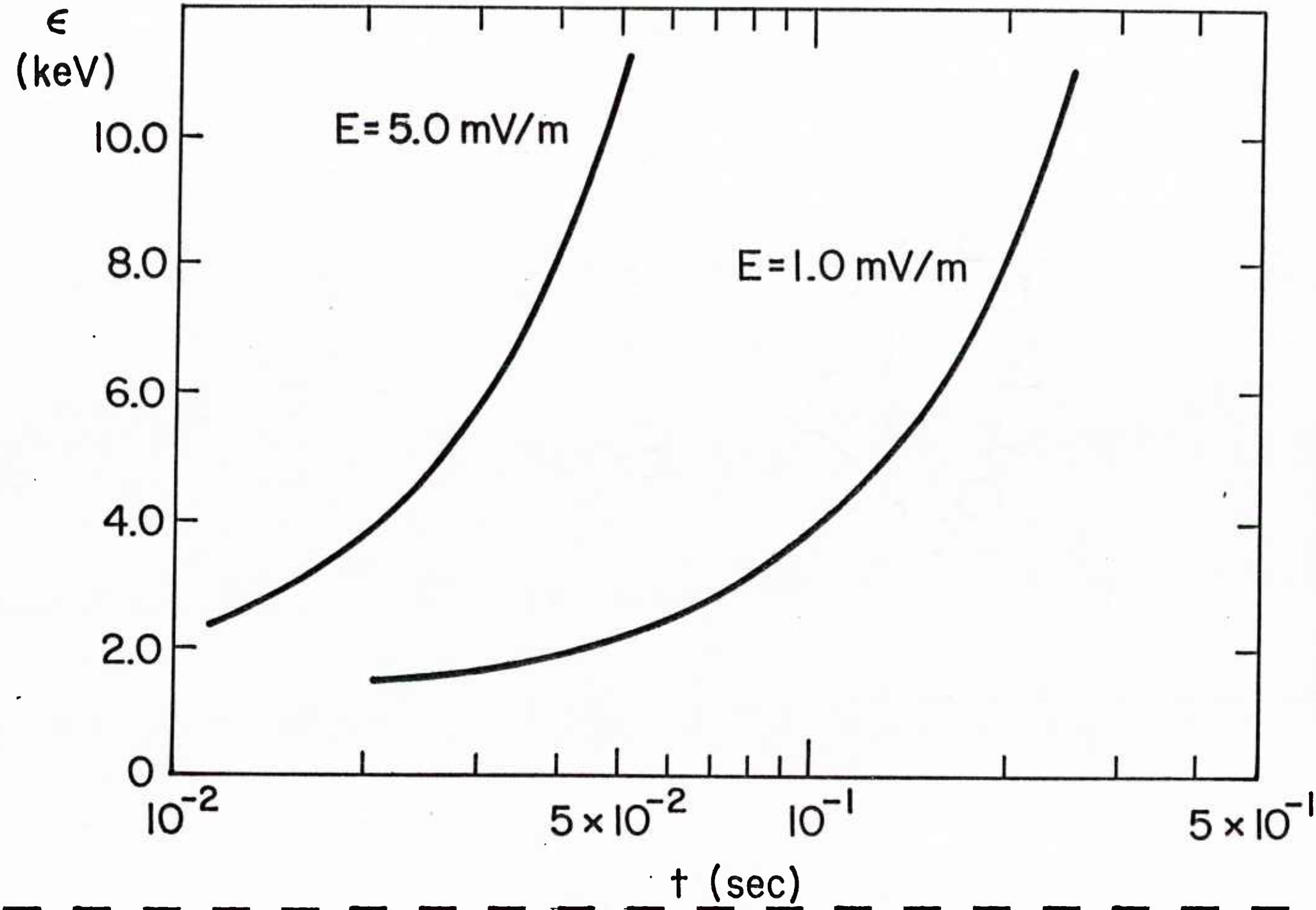
ϵ
(keV)
10.0
8.0
6.0
4.0
2.0
0
E = 5.0 mV/m
E = 1.0 mV/m
10^{-2}
5×10^{-2}
10^{-1}
5×10^{-1}
t (sec)

Figure 1

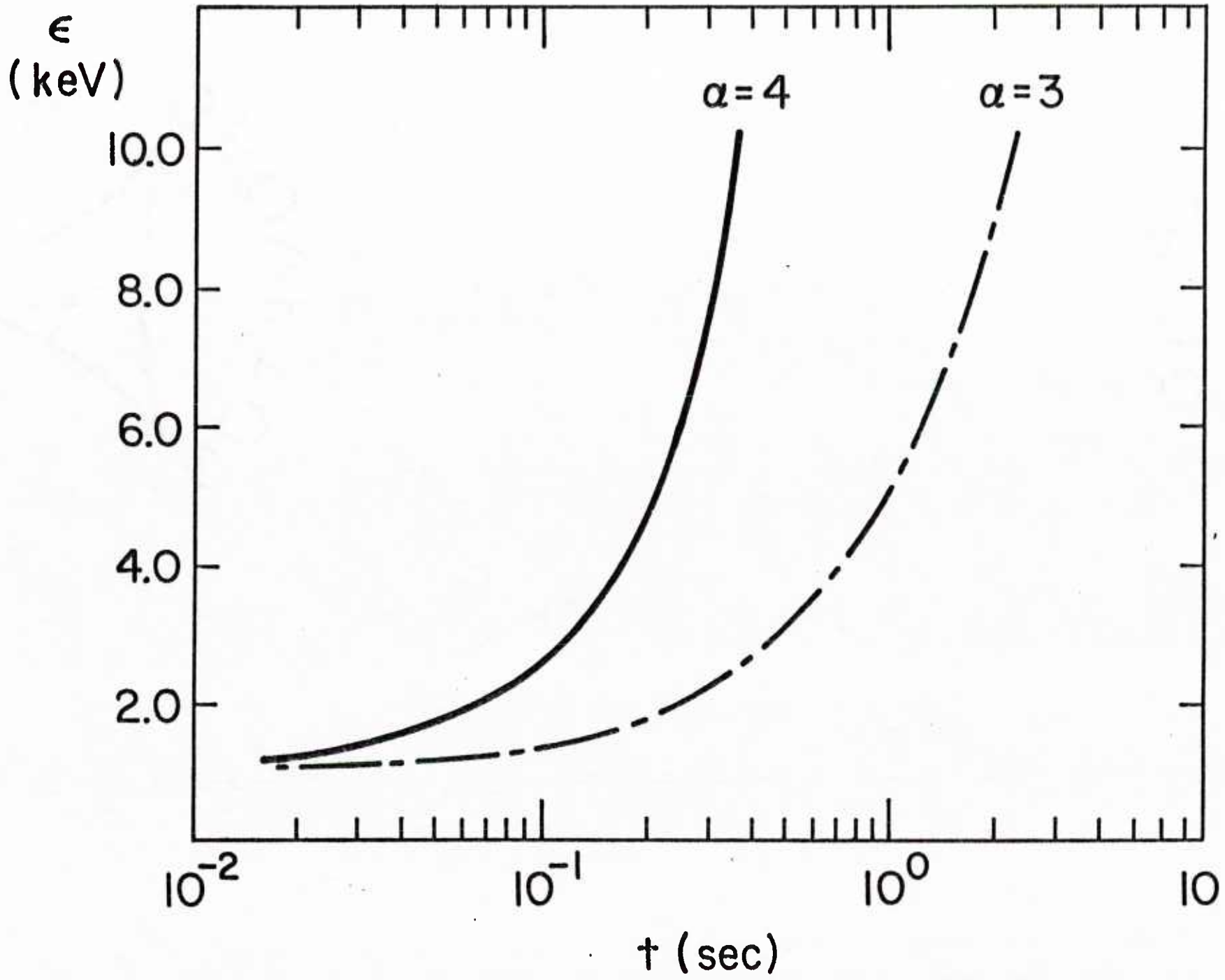

gure

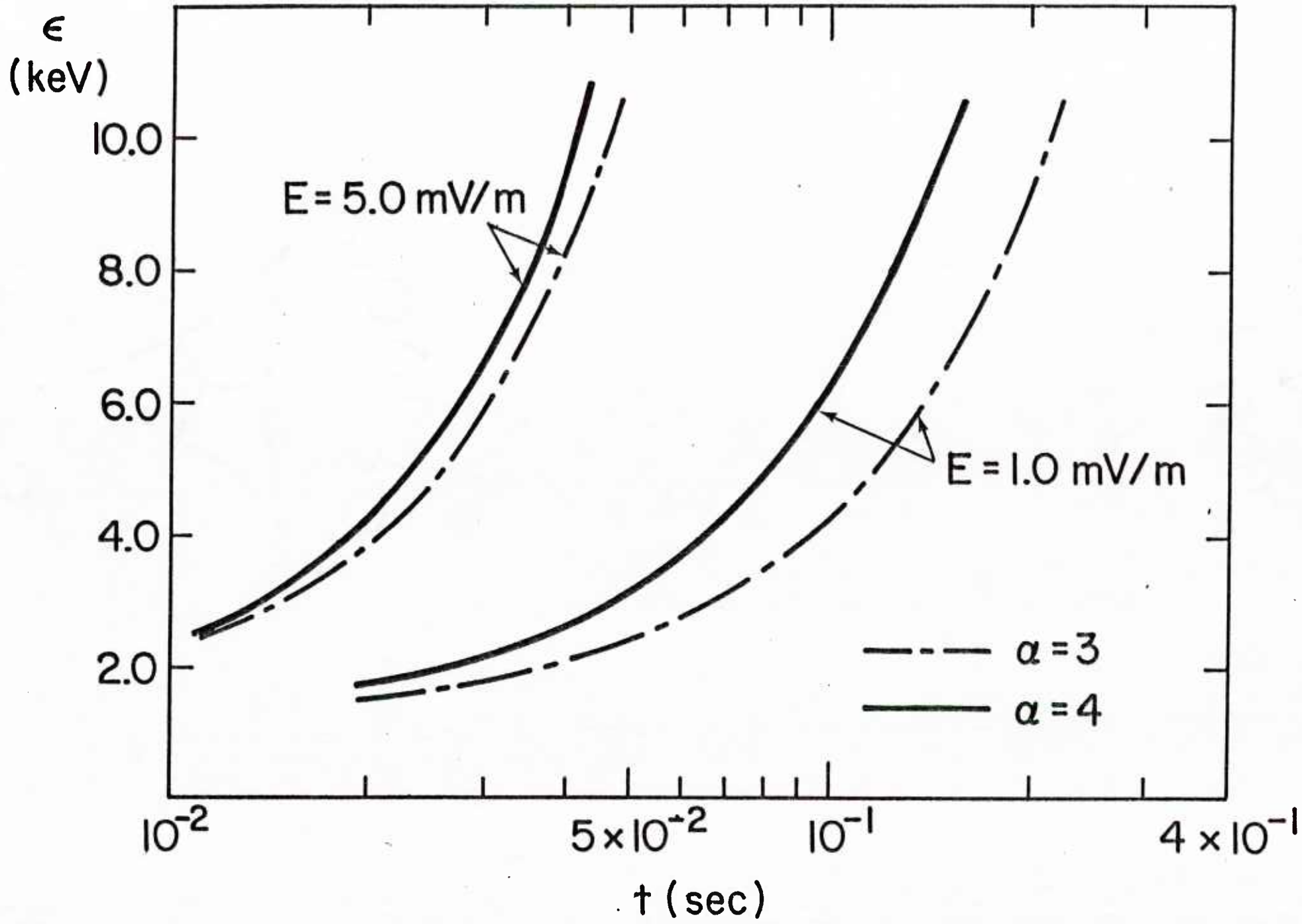

Figure

Comments on "Energization of Ionospheric Ions by Electrostatic Hydrogen Cyclotron Waves" by N. Singh, R.W. Schunk and J.J. Sojka, Geophys. Res. Lett., 8, 1249 (1981).

J.D. Gaffey, Jr.

Institute for Physical Science and Technology

University of Maryland

College Park, Maryland

20742

In a recent paper, Singh et al.(1981) make a comparison between the stochastic acceleration of ionospheric ions by electrostatic hydrogen cyclotron waves observed in their numerical simulations and the predicted acceleration of these ions based on the theory of stochastic acceleration (Papadopoulos et al., 1980). The assertion, made by Singh et al. that the heating of the helium ions observed in their simulations is appreciably larger than the heating predicted by the theory of stochastic acceleration (Papadopoulos et al.) is the result of an algebraic error. In fact, upon correcting the error, we find the agreement between the simulations and the theory to be quite good.

The error occurs in the second line of Eq. (5) of Singh et al., where the dimensionless wave amplitude α_i is defined as

$$\alpha_i \equiv \frac{k_\perp^2 q_i \Phi_o}{M_i \Omega_i^2} \quad , \tag{1a}$$

where $k_\perp$ is the perpendicular wavenumber, q_i and M_i are the ion charge and mass, the cyclotron frequency $\Omega_i \equiv q_i B/M_i c$, and Φ_o is the amplitude of the electrostatic potential of the wave. In terms of the dimensionless parameters of the background hydrogen plasma,

$$\alpha_i = \frac{1}{2} (k_\perp^2 r_H^2) \left(\frac{e\Phi_o}{T_H}\right)\left(\frac{\Omega_H}{\Omega_i}\right) \quad , \tag{1b}$$

where the Larmor radius $r_H = a_H/\Omega_H$ and the thermal velocity $a_H = (2T_H/M_H)^{1/2}$. Equation (1b) is given in Papadopoulos et al. on the line below their Eqs. (3) and (9). In proceeding from Eq. (1a) to Eq. (1b) Singh et al. omitted the factor 1/2, and thus obtained a value of α_i a factor of 2 too large.

The values of the dimensionless parameters of the background hydrogen plasma given by Papadopoulos et al. on the line below their Eq. (8) and by Singh et al. in their Eq. (3) are

$$\frac{\omega}{\Omega_H} = 1.2 \quad , \quad k_\perp r_H = 1.73 \quad , \quad \frac{e\Phi_o}{T_H} = 0.4 \quad . \tag{2}$$

Substituting the numerical values of Eq. (2) into Eq. (1b) gives

$$\alpha_i = 0.6 \frac{\Omega_H}{\Omega_i} = \frac{1}{2} \nu_i \quad , \tag{3}$$

where the frequency ratio $\nu_i \equiv \omega/\Omega_i$. The numerical values of $\alpha_i \approx \nu_i$ used by Singh et al. in their numerical simulations is a consequence of omitting the factor of 1/2 in Eq. (1b) and Eq. (3), and therefore is twice the value of the wave amplitude α_i used by Papadopoulos et al. for the same values of the parameters given in Eq. (2).

The maximum velocity achieved by stochastic acceleration, given by Singh et al. in Eq. (6) and by Papadopoulos et al. Eq. (7) is

$$v_{\perp max,i} = \left(\frac{2}{\pi}\right)^{1/3} (4\alpha_i \nu_i)^{2/3} \frac{\Omega_i}{k_\perp} \quad , \tag{4a}$$

which in terms of the dimensionless background plasma quantities becomes

$$v_{\perp max,i} = \left(\frac{2}{\pi}\right)^{1/3} \frac{(4\alpha_i \nu_i)^{2/3}}{k_\perp r_H} \frac{q_i}{e}\left(\frac{M_H T_H}{M_i T_i}\right)^{1/2} a_i \quad . \tag{4b}$$

The minimum velocity of the stochastic region, given by Singh et al. Eq. (8) and by Papadopoulos et al. Eq. (6) is

$$v_{\perp min,i} = \frac{\omega}{k_\perp}\left(1 - \frac{\alpha_i^{1/2}}{\nu_i}\right) \tag{5a}$$

which in terms of the dimensionless background plasma quantities becomes

$$v_{\perp min,i} = \frac{\nu_H}{k_\perp r_H}\left(1 - \frac{\alpha_i^{1/2}}{\nu_i}\right)\left(\frac{M_i T_H}{M_H T_i}\right)^{1/2} a_i \quad . \tag{5b}$$

In Table 1, we have calculated the minimum and maximum velocities of the stochastic region from Eqs. (4b) and (5b) for the parameters of the simulations of Singh et al., shown in their Figures 1a, 1b, 2, and 4, and also for the parameters of the simulations of Gaffey (1981) and Gaffey and Mulbrandon (1982).

The correct numerical values of $v_{\perp max,i}$ calculated from Eq. (4b) are a factor of $2^{2/3} \approx 1.6$ larger than Singh et al. have in their Figures 1a, 1b, 2, and 4 because of the error they made in calculating α_i.

The correct numerical values of $v_{\perp min,i}$ calculated from Eq. (5b) are a factor of $2^{1/2} \approx 1.4$ larger than Singh et al. have in their Figures 1a and 1b. Singh et al. did not calculate $v_{\perp min,i}$ for their Figures 2 and 4.

In Table 1, we have also summarized the results of the numerical simulations of Singh et al. and the numerical simulations of Gaffey (1981) and Gaffey and Mulbrandon (1982) for singly charged ions.

The agreement between the theoretically predicted values and the numerically calculated values is quite good in most cases. In general, it is seen that the numerically calculated $v_{\perp max,i}$ is slightly less than the

theoretically predicted value, and the numerically calculated $v_{\perp max,i}$ is slightly larger than the theoretically predicted value.

By comparing the values of $v_{\perp min,i}$ and $v_{\perp max,i}$ for $\alpha_i \approx 1/2\ \nu_i$ with those for $\alpha_i \approx \nu_i$, it is seen that the effect of increasing α_i is to decrease $v_{\perp min,i}$ and to increase $v_{\perp max,i}$, thus broadening the stochastic region.

We note that the maximum and minimum velocities given by Eqs. (4a) and (5a) depend only on the ion charge and mass, but not on the ion temperature. This is to be expected because they were derived from the equations of motion of an individual test particle. Changing the ion temperature, changes the width of the initial Maxwellian distribution, which changes the number of particles able to participate in the stochastic acceleration process, but not the maximum and minimum velocities of the stochastic region.

The theoretical minimum velocities for the 0^+ ions agree very well with the lower boundaries of the energized regions in Figures 1a and 1b of Singh et al. The theoretical maximum velocities for the 0^+ ions are about a factor of two greater than the largest velocities in Figures 1a and 1b of Singh et al. This may be due to the fact that $v_{\perp max,0^+}$ is large and Singh et al. have shown plots after only 160 0^+ cyclotron periods. In the simulations of Gaffey (1981) and Gaffey and Mulbrandon (1982) the 0^+ ions with $\alpha_{0^+} = 10$, continued to gain energy for a very long time and eventually exceeded the theoretical maximum velocity given in Table 1 and exceeded the largest velocities shown in Figures 1a and 1b of Singh et al. for $\alpha_{0^+} = 18.5$. The surface of section plots of perpendicular velocity versus gyrophase for the 0^+ ions contain a large number of islands of various orders which slow down the stochastic diffusion process. This is another reason why the 0^+ ions require a very long time

to reach the maximum velocity.

For the He^+ ions, the theoretical minimum velocity agrees very well with the lower boundary of the energized region in Figure 2 of Singh et al. The theoretical maximum velocity is about 25% greater than the largest velocities in Figure 2 of Singh et al. Again, this may be because $v_{\perp max,He^+}$ is large and Singh et al. have plotted the distribution function after only 300 He^+ cyclotron periods. In the simulations of Gaffey (1981) and Gaffey and Mulbrandon (1982) the He^+ ions with $\alpha_{He^+} = 2.4$ required a long time to gain energy and eventually exceeded slightly the theoretical maximum velocity for $\alpha_{He^+} = 2.4$.

For the He^{++} ions, the theoretical minimum and maximum velocities agree quite well with the distribution function in Figure 4 of Singh et al. Only a few ions have exceeded the theoretical maximum velocity.

In conclusion, we emphasize that the values of the minimum and maximum velocities of the stochastic region calculated from the theory of Karney (1978) and Papadopoulos et al. (1980) agree quite well with the numerical simulations of Singh et al., Gaffey, and Gaffey and Mulbrandon in most cases. The assertion made by Singh et al. that an appreciable number of helium ions are heated to velocities greatly exceeding the theoretical maximum velocity is the result of an algebraic error. Upon correcting the error we find that in all cases almost all of the energized ions are in the stochastic region between the minimum and maximum velocities predicted by the theory of stochastic acceleration.

Acknowledgment

This work was supported by the Office of Naval Research under contract N00014-82-K-0208.

REFERENCES

Gaffey, Jr., J.D. Preferential stochastic acceleration of heavy ions by coherent electrostatic hydrogen cyclotron waves in the auroral zones, EOS, 62, 1005, 1981.

Gaffey, Jr., J.D. and M.J. Mulbrandon, Preferential stochastic acceleration of heavy ions by coherent electrostatic hydrogen cyclotron waves in the auroral zones, J. Geophys. Res., 87, (to be submitted) 1982.

Karney, C.F.F., Stochastic ion heating by a lower-hybrid wave, Phys. Fluids, 21, 1584, 1978.

Papadopoulos, K., J.D. Gaffey, Jr. and P.J. Palmadesso, Stochastic acceleration of large M/Q ions by hydrogen cyclotron waves in the magnetosphere, Geophys. Res. Lett., 7, 1014, 1980.

Singh, N., R.W. Schunk and J.J. Sojka, Energization of ionospheric ions by electrostatic hydrogen cyclotron waves, Geophys. Res. Lett., 8, 1249, 1981.

TABLE 1

Theoretical and numerical minimum and maximum velocities of the stochastic region in units of the ion thermal velocity

ion species	α_i	ν_i	theoretical $\frac{T_i}{T_H}$	theoretical $\frac{v_{\perp min,i}}{a_i}$	numerical $\frac{v_{\perp max,i}}{a_i}$	numerical $\frac{v_{\perp min,i}}{a_i}$	numerical $\frac{v_{\perp max,i}}{a_i}$	Reference
O^+	18.5	19.2	1	2.2	16.1	1.9	8.3	Singh et al. Fig. 1a
O^+	10	19.2	1	2.3	10.4	1.7	14.4	Gaffey
O^+	18.5	19.2	10	0.69	5.1	0.4	3.0	Singh et al. Fig. 1b
O^+	10	19.2	10	0.73	3.3	0.5	4.5	Gaffey
He^+	4.62	4.8	0.1	2.5	16.1	1.9	13.0	Singh et al. Fig. 2
He^+	2.4	4.8	0.1	2.9	10.4	1.2	11.8	Gaffey
He^{++}	2.31	2.4	0.1	1.6	12.7	0.8	14.8	Singh et al. Fig. 4
He^{++}	1.2	2.4	0.1	2.4	8.0	-	-	Gaffey

IV. ABSTRACTS

STATISTICAL ACCELERATION OF ELECTRONS BY LOWER-HYBRID TURBULENCE IN THE PRESENCE OF A PARALLEL ELECTRIC FIELD*

J.D. Gaffey,Jr., Z.X. Liu+ and C.S. Wu (Institute for Physical Science and Technology, University of Maryland, College Park, Md. 20742)

The statistical acceleration of electrons along ambient magnetic field by large amplitude lower-hybrid turbulence in the presence of a parallel electric field is discussed. Perturbations driven by a cross-field current and propagating nearly perpendicular to the applied magnetic field are considered. It is assumed that the instability saturates rapidly and that the fluctuating electric field is predominantly electrostatic. If the turbulence is characterized by a spectrum of small parallel wavenumbers, such that the parallel phase velocity of the waves is greater than the electron thermal velocity, then the turbulence can only accelerate electrons moving with large velocities along the magnetic field. The quasilinear diffusion equation is solved using a Green's function technique, assuming a power law spectral energy density. The time evolution of an initial Maxwellian distribution is given and the time rate of change of the average electron velocity and energy are calculated for various cases. The acceleration process is also discussed in terms of a test particle problem.

*Supported by ONR and NASA

+Permanent address: Institute of Space Physics
Chinese Academy of Sciences
Beijing, China

1. Spring meeting, 1982
2. GAFF 202595
3. J.D. Gaffey, Jr.
   Institute for Physical Science ant Technology,
   U. of Md., College Park. Md. 20742
4. SM
5. None
6. P
7. 100%
8. Same as above
9. C(contributed)

Abstract Submitted
For the Twenty-fourth Annual Meeting
Division of Plasma Physics
November 1 to 5, 1982

Category Number and Subject 6.1.2, Magnetosphere

☒ Theory ☐ Experiment

Acceleration of Auroral Electrons by Lower-Hybrid Turbulence and a Quasistatic Parallel Electric Field.* J.D. GAFFEY, JR., Z.X. LIU** and S.C. GUO***, Univ. of Maryland.--The acceleration of electrons along the auroral magnetic field by large amplitude lower-hybrid turbulence and a quasistatic parallel electric field is discussed. Perturbations are excited by a cross-field current, due to a relative electron-ion drift. The fluctuating electric field is primarily electrostatic and propagates nearly perpendicularly to the auroral magnetic field. It is assumed that the instability saturates rapidly. The time evolution of the energy of an individual test electron is calculated. The quasilinear diffusion equation, with a power law spectral energy density, is solved using a Green's function method. The time evolution of an initial Maxwellian distribution is given, and the average electron energy is obtained for various cases. It is found that turbulent acceleration and electric field acceleration are comparable in some cases.
*Supported by ONR and NASA.
**Present address: Chinese Ac. of Sci.,Beijing,China.
***Present address:Chinese Ac. of Sci.,Beijing,China.

☒ Prefer Poster Session
☐ Prefer Oral Session
☐ No Preference
☐ Special Requests for placement of this abstract:
☐ Special Facilities Requested (e.g., movie projector)

Submitted by: John D. Gaffey, Jr. (John D. Gaffey,Jr.)
(signature of APS member)
IPST. Univ. of Maryland
College Park, Md. 20742
(same name typewritten)

(address)

This form, or a reasonable facsimile, plus *Two Xerox Copies* must be received NO LATER THAN NOON, July 30, 1982, at the following address:

Ms. Barbara Safarty
Princeton Plasma Physics Laboratory
P.O. Box 451
Princeton, New Jersey 08544

Instabilities Due to Transmitted and Reflected Ions and Electron Temperature Anisotropy in the Quasiperpendicular Bow Shock*

J. D. GAFFEY, JR. and E. H. DA JORNADA† (Institute for Physical Science and Technology, University of Maryland, College Park, MD 20742)
D. WINSKE (Los Alamos National Lab., Los Alamos, NM 87544)

The theory of cross-field ion streaming instabilities is generalized to treat two ion species, transmitted and reflected, and applied to the parameter regime of a high Mach number quasiperpendicular shock wave. Electron temperature anisotropy is also included in the analysis because the electrons are perferentially heated in the direction transverse to the ambient magnetic field by adiabatic compression at the shock surface. Analytical and numerical results for the linear growth rate are presented. Three waves are discussed: a nearly perpendicular propagating modified two-stream like mode, an obliquely propagating ion-ion streaming mode, and an obliquely propagating kinetic cross-field streaming mode. The first two modes are predominately electrostatic, whereas the third mode is a whistler wave with mixed electromagnetic and electrostatic polarization. The free energy which drives the instabilities is provided by the cross-field ion drift and the electron temperature anisotropy, $T_{e\perp} > T_{e\parallel}$.

*Supported by ONR, CNPq, and NASA.
†Permanent address: Instituto de Fisica, Universidade Federal do Rio Grande do Sul, 90000 Porto Alegre, RS, Brasil.

1. Spring Meeting 1984
2. GAFF 202959
3. Corresponding address:

   Institute for Physical Science and Technology
   University of Maryland
   College Park, MD 20742

   (301) 454-4654
4. SM (Magnetospheric Physics)
5. Special Session:

   Waves, Instabilities, and Turbulence in Space Plasmas.
6. P (poster)
7. 50% at Spring Meeting 1983.
8. (a). Same as #3. above.
9. C (contributed)

Instabilities at the Bow Shock I: Kinetic Cross-Field Streaming Instability*

M. TANAKA, J. D. GAFFEY, JR., D. WINSKE, C. S. WU, Y. M. ZHOU, S. T. TSAI AND K. PAPADOPOULOS
(University of Maryland, College Park, MD 20742)

The kinetic cross-field streaming instability is the high beta generalization of the modified-two-stream instability. It propagates at oblique angles ($\theta << 90^{o}$) to the magnetic field and is not stabilized by electromagnetic effects when the drift speed exceeds the Alfven speed. It is shown that the mode in fact is an obliquely propagating whistler. Particle simulations of the instability are presented and compared with detailed linear, quasilinear and nonlinear theory. The results are applied to the earth's bow shock--the instability is expected to occur in the foot region of the quasi-perpendicular shock--to explain electron and ion heating and the observed low frequeny (< 100 Hz) electromagnetic waves.

*Supported by NASA Solar Terrestrial Theory Program and ONR.

1. Fall Meeting

2. 207734 Tanaka

3. M. Tanaka
IPST
Univ. of Maryland
College Pk, MD 20742
301-454-2061

4. SM

5. None

6. P

7. 30% APS

8. a. Astronomy Program
Univ. of Maryland
College Pk, MD 2074

9. C

nstabilities at the Bow Shock III: Cross-Field Streaming Instability with Temperature Anisotropy*

S. T. TSAI, M. TANAKA, C. S. WU AND J. D. GAFFEY, JR.
(University of Maryland, College Park, MD 20742)

The fact that whistlers with oblique propagation can e amplified by a cross-field ion stream implies that lectron Landau damping is unable to stabilize growth due to the ion drift. On the other hand it is also ell known that electron thermal anisotropy $T_\perp > T_\parallel$ an result in whistler instability with $k_\perp \neq 0$. It is natural to question what happens if both the ion rift and electron thermal anisotropy are included in he analysis. The present study finds the thermal nisotropy enhances the peak growth rate significantly. Since in a perpendicular shock lectrons can be heated preferentially in the ransverse direction, the inclusion of the effect of temperature anisotropy is not only realistic but ecessary.

*Supported by NASA Solar Terrestrial Theory Program and ONR.

1. Fall Meeting

2. Wu 20084

3. C.S. Wu
IPST
Univ. of Maryland
College Pk, MD 20742
301-454-4399

4. SM

5. None

6. P

7. 0%

8. a. Astronomy Program
Univ. of Maryland
College Pk, MD
20742

9. C

2P24

A CROSS-FIELD STREAMING INSTABILITY WITH ELECTRON TEMPERATURE ANISOTROPY IN TANDEM MIRRORS*

J.D. Gaffey, Jr., M. Tanaka, S.T. Tsai

Institute for Physical Science and Technology

University of Maryland

College Park, Maryland 20742

The kinetic cross-field streaming instability, which is the high beta generalization of the modified-two-stream instability, has been studied in detail, including the effect of an electron temperature anisotropy $T_{\perp e} > T_{\parallel e}$. The mode propagates at oblique angles, much less than 90°, to the magnetic field, and it is not stabilized by electromagnetic effects when the drift velocity exceeds the Alfvén velocity. In fact, it has been shown that this mode is an obliquely propagating whistler wave. The fact that obliquely propagating whistler waves can be amplified by cross-field ion streaming implies that the electron Landau damping is unable to stabilize the growth due to the ion drift. Because mirror machines are often heated by energetic neutral beams injected perpendicular to the magnetic field, it is natural to investigate what happens when both the ion drift and the electron temperature anisotropy are included in the analysis. Since the electrons can be preferentially heated in the transverse direction in a mirror machine, the inclusion of the effect of the temperature anisotropy is not only realistic but also necessary. The present study has found that the temperature anisotropy significantly enhances the peak growth rate. The results have been applied to the end cells of the Tandem Mirror device.

*Supported by ONR and NASA

Effect of Electron Thermal Anisotropy on the Kinetic Cross-Field Instability in the Bow Shock*

J.D. GAFFEY, JR., MOTOHIKO TANAKA, C.S. WU AND E.H. DA JORDANA** (all at Institute for Physical Science and Technology, Univ. of Md., College Park, Md. 20742)

The investigation of the kinetic cross-field streaming instability (Wu et al., (1983), which is motivated by the research of collisionless shock waves and applied to the earth's bow shock, is discussed more fully in the present paper. Since in the quasiperpendicular bow shock electrons are preferentially heated in the direction transverse to the ambient magnetic field, the inclusion of the effect of the temperature anisotropy is both desirable and necessary. The present study has found that $T_{e\perp} > T_{e\parallel}$ significantly enhances the peak growth rate of the cross-field streaming instability when the electron beta is of order unity. Furthermore, the present analysis also improves the analytical and numerical solutions of the dispersion equation obtained by Wu et al. (1983).

Wu, C.S., Zhou, Y.M., Tsai, S.T., Guo, S.C., Winske, D. Papadopoulos, K., 1983, Phys. Fluids, 26, (in press).

*Supported by ONR, NASA, CNPq and FINEP.

** Permanent address: Insituto de Fisica, Universidade Federal do Rio Grande do Sul, 90,000 Porto Alegre, Brasil.

1. Spring Meeting 1983
2. GAFF 202595
3. Corresponding address:
   Institute for Physical Science and Technology
   University of Maryland
   College Park, Md. 20742
   301 454-4654
4. SM (Magnetospheric Physic
5. Special Session:
   Waves, Instabilities, and Turbulence in Space Plasmas.
6. P (poster)
7. 50 % at the Fall Meeting 1982
8. Prepaid, $ 30.00 check enclosed
9. C (contributed)

Abstract Submitted
For the Twenty-fifth Annual Meeting
Division of Plasma Physics
November 7 to 11, 1983

Category Number and Subject 1.4 - Scattering, Emission and Absorption of Radiation

[X] Theory [ ] Experiment

Spontaneous Emission of Radiation at Cyclotron Harmonics by Electrons With A Loss-Cone or Hollow-Beam Distribution Function.* C. S. WU, H. P. FREUND** AND J. D. GAFFEY, Jr., U. of Maryland -- The spontaneous emission of radiation at cyclotron harmonics by electrons with a loss-cone or hollow beam distribution function is investigated. The characteristic energies of these electrons are assumed to be from several keV to several tens keV. In addition to these energetic electrons there also exists a component of low-energy background electrons which has a higher density. The present investigation is motivated by the research on the auroral kilometric radiation and cyclotron emissions in mirror machines. The emissivity is calculated based on an approach similar to that discussed in a previous paper by Freund and Wu[1] in which the general expression for the emissivity is derived and the relativistic effect on the cyclotron resonance is included in the calculation.

*Supported by NASA and ONR

**Permanent address: Science Applications, Inc. McLean, VA 22102

1.H. P. Freund and C. S. Wu., Phys. Fluids 20, 1697 (1977)

[X] Prefer Poster Session
[ ] Prefer Oral Session
[ ] No Preference
[ ] Special Requests for placement of this abstract:
[ ] Special Facilities Requested (e.g., movie projector)

Submitted by:

C. S. Wu
(signature of APS member)

C. S. Wu
(same name typewritten)

IPST,
Univ. of Md., College Pk., Md.
(address)

This form, or a reasonable facsimile, plus *Two Xerox Copies* must be received NO LATER THAN Noon, Friday, July 15, 1983, at the following address:

Division of Plasma Physics Annual Meeting
c/o Ms. Barbara Sarfaty
Princeton Plasma Physics Laboratory
P. O. Box 451
Princeton, New Jersey 08544

Abstract Submitted
For the Twenty-fifth Annual Meeting
Division of Plasma Physics
November 7 to 11, 1983

Category Number and Subject 2.2.5 Microinstabilities

[X] Theory [ ] Experiment

Effect of Electron Temperature Anisotrophy on the Kinetic Cross-Field Streaming Instability in Tandem Mirrors* J. D. GAFFEY, JR., E. H. DA JORNADA,+ M. TANAKA, D. WINSKE, and C. S. WU, I.P.S.T., Univ. of Md. -- The theory of the kinetic cross-field streaming instability[1] which is the high beta generalization of the modified-two-stream instability, is extended to include the effects of electron temperature anisotropy since the electrons in magnetic mirrors are preferentially heated perpendicular to the magnetic field. Because supplemental heating in mirror machines is often supplied by neutral beams injected across the magnetic field, the ion drift as well as the electron thermal anisotropy is included in the analysis. Furthermore, the present study also improves the analytical and numerical solutions obtained previously by Wu, et al.[1] The results are applied to the end cells of the Tandem Mirror device. The unstable mode is identified as a whister wave propagating obliquely to the magnetic field. The peak growth rate is significantly enhanced by the electron temperature anisotropy $Te_{\perp} > Te_{\parallel}$ when the electron beta is sufficiently high.
*Supported by CNPq, NASA and ONR
+Permanent address: Instituto de Fisica, Univerisidade Federal do Rio Grande do Sul, Porto Alegre, Brasil
1. C. S. Wu et al., Phys. Fluids 26, 1259 (1983).

[X] Prefer Poster Session
[ ] Prefer Oral Session
[ ] No Preference
[ ] Special Requests for placement of this abstract:
[ ] Special Facilities Requested (e.g., movie projector)

Submitted by:
John D. Gaffey, Jr.
(signature of APS member)

John D. Gaffey, Jr.
(same name typewritten)

IPST,
Univ. of Md., College Pk., Md.
(address)

This form, or a reasonable facsimile, plus *Two Xerox Copies* must be received NO LATER THAN Noon, Friday, July 15, 1983, at the following address:

Division of Plasma Physics Annual Meeting
c/o Ms. Barbara Sarfaty
Princeton Plasma Physics Laboratory
P. O. Box 451
Princeton, New Jersey 08544

ELECTRON-CYCLOTRON MASER INSTABILITY IN MAGNETIC MIRROR MACHINES*

H. K. Wong**
Laboratory for Extraterrestrial Physics
NASA-Goddard Space Flight Center
Greenbelt, Maryland 20771

J. D. Gaffey, Jr. and C. S. Wu
Institute for Physical Science and Technology
University of Maryland
College Park, Maryland 20742

The electron-cyclotron maser instability for energetic electrons with a loss-cone distribution function is studied for magnetic mirror machines. The instability can occur at all angles of propagation for a wide range of parameters. The growth rate is significantly reduced by the presence of a population of cold electrons, and the instability can be suppressed if the density of the cold electrons is sufficiently large and the temperature of the energetic electrons is not too high.

*Research supported by ONR and NASA

**NAS/NRC Resident Research Associate